US Army Corps of Engineers

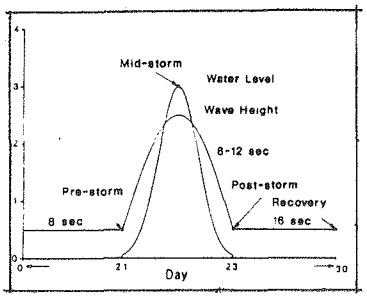

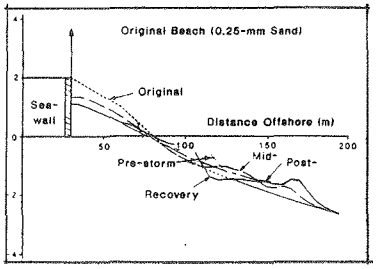

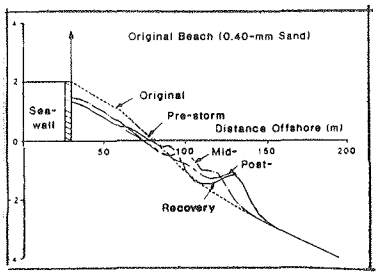

COASTAL ENGINEERING RESEARCH CENTER

TECHNICAL REPORT CERC-89-9

SBEACH: NUMERICAL MODEL FOR SIMULATING STORM-INDUCED BEACH CHANGE

Report 2
NUMERICAL FORMULATION AND MODEL TESTS

by

Magnus Larson

Department of Water Resources Engineering
Institute of Science and Technology
University of Lund
Box 118, Lund, Sweden S-221 00

and

Nicholas C. Kraus, Mark R. Byrnes

Coastal Engineering Research Center

DEPARTMENT OF THE ARMY
Waterways Experiment Station, Corps of Engineers
3909 Halls Ferry Road, Vicksburg, Mississippi 39180-6199

May 1990
Report 2 of a Series

Prepared for DEPARTMENT OF THE ARMY
US Army Corps of Engineers
Washington, DC 20314-1000
Under Calculation of Cross-Shore Sediment Transport and Beach Profile Change Work Unit 32530

Destroy this report when no longer needed. Do not return it to the originator.

The findings in this report are not to be construed as an official Department of the Army position unless so designated by other authorized documents.

The contents of this report are not to be used for advertising, publication, or promotional purposes. Citation of trade names does not constitute an official endorsement or approval of the use of such commercial products.

REPORT DOCUMENTATION PAGE

Form Approved
OMB No. 0704-0188

1a. REPORT SECURITY CLASSIFICATION Unclassified	1b. RESTRICTIVE MARKINGS
2a. SECURITY CLASSIFICATION AUTHORITY	3. DISTRIBUTION/AVAILABILITY OF REPORT Approved for public release; distribution unlimited.
2b. DECLASSIFICATION/DOWNGRADING SCHEDULE	
4. PERFORMING ORGANIZATION REPORT NUMBER(S) Technical Report CERC-89-9	5. MONITORING ORGANIZATION REPORT NUMBER(S)
6a. NAME OF PERFORMING ORGANIZATION See reverse. 6b. OFFICE SYMBOL (If applicable)	7a. NAME OF MONITORING ORGANIZATION
6c. ADDRESS (City, State, and ZIP Code) See reverse.	7b. ADDRESS (City, State, and ZIP Code)
8a. NAME OF FUNDING/SPONSORING ORGANIZATION US Army Corps of Engineers 8b. OFFICE SYMBOL (If applicable)	9. PROCUREMENT INSTRUMENT IDENTIFICATION NUMBER
8c. ADDRESS (City, State, and ZIP Code) Washington, DC 20314-1000	10. SOURCE OF FUNDING NUMBERS PROGRAM ELEMENT NO. / PROJECT NO. / TASK NO. / WORK UNIT ACCESSION NO. 32530

11. TITLE (Include Security Classification)
SBEACH: Numerical Model for Simulating Storm-Induced Beach Change; Report 2, Numerical Formulation and Model Tests

12. PERSONAL AUTHOR(S)
Larson, Magnus; Kraus, Nicholas C.; Byrnes, Mark R.

13a. TYPE OF REPORT	13b. TIME COVERED	14. DATE OF REPORT (Year, Month, Day)	15. PAGE COUNT
Report 2 of a series	FROM _____ TO _____	May 1990	121

16. SUPPLEMENTARY NOTATION
Available from National Technical Information Service, 5285 Port Royal Road, Springfield, VA 22161.

17. COSATI CODES			18. SUBJECT TERMS (Continue on reverse if necessary and identify by block number)
FIELD	GROUP	SUB-GROUP	See reverse.

19. ABSTRACT (Continue on reverse if necessary and identify by block number)

This report is the second in a series on the numerical model SBEACH (Storm-induced BEAch CHange). SBEACH calculates dune and beach erosion produced by storm waves and water levels; bar formation and movement produced by breaking waves are also simulated. The model is empirically based and was originally developed from a large data set of net cross-shore sand transport rates and beach profile change observed in large tanks. The empirical formulation, model sensitivity tests, and a field validation case are described in Report 1. In the present report, Report 2, the capability of the model to simulate berm and dune erosion is evaluated using recently acquired field data from both US east and west coasts. Hypothetical storm events are also simulated to demonstrate model applicability and potential uses for predicting initial adjustment of beach fill and its response to storm action, including poststorm recovery.

(Continued)

20. DISTRIBUTION/AVAILABILITY OF ABSTRACT	21. ABSTRACT SECURITY CLASSIFICATION
☒ UNCLASSIFIED/UNLIMITED ☐ SAME AS RPT. ☐ DTIC USERS	Unclassified
22a. NAME OF RESPONSIBLE INDIVIDUAL	22b. TELEPHONE (Include Area Code) / 22c. OFFICE SYMBOL

6a. NAME OF PERFORMING ORGANIZATION (Continued).

University of Lund
Institute of Science and Technology
Department of Water Resources Engineering;

USAEWES, Coastal Engineering Research Center

6c. ADDRESS (Continued).

Box 118, Lund, Sweden S-221 00;
3909 Halls Ferry Road, Vicksburg, Mississippi 39180-6199

18. SUBJECT TERMS (Continued).

Accretion	Erosion
Beach erosion	Longshore bars
Berms	Numerical models
Cross-shore sand transport	Storm erosion
Dune erosion	

19. ABSTRACT (Continued).

In addition to describing the field tests, Report 2 provides a complete description of the mathematical formulation of the model and numerical algorithms comprising the solution scheme. Improvements of the model made since publication of Report 1 are also presented. The associated wave model has been generalized by using complete linear wave theory everywhere on the profile without shallow-water approximations, a capability important in general applications for irregular bottom profiles subjected to waves of widely ranging characteristics. Refraction has been included, and an option is provided to randomize the wave input for better representing forcing conditions in the field.

PREFACE

This study was conducted at the Coastal Engineering Research Center (CERC), US Army Engineer Waterways Experiment Station (WES), Vicksburg, MS, and the Department of Water Resources Engineering (DWRE), Institute of Science and Technology, University of Lund (UL), Lund, Sweden. Work at WES was authorized as part of the Civil Works Research and Development Program by Headquarters, US Army Corps of Engineers (HQUSACE), and was performed under the Calculation of Cross-Shore Sediment Transport and Beach Profile Change Work Unit 32530, Shore Protection and Restoration Program, CERC. Messrs. John H. Lockhart, Jr., and John G. Housley were HQUSACE Technical Monitors. Dr. C. Linwood Vincent was CERC Program Manager.

This study was performed as a cooperative study between investigators at CERC and DWRE with partial support provided by CERC to DWRE through the US Army Research, Development, and Standardization Group, UK, under Contract No. WESCW 89-238. The associated studies were performed and this report was written over the period 1 August 1988 through 30 August 1989 by Dr. Magnus Larson, Assistant Professor, DWRE, UL; Dr. Nicholas C. Kraus, Senior Scientist, Research Division (RD), CERC; and Dr. Mark R. Byrnes, Research Physical Scientist, Coastal Processes Branch (CPB), RD, and Principal Investigator of the Calculation of Cross-Shore Sediment Transport and Beach Profile Change Work Unit. Ms. Kathryn J. Gingerich and Mr. Mark B. Gravens, CPB, provided valuable reviews of this report.

The portion of the study performed at UL was under general supervision of Dr. Gunnar Lindh, Head, DWRE. The portion performed at CERC was under general supervision of Dr. James R. Houston and Mr. Charles C. Calhoun, Jr., Chief and Assistant Chief, CERC, and administrative supervision of Mr. H. Lee Butler, Chief, RD, and Mr. Bruce A. Ebersole, Chief, CPB. This report was edited by Ms. Lee T. Byrne, Information Technology Laboratory, WES.

COL Larry B. Fulton, EN, was Commander and Director of WES during publication of this report. The Technical Director was Dr. Robert W. Whalin.

CONTENTS

LIST OF TABLES

LIST OF FIGURES

LIST OF FIGURES (Continued)

CONVERSION FACTORS, NON-SI TO SI (METRIC)
UNITS OF MEASUREMENT

Non-SI units of measurement used in this report can be converted to SI (metric) units as follows:

Multiply	By	To Obtain
degree (angle)	0.01745329	radians
feet	0.3048	metres
miles (US statute)	1.6093	kilometers
tons (2,000 pounds, mass)	907.1847	kilograms

SBEACH: NUMERICAL MODEL FOR SIMULATING STORM-INDUCED BEACH CHANGE
NUMERICAL FORMULATION AND MODEL TESTS

PART I: INTRODUCTION

Problem Statement and Objectives

1. Beach stabilization and coastal flood protection are major areas of concern in the field of coastal engineering. Beach erosion, accretion, and change in the offshore bottom topography occur naturally through the transport of sediment by waves and currents. Additional changes result from perturbations introduced by coastal structures, beach fills, and other engineering activities. Beach change is controlled by wind, waves, currents, water level, sediment characteristics and supply, and constraints on sediment movement such as those imposed by coastal structures. These controlling factors are nonlinear and have great variability in space and time. Although it is a challenging problem to predict the course of beach change, such estimations are necessary to design and maintain shore protection projects.

2. The beach can be considered as a flexible structure that provides protection to life and resources along the coast. However, over an interval of just a few hours, storms can produce serious damage and life-threatening situations by rapid erosion of the beach and upland inundation. Quantitative estimation of storm-induced beach change (e.g., contour retreat and volume of eroded material) as a function of the time-dependent forcing conditions is therefore of great importance. Another important aspect of beach response to storm action is the recovery phase normally occurring at the end of a storm and during periods of mild wave conditions. As wave height decreases during the waning stages of a storm, waves transform from erosive to accretive, and the foreshore is rebuilt. It is vital to describe the process of recovery if storm impact is to be assessed and the amount of material lost from the beach quantified. The recovery process must also be modeled if the impacts of successive storms are to be estimated.

3. Seasonal changes in profile shape are readily apparent, produced by smaller, longer period waves in the summer and higher, shorter period waves in the winter. Waves associated with summer conditions tend to produce sand

movement directed toward shore to build up the subaerial beach, whereas winter waves typically erode the inshore part of the beach profile and deposit material offshore, creating one or more longshore bars. It is important to reproduce these seasonal changes in profile shape if predictions or simulations are to be valid for long periods. Also, the capability to estimate variability in shoreline position due to seasonal and shorter time changes in wave climate provides a basis for managing coastal resources rationally and identifying if and when a net loss in beach volume has taken place.

4. Initial adjustments of beach fill to wave action and the response of beach fills to storm processes are of central interest in the design of fill schemes for artificial nourishment. Prediction of protective dune and beach profile evolution for different geometric fill configurations and grain sizes can provide guidance for an efficient benefit-cost analysis of proposed nourishment designs. Different nourishment templates must be evaluated and compared objectively to assist in finding the optimal design to satisfy criteria based on storm protection and recreation benefits.

5. Structures located in the nearshore zone can alter beach evolution, restricting sand transport in a manner dependent on the type, size, and location of the structure. In particular, potential profile change on a seawall-fronting beach must be estimated to determine if the wall will be damaged during storm attack. Likewise, the influence of the wall on modifying the beach is of interest in project design. Knowledge of beach change induced by seawalls will help in their design for optimal performance of the structure and to appraise its impact on the beach (cf. Kraus 1988).

6. Prediction of beach evolution with numerical models has proven to be a powerful technique that can be applied to assist in determining project design. Models provide a framework for developing project problem formulation and solution statements, organizing data collection and analysis, evaluating alternative designs, and optimizing the selected design. Problems related to beach profile response during storms, initial adjustments of a beach fill, seasonal changes in profile shape, and the influence of seawalls on profile evolution are conveniently evaluated using numerical models.

7. This report is the second in a series describing development of a numerical simulation model for engineering use for predicting beach profile evolution, including the formation and movement of major morphologic features

such as longshore bars, troughs, and berms. The model is called SBEACH, an acronym for Storm-induced BEAch CHange. The first report in the SBEACH series (Larson and Kraus 1989a), hereafter referred to as Report 1, describes model development, including the approach, empirical foundation of the model, and initial tests and verification with large-scale laboratory data and limited field data. The objectives of the present report are to describe the numerical solution procedure and to demonstrate applicability of the model with newly acquired field data pertaining to realistic situations encountered in engineering practice. Report 3 in this series will provide details on the operation of SBEACH in the form of a User's Manual.

Review of Methodology

8. The model SBEACH was developed using data obtained from experiments performed in large wave tanks with monochromatic waves of prototype-scale heights and periods. Report 1 gives a thorough discussion of the data base, including a wide-ranging empirical analysis of the data to establish cause-and-effect relationships between the waves and beach profile change. Based on this analysis and physical considerations, a numerical model was developed and tested for simulating profile evolution generated in the large wave tanks. The model was then tested using field data obtained at the Coastal Engineering Research Center's (CERC's) Field Research Facility (FRF) in Duck, NC, and was shown to give reasonable agreement between calculated and measured bar formation and movement.

9. In this report, the capability of the model to predict berm and dune erosion is evaluated using recently acquired field data from both the US east and west coasts. Hypothetical cases are also simulated to demonstrate applicability and potential uses of the model to predict the initial adjustment of a beach fill and its response to storm action, including poststorm recovery. Two different synthetic storms are developed, corresponding to tropical (hurricane) and extratropical (northeaster) events.

10. Improvements in the numerical model have been made beyond those presented in Report 1. The wave transformation model has been generalized by using complete linear wave theory everywhere along the profile without any shallow-water wave approximations. This capability becomes important in

applications encountered in engineering practice, in which differing wave conditions can place the active calculation at various locations on the calculation grid. Also, it is now possible to specify an arbitrary angle between the incident waves and the bottom contours, thus taking into account wave refraction. An option has been included to randomize the wave input to better represent forcing conditions in the field. This is done by randomly changing the input wave height by a predetermined percentage around its input value. Such a modification of the wave height makes the break point move back and forth and thus produces smoother profile features more in accordance with the topography observed in the field. Wave runup is presumably better represented in this process, thereby taking another step toward improved representation of sediment movement on the foreshore.

Scope of Report

11. Part I provides an introduction and short review of Report 1. Part II reviews the empirical foundation of the model, with information on the model's capabilities and limitations, as well as related subjects for future work. Part III describes the wave model that provides input to the empirically developed transport formulas and a realistic estimate of the water level under storm surge, tide, and waves, as described in Part II. Part IV describes the profile change model, focusing on the numerical solution scheme and data input requirements. Part V first reviews sensitivity tests of the model and then describes two case studies, one for the US east coast and one for the US west coast. In Part VI, the model is applied for hypothetical examples to demonstrate a range of uses in beach-fill design. Part VII provides concluding observations of the present capabilities and limitations of SBEACH, leading to recommendations for further study and development of the model.

PART II: REVIEW OF EMPIRICAL FOUNDATION

12. This chapter gives a summary of the empirical foundation of the beach profile change numerical simulation model SBEACH. The data base used in model development is outlined, and the relevance of laboratory data is discussed with reference to field conditions. Salient aspects of cross-shore sand transport characteristics derived from the data are presented, focusing on direction and distribution of transport. The four different transport regions used in the model are introduced and related to findings in nearshore wave dynamics. In addition, the semi-empirical cross-shore sand transport rate equations are summarized.

Data Base

13. The complexity and randomness of nearshore sediment processes, the limited capability of quantifying nearshore fluid and sediment movement, and the limited availability of input data in realistic applications all indicate that numerical models for simulating beach profile change in engineering situations must be based on empirical relations. In Report 1, it was argued that a macroscale approach of model development based on a firm empirical foundation provided a reasonable approach which paralleled the regularities in morphologic change exhibited by beaches. These changes are on a spatial scale of meters and on a time scale of hours to days. Such regularity contrasts markedly from the randomness and complexity of individual particle movement. However, the lack of detailed field data encompassing high-resolution measurements in time and space together with associated wave and water level conditions made it necessary to use laboratory data to enhance development of such a model.

14. Use of laboratory data must address the problem of scaling in attempts to transfer observations and results to the prototype. It is desirable to perform experiments at a scale which is close to that of waves producing significant change on a natural beach, without distorting the kinematic and dynamic interaction between fluid and sediment motion. However, only a small number of experiment programs have been carried out on a scale comparable to the field situation (Saville 1957, Kajima et al. 1982, Vellinga

1982, Dette and Uliczka 1987). Data from the first two laboratory programs were used for numerical model development in this study (Report 1) because they provided an extensive range of conditions that reasonably replicated a naturally sloping beach. In the combined data set, a large number of wave and beach conditions were available for analysis, and the empirical relations obtained were less likely to be influenced by experiment-specific conditions.

15. Model development was largely based on data obtained in the prototype-scale experiments, whereas model verification also used data from a natural beach. Larson (1988) and Larson and Kraus (1989a) give a detailed discussion of the two laboratory experiment programs together with the results of extensive data analysis of the geometric characteristics of the profile and their relation to wave and sand-beach properties.

16. In this report, only a short review of the experiments is presented to provide a background for discussion of the numerical model. The first data set was obtained in experiments performed by the US Army Corps of Engineers (CE) in the years 1956-57 and 1962 (Saville 1957, Caldwell 1959, Kraus and Larson 1988) at Dalecarlia Reservation, Washington, DC. The second data set was derived from experiments carried out at the Central Research Institute of Electric Power Industry (CRIEPI) in Japan (Kajima et al. 1982, 1983).

CE experiments

17. The CE experiments were conducted in a concrete tank 193.5 m long, 4.6 m wide, and 6.1 m deep and having a standard operating depth of 4.6 m (for details of the experimental facility see Raynor and Simmons (1964) and Kraus and Larson (1988)). Most cases were started from a plane initial beach slope of 1:15, and waves of constant height and period were applied until near-equilibrium conditions were attained. A run typically lasted 40 to 60 hr, and the water level was held constant for all cases except one in which a step-type sinusoidal variation was employed. On the order of 10 to 15 profile surveys were made during a typical case, and the survey interval was 1.2 m.

18. Two different sands were used with median grain sizes of 0.22 and 0.40 mm. Eighteen distinct cases have been documented (Kraus and Larson 1988) of which sixteen started from a plane slope. Wave height varied between 0.55 and 1.68 m in the horizontal portion of the tank, and wave period ranged between 3.75 and 16.0 sec. Some observations were made of the breaking wave

height and location during the runs, and a limited number of wave runup measurements were performed as well.

CRIEPI experiments

19. The CRIEPI experiments were similar to the CE experiments in design, and wave tank dimensions (205 by 3.4 by 6 m) were comparable to those of the CE tank. The experiment program consisted of 24 cases with a varying initial beach profile, including both plane initial slopes and profiles of arbitrary shape. The generated wave height ranged between 0.3 and 1.8 m and the wave period between 3 and 12 sec. All cases were run with monochromatic waves and a fixed water level. For cases starting from a plane beach slope (17 of the 24 cases), the initial slope varied from 1:50 to 1:10. Two different sands with median diameters of 0.27 and 0.47 mm were used.

20. Wave height and wave setup along the profile were measured. The number of profile surveys made during a run was somewhat fewer than for the CE experiments, but the spatial resolution of the measurements was considerably higher. Refer to Report 1 for details of data analysis.

Relevance of large wave tank experiments

21. Although scale effects in the large wave tanks were probably small, some differences in response of the beach profile as compared with a natural beach are expected. The main questions concern the relevance of the laboratory data; that is, have the main mechanisms governing cross-shore sand transport on a natural beach been reproduced in the wave tank, and have additional effects been induced in the tank environment which are not found on a beach? One procedure for evaluating the appropriateness of wave tank data is to compare observed profile evolution with that found in the field; such comparisons are summarized below.

22. The speed of bar movement calculated from the large wave tank data (Report 1) was very similar to observations made by Sallenger, Holman, and Birkemeier (1985) on a natural beach during a storm event. In general, the time scale of profile change, both onshore and offshore, was rapid for the field measurements and in accordance with what was observed in the large wave tank experiments. In particular, onshore bar movement occurring during the poststorm recovery stage took place rapidly in the field just as was noted during the accretionary cases in the large wave tanks.

23. The ratio between depth to trough bottom and depth to bar crest obtained in the large tanks displayed properties in good agreement with field observations reported by Shepard (1950). Bars in the field exposed to waves with longer wave periods showed a smaller value of the ratio between depth to trough and depth to crest in accordance with the wave tank data. The value of this ratio was preserved during offshore bar movement in the large wave tank experiments; Sallenger, Holman, and Birkemeier (1985) also found this to be the case during a storm event recorded in the field.

24. A criterion to predict overall profile response (on- or offshore sand movement) based on the sand fall speed and the deepwater wave steepness was derived from the large wave tank data. This criterion proved to be valid for natural beaches if the mean wave height was used in the criterion as the representative statistical wave height. The two empirical coefficients in the formula expressing the criterion were the same for the wave tank data and field data, further emphasizing the relevance of wave tank experiments as well as the apparent lack of scale effects in the experiments.

25. Hallermeier (1987) pointed out the pertinence of results obtained in the large-scale laboratory tests. He found quantitative agreement in terms of shoreline retreat and erosive geometry between a large wave tank case and measured erosion during a storm at Bethany Beach, Delaware, where the conditions in the tank and in the field were similar. The capability of SBEACH to predict eroded volume as well as breakpoint bar movement in field situations also supports the validity of large wave tank studies (Report 1).

26. An obvious restriction of the wave tank data, which is an advantage from the viewpoint of clarifying cross-shore transport characteristics, is the absence of longshore fluid and sand motion. However, one of the main reasons for conducting profile change experiments in wave tanks is to gain insight into the physical processes of cross-shore sand movement. The large wave tank experiments were conducted using waves with a constant height and constant period (monochromatic waves) during a run. Thus, it is an underlying assumption that quantitative understanding of profile evolution may be obtained by studying the response to monochromatic waves of uniform height. In the model, the effect of irregular waves is simulated by using a time series of waves of different heights and periods. This procedure is probably adequate for

simulating profile change by individual irregular waves but neglects the contribution of other types of waves such as infragravity waves.

27. An alternative approach is to employ a statistical or probabilistic description of the incident waves, which would certainly lead to, for example, more gently sloping bars that develop in the field as opposed to the steeper bars that develop under monochromatic waves of constant height in tanks. A proper limit of such models is replication of profile change and bar growth under an extremely narrow-banded wave height and period distribution. In development of SBEACH, there was concern that an *a priori* probabilistic or statistical description would introduce smoothing and mask or obliterate the significance of individual wave components. Therefore, the approach used is founded on profile change produced under elemental monochromatic waves of constant height and proceeds to describe change under irregular waves by superposition.

28. Randomly varying wave height, period, and direction produce a break point that continually changes position, leading to smoother profile development with features less pronounced than in the monochromatic wave case (Keulegan 1948). In the large wave tank experiments, beach slopes tended to become steep as the profile approached equilibrium, especially around the bar or at the foreshore step (Report 1). This was attributed to the applied constant wave height, wave period, and water level, which promoted gradual breakpoint movement and the consequent buildup of steep beach slopes. In summary, a fundamental assumption guiding model development is that short-period breaking waves during storm events are the dominant cause of beach change in the surf zone and thus of bar formation and movement.

Long-period waves

29. Investigations on several coasts (e.g., Guza and Thornton 1982, Greenwood and Sherman 1984, Wright and Short 1984) have found that significant amounts of energy can be contained in lower frequencies of the wave power spectra in very shallow water and in the swash. The presence of lower frequency wave motion cannot be predicted at present, but it appears to be significant in association with storms. It has also been shown that long waves and periodic arrival of high (short-period) wave groups can be responsible for as much or more sediment suspension than individual short-period waves (e.g., Downing 1984; Sternberg, Shi, and Downing 1984; Beach and

Sternberg 1987) in shallow portions of the surf zone. Thus, if long-period waves or wave groups are present, their contribution to the total sediment transport is expected to be significant. An equally if not more important role played by long waves and wave groups than in direct movement of sediment is their contribution to elevating water level near the shore. This allows short-period waves to attack higher on the beach than might be expected.

30. Quantitative engineering relationships for predicting sediment transport produced by long waves and groups have not yet been developed. Therefore, their contribution is not directly represented in the model. When such transport relations become available, it should be possible to incorporate them in SBEACH if they can be expressed in a macroscale framework.

Field data

31. Field data from the FRF were used to verify the numerical model, primarily with regard to bar movement (Report 1). Temporal changes in shoreline position at the FRF are relatively small, making the data potentially unsuitable for testing the predictive capabilities of the model for evaluating dune and foreshore change. In the present report, dune and foreshore change predictions are evaluated using two recently acquired field data sets augmenting field verification given in Report 1.

Cross-Shore Transport Direction and Distribution

32. Cross-shore movement of sediment is governed by properties of the velocity field and sediment concentration. Thus, a first-principles description of the waves, velocity, and concentration is necessary not only across the surf zone but also through the water column at every point on the calculation grid. Presently, such a detailed prediction is not possible in numerical models of beach profile change for engineering use to describe the evolution of natural beaches. However, Dally and Dean (1984) and, more recently, Roelvink and Stive (1989) have had success with first-principles type models in reproducing specific occurrences of profile change.

33. Sediment concentration in the surf zone is closely related to the generation of turbulent motion, which depends on wave breaking. Accordingly, it is plausible that sediment concentration, and thus the amount of material available for transport, is closely related to wave energy dissipation

produced by wave breaking (Dean 1977, Kriebel 1982, Moore 1982, Kriebel and Dean 1985). This macroscale approach is used in SBEACH. In the model, prediction of the cross-shore velocity field is avoided by expressing the cross-shore sand transport rate directly in terms of wave and profile properties. The direction of transport is predicted from an empirical criterion derived from the large wave tank data and verified with field data, and the magnitude of transport in the main portion of the surf zone is related to the wave energy dissipation per unit water volume. This simplified approach implies a transport rate distribution directed either onshore or offshore along the entire profile at a specific instant in time.

Cross-shore transport direction

34. Criteria for predicting whether a beach will erode or accrete through cross-shore sand transport processes have been suggested by a number of authors (see Larson and Kraus 1989a). Most criteria refer to general types of profile configuration, such as winter/summer, storm/normal, bar/berm, dissipative/reflective, which evolve under certain wave and sediment conditions, whereas some authors have focused on predicting the transport direction. In general, there is no contradiction between the two types of criteria, and they can be regarded as equivalent in a macroscopic sense. A profile on which bars develop has transport directed predominantly offshore, whereas a profile exhibiting berm buildup mainly experiences onshore sand movement. However, if a criterion for predicting transport direction is expressed in terms of local wave properties, there could be a significant difference between transport direction and the overall profile type that evolves.

35. Criteria for predicting profile type or overall transport direction typically include one parameter for characterizing the incident wave condition and another parameter involving some property of the sediment (grain size or fall speed) and/or beach slope. Deepwater wave steepness H_o/L_o* is the most commonly used descriptor of the waves (Waters 1939, Rector 1954, Iwagaki and Noda 1962, Nayak 1970, Dean 1973, Sunamura and Horikawa 1974), whereas several different parameters for describing sediment properties have been proposed, such as D_{50}/L_o (Rector 1954), H_o/D_{50} (Iwagaki and Noda 1962), and $\pi w/gT$ (Dean 1973), in which

* For convenience, symbols and abbreviations are listed in Appendix A.

H_o = deepwater wave height, m

L_o = deepwater wavelength, m

D_{50} = median grain size, mm

w = sand fall speed, m/sec

g = acceleration due to gravity, m/sec^2

T = wave period, sec

In development of SBEACH, the deepwater wave steepness H_o/L_o and the parameter H_o/wT , called the dimensionless fall speed or fall speed parameter, were found to give a good distinction between profiles exhibiting mainly bar and berm formation. The fall speed parameter also emerged naturally in the course of regression analysis relating morphodynamic properties of the profile to the incident waves (Larson 1988; Larson, Kraus, and Sunamura 1988; Larson and Kraus 1989a).

36. Figure 1 shows the criterion for distinguishing erosion and accretion developed for data from the large wave tank experiments. Separation of eroded and accreted (bar and berm) profiles is achieved by the equation expressing the solid line drawn in the figure and given by

$$\frac{H_o}{L_o} = M\left[\frac{H_o}{wT}\right]^3 \tag{1}$$

in which $M = 0.00070$ is an empirically determined coefficient. If the left side of Equation 1 is less (greater) than the right side, the profile is predicted to erode (accrete). Wave steepness describes the wave asymmetry, whereas wave height and period appearing in the fall speed parameter account for the absolute magnitudes of those quantities. The fall speed accounts for the settling characteristics of sand particles. Saville (1957) showed on the basis of the early CE experiments that the magnitude of the wave height controls erosion and accretion in addition to the wave steepness.

37. Viewing Figure 1, it is seen that higher waves and shorter periods tend to promote erosion. Coarser grained beaches, for which the fall speed is greater, tend to more readily accrete than do finer grained beaches exposed to the same wave conditions. These predictions conform with field observations.

38. In describing profile change in the wave tank studies, specification of wave and sediment properties to be used in Equation 1 is unambiguous

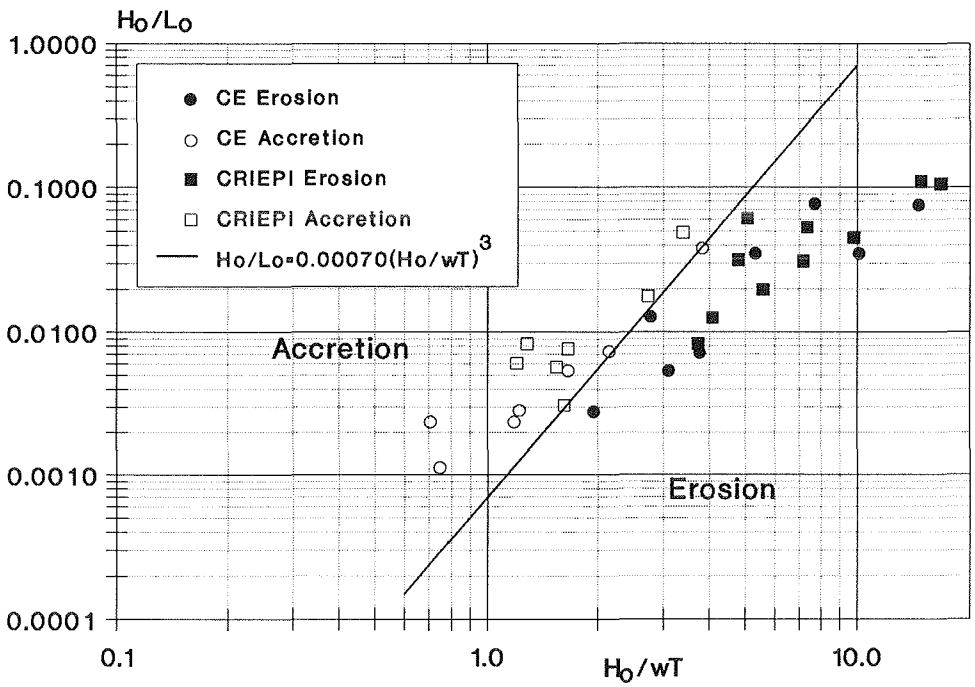

Figure 1. Criterion for predicting beach erosion and accretion based on monochromatic laboratory wave data

because of the fixed wave height and period and well-defined sand size. However, in order to apply the equation to a natural beach, appropriate wave and sediment characteristics must be available. Field data were collected from various investigations around the world to establish the proper statistical descriptors to be used in Equation 1. The data used are summarized in Sunamura (1980a) and Seymour (1986), where movement of the deeper contours was used to evaluate profile change and transport direction in the latter investigation. Report 1 gives a more complete description of the field data used in evaluating the performance of Equation 1.

39. Three deepwater statistical wave heights (mean wave height $\bar{H}_o$, root-mean-square wave height H_{rms}, significant wave height H_{so}) were tested in Equation 1 to obtain the best division between accretionary and erosional profiles for field measurements. Although reasonable delineation could be obtained with each of the wave heights, use of mean wave height provided the best delineation with the same value of M as found for the large wave tank data. Figure 2 displays in analogy to Figure 1 the criterion (solid line) together with the data from natural beaches. If deepwater significant wave

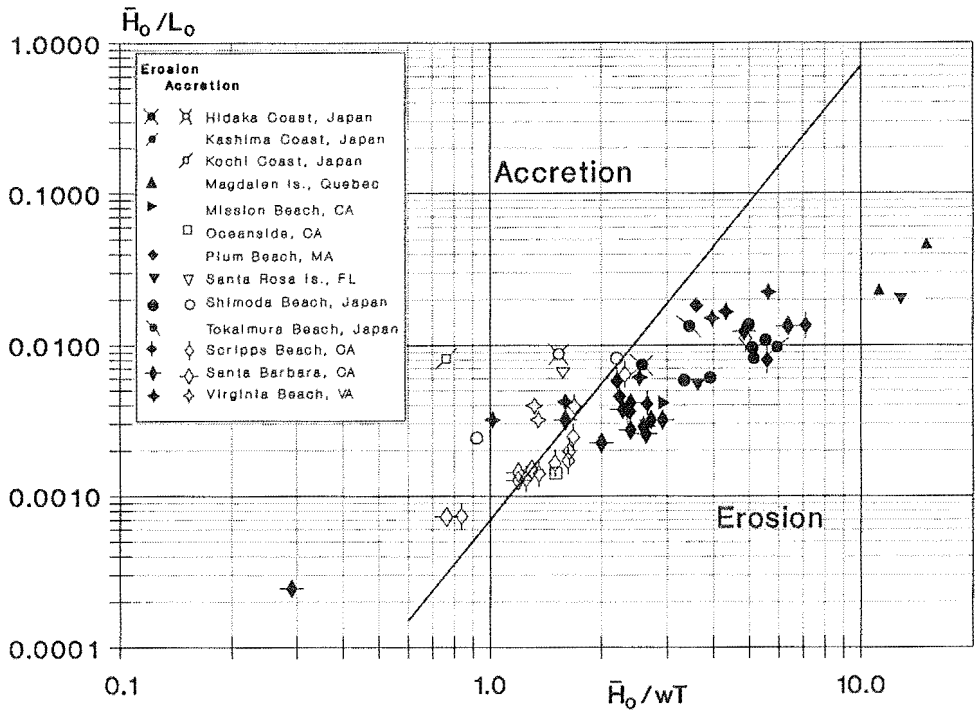

Figure 2. Criterion for predicting beach erosion and accretion

height was reported in the field data, mean wave height was calculated as $\bar{H}_o = 0.626\ H_{so}$ assuming a Rayleigh distribution. The mean or peak period of the spectra was chosen as the representative period to be used in Equation 1 together with median grain size of the beach sediment.

40. Mimura, Otsuka, and Watanabe (1986) compared profile change, transport direction, and transport rate produced in a small wave tank in comparable cases using regular and irregular waves. They observed that the criterion developed by Sunamura and Horikawa (1974) gave the best delineation between erosion and accretion if mean wave height was used in analyzing the irregular wave tests. Profile change proceeded at a slower rate for irregular waves, and this was attributed to the presence of both accretionary and erosional wave components in a wave train. Their observation supports the method of superimposing the effects of individual waves to obtain profile evolution for irregular waves in SBEACH. Kraus and Horikawa (1990) further discuss the difference in sand transport under regular and irregular waves.

Cross-shore sand transport rate distribution

41. Cross-shore sand transport rate distributions were calculated from consecutive profiles in time by integrating the mass conservation equation.

This technique has been applied by van Hijum (1974, 1976), Hattori and Kawamata (1980), and Shimizu et al. (1985). The transport rate obtained constitutes an average net rate for the period between the two profile surveys. Report 1 describes a wide range of analyses of cross-shore transport rate characteristics and transport rate formulas derived on the basis of physical considerations and observations from the data. In the following, some important aspects of the cross-shore sand transport rate are discussed regarding typical distribution shapes in time and space.

42. An important property of the cross-shore sand transport rate as calculated from measured profile change is the temporal decay of the rate of change for profiles exposed to constant waves and water level. The calculated maximum sand transport rate was more than one order of magnitude smaller at the end of a run as compared with the earliest part of the run. A small amount of transport activity still occurred at the end of the runs, attributed in part to profile change introduced by small variations in forcing conditions and randomness in fluid and sand particle motion. Thus, in fitting empirical functions by least-squares to calculated maximum transport rates, an inverse dependence on time gave a better description than an exponential decay because of the finite amount of transport prevailing at the end of the run.

43. By calculating the cross-shore transport rate distribution using initial and final profiles of a run, termed equilibrium distributions, a picture of the overall profile response is obtained. Equilibrium transport rate distributions were classified as three main types (Larson and Kraus 1989a). Figure 3 illustrates the characteristics of these types by displaying the calculated distributions from selected large wave tank cases. The equilibrium distribution types may be summarized as:

a. Erosional (Type E); transport directed offshore along the entire profile.

b. Accretionary (Type A); transport directed onshore along the entire profile.

c. Mixed accretionary and erosional (Type AE); transport directed onshore along the seaward part of the profile and transport directed offshore along the shoreward part of the profile.

44. A majority of cases fell in the classifications of Type E or Type A, indicating predominantly unidirectional transport during the run. Cases having Type AE distributions correspond to profiles where little change

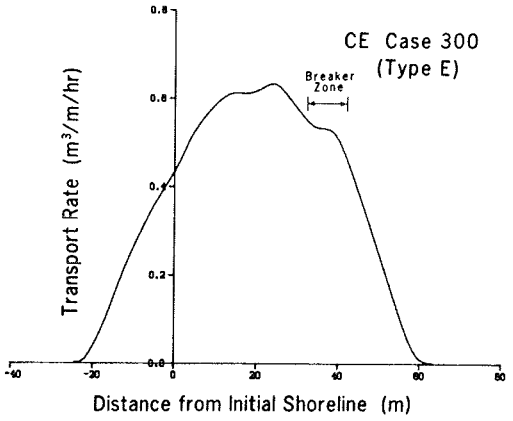

a. Erosional

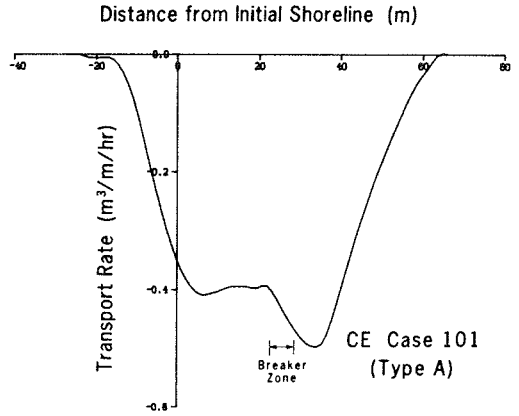

b. Accretionary

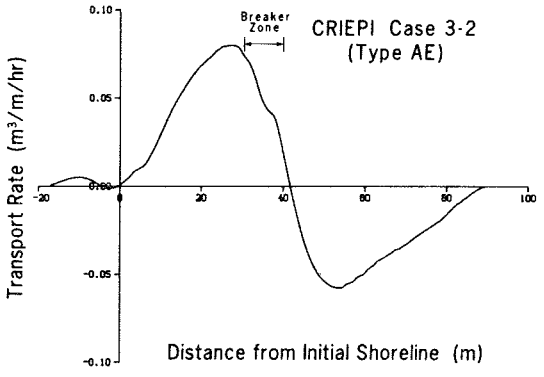

c. Mixed accretionary and erosional

Figure 3. Net cross-shore sand transport rate distributions

place, implying a transport direction that was not so distinct. If significant profile change occurred, transport was directed primarily onshore or offshore. Thus, in the numerical model, which has as a primary objective simulation of events producing significant profile change, it is reasonable to assume a unidirectional transport rate distribution as a first approximation.

45. Sand transport rate distributions calculated from consecutive profile surveys did not show as clear a trend as did the equilibrium distributions, particularly for consecutive surveys taken at later times. In the beginning of a run, when large profile change took place, the transport rate distribution was typically unidirectional. Complexity in transport rate distributions at later times probably reflects a close balance among the many factors contributing to sand movement, for which small instabilities away from equilibrium could produce relatively large localized contributions to the transport. In order to model beach change in situations where the beach is in near-equilibrium with the water level and incident waves, prediction of more complex distributions will probably have to be included.

Transport Regions and Transport Rates

46. Report 1 describes analyses of individual net sand transport rate distributions with the aim of relating the local transport rate to wave and sediment characteristics. Research in nearshore wave dynamics has identified regions of different hydrodynamic properties associated with wave shoaling, wave decay, and intensity of small- and large-scale motion. Svendsen, Madsen, and Buhr Hansen (1978) defined an outer and inner region of the surf zone according to the character of wave and wave-induced water motion. The outer region, located immediately shoreward of the wave break point, is distinguished by a rapid transition in wave height with large-scale flow patterns. At some location landward of the break point, the large-scale flow decays and turns into small-scale turbulent fluctuations; simultaneously the wave changes character and becomes borelike. The region shoreward of this point is known as the inner region and extends to the location where wave runup begins.

47. The concept of two different regions in the surf zone had already been suggested by Miller (1976), who distinguished a vortex and a bore region (see also Basco 1985 and Jansen 1986). Miller also noted that the main

difference between plunging and spilling breakers was the generation of vortices in the outer region. In the inner (bore) region, flow conditions were similar and independent of breaker type, as also noted by Svendsen, Madsen, and Buhr Hansen (1978). Svendsen (1987) analyzed flow measurements to determine the turbulent kinetic energy in the surf zone. He found that the variation over depth of the time-mean turbulent kinetic energy was small (Peregrine and Svendsen 1978), and he attributed this to a strong mixing created by large-scale vortices. Skjelbreia (1987) studied breaking of solitary waves in the laboratory and defined four different zones of wave transformation: gradual and rapid shoaling, and gradual and rapid decay.

48. The identification of regions with different wave characteristics in the nearshore stimulated a separate analysis of the calculated net transport rates in these regions. An important assumption underlying the numerical model SBEACH is the significance of breaking and broken waves in determining the cross-shore sand transport rate. Quite different transport characteristics should be found inside and outside the surf zone, making it reasonable to assume that the transport relationships are different in a macroscopic sense. Furthermore, the dynamics of transport in the swash are governed by properties of the uprush bore and the backwash, sediment characteristics (grain size, porosity, grain density, etc.), and beach slope, which makes it logical to define the swash zone as another distinct region of transport.

49. Based on the division of the profile applied in nearshore wave dynamics and the physical characteristics of sediment transport under various flow conditions, four different zones of transport (Figure 4) were introduced (Larson, Kraus, and Sunamura 1988; Larson and Kraus 1989a). These zones are:

a. Zone I: From the seaward depth of effective sand transport to the break point (prebreaking zone).

b. Zone II: From the break point to the plunge point (breaker transition zone).

c. Zone III: From the plunge point to the point of wave reformation or to the swash zone (broken wave zone).

d. Zone IV: From the shoreward boundary of the surf zone to the shoreward limit of runup (swash zone).

50. The zone located between the break point and the plunge point is analogous to the outer region (vortex region) proposed by Svendsen, Madsen, and Buhr Hansen (1978). A certain distance is required after breaking before

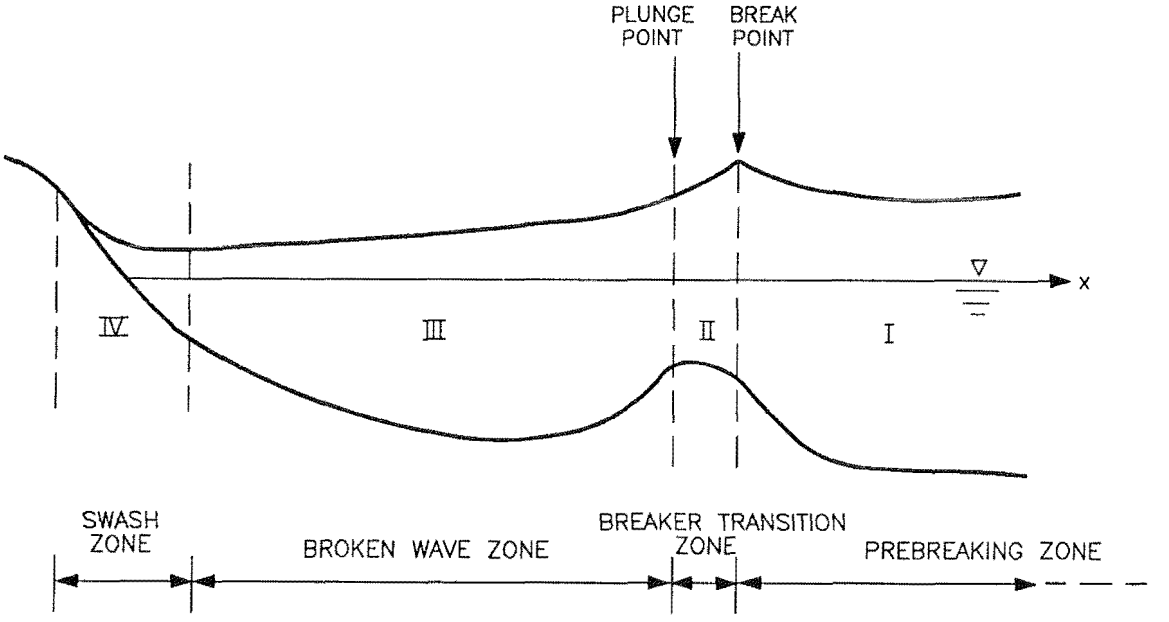

Figure 4. Principal zones of cross-shore transport

turbulent conditions are approximately uniform through the water column. Assuming the cross-shore transport rate is proportional to energy dissipation per unit water volume, the recognition of this zone is important and physically motivated. In this report only empirically based transport relationships for the zones derived from the large wave tank data will be presented. These formulas are used in the numerical model to determine the transport rate distribution across-shore and are discussed in detail in Report 1.

51. The derived transport rate relationships, based on physical considerations and analysis of the large wave tank data, are summarized as:

$$\text{Zone I:} \quad q = q_b \, e^{-\lambda_1 (x - x_b)} \qquad x_b < x \tag{2}$$

$$\text{Zone II:} \quad q = q_p \, e^{-\lambda_2 (x - x_p)} \qquad x_p < x \leq x_b \tag{3}$$

$$\text{Zone III:} \quad q = \begin{cases} K \left[D - D_{eq} + \dfrac{\varepsilon}{K} \dfrac{dh}{dx} \right] & D > \left[D_{eq} - \dfrac{\varepsilon}{K} \dfrac{dh}{dx} \right] \\ 0 & D \leq \left[D_{eq} - \dfrac{\varepsilon}{K} \dfrac{dh}{dx} \right] \end{cases} \tag{4}$$

for $x_z \leq x \leq x_p$

$$\text{Zone IV:} \quad q = q_z \left[\frac{x - x_r}{x_z - x_r} \right] \qquad x_r < x < x_z \tag{5}$$

where

q = net cross-shore sand transport rate, $m^3/m\text{-sec}$

$\lambda_{1,2}$ = spatial decay coefficients in Zones I and II, $1/m$

x = cross-shore coordinate directed positive offshore, m

K = sand transport rate coefficient, m^4/N

D = wave energy dissipation per unit water volume, $N\text{-}m/m^3\text{-sec}$

D_{eq} = equilibrium wave energy dissipation per unit water volume, $N\text{-}m/m^3\text{-sec}$

ε = slope-related sand transport rate coefficient, m^2/sec

h = still-water depth, m

The subscripts b , p , z , and r stand for quantities evaluated at the break point, plunge point, end of the surf zone, and runup limit, respectively. Different spatial decay coefficients are used in Zones I and II, denoted by the subscripts 1 and 2, to describe the decrease in sand transport rate with distance.

52. Empirical expressions for the spatial decay coefficients were derived from large wave tank data (Report 1). The decay coefficient in Zone I was empirically related to median grain size (D_{50}) and breaking wave height (H_b) as (with D_{50} in mm and H_b in m)

$$\lambda_1 = 0.4 \left[\frac{D_{50}}{H_b} \right]^{0.47} \tag{6}$$

For Zone II, limited data suggested that

$$\lambda_2 = 0.2 \, \lambda_1 \tag{7}$$

In calculating the transport rate in Zones I and II, the transport rate is first determined at the plunge point from Equation 4, and then the exponential decay rates are applied seaward in the respective zones.

53. The cross-shore transport rate in zones of fully broken waves is related to the wave energy dissipation per unit water volume. This type of transport formula has previously been used by Moore (1982), Kriebel (1982, 1986), and Kriebel and Dean (1985). Analysis of the large wave tank data substantiated this type of transport relationship in zones of broken waves (Larson 1988, Larson and Kraus 1989a). The transport relationships in the other zones are empirical and based directly on the data from the wave tank experiments. For example, in the swash zone the transport rate is designed to decrease linearly from the end of the surf zone to the runup limit. This property of the transport rate distribution was manifested in many large wave tank cases, occurring with both onshore and offshore transport. Similar characteristics have been noted on a natural beach where the foreshore changed uniformly during erosional and accretionary events (Seymour 1987). However, no direct measurements have been made of transport rates on the foreshore, and transport in this region of the profile deserves further study.

PART III: WAVE MODEL

54. The wave model provides input to calculate cross-shore sand transport rates from which profile change is obtained. In this chapter, an overview is given of the capabilities and limitations of the wave model including a summary of the governing equations. The equations are expressed in an explicit finite-difference form and presented together with the numerical solution method. Finally, the interaction of the wave model with other modules in the full profile change model is discussed with reference to input and output requirements.

55. The wave model is a generalized version of the model described in Report 1. Significant improvements include:

a. Use of complete linear wave theory expressions rather than shallow-water wave approximations.

b. Addition of an option for specifying an arbitrary incident wave angle with respect to the bottom contours. The bottom contours are assumed to be straight and parallel.

c. Use of a more general numerical solution scheme based on the energy flux equation.

Model Capabilities and Limitations

56. Linear wave theory is used to determine wave characteristics across-shore from deep water or a specified water depth offshore to the break point. Shoreward of the break point, a slightly generalized form of the wave decay model of Dally, Dean, and Dalrymple (1984, 1985) calculates the wave height distribution. The point of incipient wave breaking is determined from an empirical criterion expressed in terms of the surf similarity parameter defined with the deepwater wave steepness and the local beach slope seaward of the breakpoint, evaluated over one-third of the wavelength.

57. An input wave height, period, and incident wave angle must be given either in deep water or at a specified depth. The model uses mean wave height to calculate transport direction and significant wave height to calculate the break point and transport rate (Report 1). Wave information is transformed by shoaling and refraction over straight and parallel bottom contours to the most seaward point of the model grid. Energy dissipation in the viscous layer

along the bottom is neglected since the effect on wave height is negligible in comparison to the amount of energy dissipation in the surf zone.

58. Calculation of the wave height across-shore starts in the most seaward calculation cell and proceeds shoreward cell by cell. The local wave height and angle with respect to the bottom contours are determined from conservation of energy flux and Snell's Law. In regions of wave breaking, energy dissipation due to increased turbulence in the water column is included in the energy flux equation. It is possible to specify bottom contours with an orientation that is not parallel to the baseline (y-axis).

59. Energy dissipation in the surf zone is assumed proportional to the excess energy flux beyond a stable energy flux that is a function of water depth (Horikawa and Kuo 1966). Wave properties in the surf zone are calculated using linear wave theory without invoking shallow-water approximations. The wave height calculation is carried out to a water depth that is less than the depth where the surf zone ends in accordance with the definition of the different hydrodynamic regions in the nearshore. The depth at the shoreward end of the surf zone is roughly equal to the seaward limit of the backrush.

60. The wave model allows wave reformation to take place and the possibility of multiple break points across the nearshore zone. Wave reformation occurs if the local wave height reaches the stable wave height, implying no wave energy dissipation. After energy dissipation ceases, shoaling and refraction become dominant until wave breaking occurs and dissipation is initiated once more.

61. Generalizing the breaker decay model of Dally, Dean, and Dalrymple (1984, 1985), the two-dimensional equation for conservation of energy flux incorporating energy dissipation associated with wave breaking may be written

$$\frac{\partial}{\partial x}(F\cos\theta) + \frac{\partial}{\partial y}(F\sin\theta) = \frac{\kappa}{d}(F - F_s) \tag{8}$$

where

x = cross-shore coordinate, positive directed seaward, m

F = wave energy flux, N-m/m-sec

θ = wave angle with respect to the bottom contours

y = longshore coordinate, m

κ = empirical wave decay coefficient

d = total water depth, m

F_s = stable wave energy flux, N-m/m-sec

The total water depth d is given by

$$d = h + \eta \tag{9}$$

where η is the mean water surface elevation (setup or setdown) produced by wave motion. The wave energy flux is given by

$$F = EC_g \tag{10}$$

where

E = wave energy density, N-m/m^2

C_g = wave group speed, m/sec

The wave energy density is written using linear wave theory as

$$E = \frac{1}{8} \rho g H^2 \tag{11}$$

where

ρ = density of water, kg/m^3

H = wave height, m

Assuming the wave conditions to be uniform alongshore and the bottom contours to be straight and parallel, Equation 8 may be reduced to

$$\frac{d}{dx} (F \cos\theta) = \frac{\kappa}{d} (F - F_s) \tag{12}$$

62. Wave group speed is related to wave phase speed C through a factor n which is a function of the water depth and the wavelength L (or wave period T) as

$$C_g = nC \tag{13}$$

where

$$n = \frac{1}{2}\left[1 + \frac{\frac{2\pi d}{L}}{\sinh\left[\frac{2\pi d}{L}\right]}\right] \tag{14}$$

The wave phase speed is determined through the dispersion relationship

$$C = C_o \tanh\left[\frac{2\pi d}{L}\right] \tag{15}$$

where

$$C_o = \frac{gT}{2\pi} \tag{16}$$

in which C_o is the wave phase speed in deep water. Equation 14 is an implicit equation that must be solved numerically or by rational approximations since C contains a dependence on the wavelength, that is, $C = L/T$.

63. The wave decay coefficient controls the rate of energy dissipation, whereas the stable energy flux determines the amount of energy dissipation necessary for stable conditions to occur once breaking is initiated. In this respect, the stable wave condition refers to a state in which energy dissipation during breaking ceases, allowing waves to reform. The stable energy flux may be expressed as

$$F_s = E_s C_g \tag{17}$$

where E_s = stable wave energy density, N-m/m^2 . The stable wave energy flux corresponds to a stable wave height that is a function of the water depth

$$H_s = \Gamma d \tag{18}$$

where H_s is the stable wave height and Γ is the stable wave height coefficient (empirical).

64. Two empirical coefficients enter in the breaker decay model, κ and Γ. However, the values of these coefficients seem to vary little over a wide range of conditions, both in the laboratory and on natural beaches. On the basis of small- and large-scale tank data, Dally, Dean, and Dalrymple (1984) recommended the values of $\kappa = 0.15$ and $\Gamma = 0.40$ for use as averages for a varying bottom slope. Ebersole (1987) evaluated the performance of the breaker decay model using field measurements and found good agreement for engineering applications.

65. Report 1 verified the applicability of the breaker decay model for a barred beach profile using the large-wave tank measurements of Kajima et al. (1983). Values obtained for the two empirical coefficients were in general agreement with values obtained by the aforementioned authors. An apparent dependence on beach slope for the coefficients was noted, but no specific relationships could be developed.

66. Kraus and Larson (in preparation) evaluated the performance of the breaker decay model for waves approaching the beach at an angle with respect to the bottom contours for both laboratory (Visser 1982) and field data (Wu, Thornton, and Guza 1985). In these cases, the coefficients were fixed at the standard values of $\kappa = 0.15$ and $\Gamma = 0.40$. In all cases, the breaker decay model produced satisfactory agreement. For the field data, a statistical approach was used in which wave heights were randomly selected from a Rayleigh distribution for a large number of waves, and the calculated wave height distributions were averaged to obtain a representative distribution.

67. As waves propagate toward shore, a flux of momentum (radiation stress) arises and causes displacement of the mean water elevation if changes in this flux occur due to shoaling or breaking. Seaward of the break point, shoaling produces an increase in wave height, which causes a corresponding increase in the momentum flux. This flux increase is balanced by lowering of the mean water elevation, called setdown (Longuet-Higgins and Stewart 1963). Inside the surf zone, as waves continue to break and decrease in height, the momentum flux decreases, and an increase in mean water elevation occurs (setup).

68. Displacement of the mean water surface (setup or setdown) may be determined from the momentum equation

$$\frac{dS_{xx}}{dx} = - \rho g d \frac{d\eta}{dx} \tag{19}$$

where S_{xx} is the radiation stress component directed onshore (N/m). The radiation stress component S_{xx} is given by linear wave theory for an arbitrary wave angle of incidence as

$$S_{xx} = \frac{1}{8} \rho g H^2 \left[n(\cos^2\theta + 1) - \frac{1}{2} \right] \tag{20}$$

69. The energy flux conservation equation (Equation 8), the wave dispersion relationship (Equation 15), and the cross-shore momentum equation (Equation 19) are not sufficient to specify the wave height across-shore if the waves arrive at an oblique angle to the bottom contours. In this case, an additional equation must be solved that expresses the conservation of wave number. The wave number conservation equation is written in the general form, not taking into account diffraction, as

$$\frac{\partial}{\partial x} \left[\frac{\sin\theta}{L} \right] - \frac{\partial}{\partial y} \left[\frac{\cos\theta}{L} \right] = 0 \tag{21}$$

70. For straight and parallel bottom contours, implying no alongshore variation in wave properties, Equation 21 may be simplified to yield

$$\frac{d}{dx} \left[\frac{\sin\theta}{L} \right] = 0 \tag{22}$$

Integration of Equation 22 gives Snell's Law, which states that the quantity $\sin\theta/L$ is constant across-shore. Equations 8, 15, 20, and 22 allow the wave height to be determined once boundary conditions have been established.

71. As mentioned previously, the wave height, period, and incident angle are calculated at the seaward end of the profile from deepwater or equivalent conditions, providing the necessary boundary conditions. The end of the grid should be located seaward of the break point for all simulations.

From the wave properties, it is possible to determine analytically the setdown at the most seaward point (Longuet-Higgins and Stewart 1962).

$$\eta = - \frac{\pi H^2}{4L \sinh\left[\frac{4\pi d}{L}\right]} \tag{23}$$

72. Also, a condition for the initiation of breaking is needed, indicating the location at which energy dissipation due to breaking begins and the wave decay coefficient becomes different from zero. Breaking occurs when the ratio between the wave height and the water depth exceeds a certain value which is a function of the surf similarity parameter expressed in terms of the deepwater wave steepness and profile slope prior to breaking.

$$\gamma = 1.14\ \xi^{0.21} \tag{24}$$

where

γ = breaker ratio = H_b/h_b

ξ = surf similarity parameter

The surf similarity parameter is given by

$$\xi = \tan\beta \left[\frac{H_o}{L_o}\right]^{-0.5} \tag{25}$$

where $\tan\beta$ is the local beach slope seaward of the break point.

73. Equation 24 was derived in Report 1 from data given by Kajima et al. (1983), but very similar relationships were previously reported in Singamsetti and Wind (1980) and Sunamura (1980b). Report 1 used data from prototype-scale experiments, whereas the two latter studies were based on small-scale laboratory experiments. Thus, in Equation 24 scale effects are absent, although it should be observed that only monochromatic waves were used in the tests.

74. The laboratory data of Kajima et al. (1983) included cases with a maximum wave period of 12 sec, although most cases had periods in the range of 3 to 9 sec. The limited data available for longer period waves indicate that

Equation 24 should be used with care. Also, since the relationship was determined mainly from barred profiles exposed to monochromatic waves, the profile slope seaward of the break point was steeper than what is typically found in the field. Thus, Equation 24 tends to underestimate the breaker ratio for gentle slopes in field applications.

75. An expression for energy dissipation due to wave breaking is needed in the prediction of the cross-shore sand transport rate. In the process of wave height decay after breaking, turbulent motion is induced in the surf zone. The turbulent kinetic energy is converted into heat through transfer of energy from larger to smaller eddies. In the macroscale approach of the beach profile model, it is satisfactory to derive energy dissipation from wave height decay without resolving the internal structure of this process. However, the difference between the production of turbulent kinetic energy and the corresponding dissipation with reference to the time scale (Roelvink and Stive 1989) is observed as well as the process of energy reordering (Svendsen, Madsen, and Buhr Hansen 1978).

76. The wave energy dissipation D per unit water volume is

$$D = \frac{1}{d} \frac{d}{dx} (F \cos\theta) \tag{26}$$

Using Equation 12, the following relationship for D is obtained

$$D = \frac{\kappa}{d^2} (F - F_s) \tag{27}$$

Once the cross-shore wave height distribution is calculated, the energy dissipation per unit water volume in the surf zone is determined explicitly from Equation 27. Outside the surf zone, κ is set to zero, and no energy dissipation takes place since bottom friction is neglected.

Numerical Solution Scheme

77. An explicit finite-difference scheme is used to solve the equations for determining cross-shore wave height. In the following section, an outline is given of the numerical solution scheme and the difference equations employed. Figure 5 is a definition of the grid and illustrates where the various quantities in the difference equations are defined.

78. In the model, a quasi-stationary approach is applied, implying that a steady-state solution of the wave height distribution is determined at every time step. Propagation of individual waves is not described, but it is assumed that the model time step is significantly larger than the wave period.

79. For irregular wave conditions, the wave height used at each time step may be regarded as a statistical measure that represents the average properties of the breaking waves during the time step. This wave height is different from the wave height needed to reproduce the average wave height distribution during a time step, which includes all broken and unbroken waves at specific locations. The selected wave height parameter should represent the average location of the surf zone, giving a clear distinction between regions of broken and unbroken waves. From experience with field simulations, significant wave height is satisfactory in this respect (Report 1).

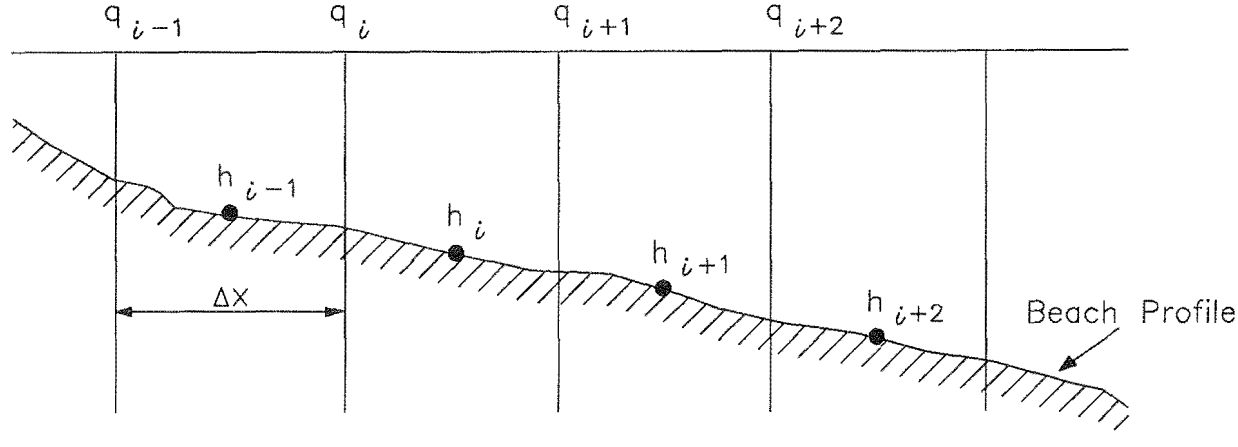

Quantities evaluated at q-points: q, H, θ, L, F, C_g

Quantities evaluated at h-points: h, η, F_s, D

Figure 5. Definition sketch of numerical grid

80. Numerical calculations start at the seaward end of the grid and proceed onshore through an explicit solution scheme in which quantities known at a specific grid point are used to determine corresponding quantities at the next grid point. In the difference equations presented, the index i is used to denote the number of a specific grid point. A staggered grid is used with different quantities taken at points in the middle of calculation cells or at the boundaries between cells (Figure 5). The primary quantity in the middle of a cell is water depth, and these grid points are termed h-points. At the boundaries of calculation cells, the main quantity is the cross-shore transport rate, and quantities defined here are termed q-points.

81. As previously mentioned, the wave height, period, and incident angle must be known at the most seaward grid point (given or calculated from some reference depth offshore) prior to starting the calculation. From these wave properties, wave setdown is determined from Equation 23. Profile depth is given in the middle of each calculation cell, whereas setdown and setup are calculated at q-points. Depths at the boundaries of the cells are given by linear interpolation. Also, energy flux and radiation stress in the direction of the waves are determined from knowledge of the depth and wave quantities at the first q-point.

82. Moving from a specific q-point to the next, wave refraction is first determined if the incident wave approaches with an angle to the bottom contours. From Equation 22, the angle between the wave crests and the bottom contours at the next shoreward q-point is given by

$$\theta_i = \arcsin\left[\frac{L_i}{L_{i+1}} \sin\theta_{i+1}\right] \tag{28}$$

Note that grid point numbering increases in the seaward direction since the x-axis points offshore, but the calculation proceeds from offshore in the shoreward direction. Water depth at grid point i in Equation 28 is corrected with setdown (setup) using the value at grid point $i+1$ to avoid use of an implicit or iterative scheme. Wavelengths are calculated using the dispersion relationship (Equation 15) solved by a Padé approximation (Hunt 1979).

83. The next step in the calculation is to determine the energy flux and thus the wave height. Equation 10 is written in difference form as

$$F_i = \frac{1}{\cos\theta_i + 0.5A_{c_i}} \left[F_{i+1} \left(\cos\theta_{i+1} - 0.5A_{c_i}\right) + A_c F_{s_i}\right] \tag{29}$$

where

$$A_{c_i} = \frac{\kappa \Delta x}{h_i + \eta_{i+1}} \tag{30}$$

and Δx = length step (m). The stable wave energy flux is determined from

$$F_{s_i} = \frac{1}{8} \rho g \left[\Gamma \left(h_i + \eta_{i+1}\right)\right]^2 \frac{C_{g_i} + C_{g_{i+1}}}{2} \tag{31}$$

An average value for the wave group speed is used because this quantity is taken at q-points, and the stable wave energy flux is evaluated at h-points. Seaward of the break point, κ is set to zero, indicating that A_{c_i} is also zero, since no energy dissipation due to breaking occurs.

84. After the energy flux has been calculated at a specific point, the corresponding wave height is determined from Equations 10 and 11 as

$$H_i = \left[\frac{8F_i}{\rho g C_{g_i}}\right]^{0.5} \tag{32}$$

Using the wave height, radiation stress is calculated from Equation 20 and setdown (setup) is given from Equation 19, expressed in difference form as

$$\eta_i = \eta_{i+1} + \frac{(S_{xx})_{i+1} - (S_{xx})_i}{\rho g (h_i + \eta_{i+1})} \tag{33}$$

85. At every calculation step, a check is made to determine if wave breaking has occurred according to Equation 24. Once breaking is initiated, the wave decay coefficient is given the value $\kappa = 0.15$, and energy dissipation takes place. Also, if breaking has occurred, a check is made to determine whether wave reformation is possible, that is, whether the wave energy

flux is lower than the stable energy flux. The stable wave height coefficient is set to $\Gamma = 0.40$, and if there is wave reformation, κ is given the value zero. An arbitrary number of surf zones with intermediate zones of wave reformation may occur.

86. The breaker ratio is determined from Equation 24 for the most seaward break point. If multiple breaking occurs, a constant breaker ratio $\gamma = 1.0$ is applied at the more shoreward break points to avoid extreme values that may occur by use of Equation 24 at steep-sloped, small bars created in the inner surf zone. The shoreward boundary of the calculation grid is located at a predetermined water depth approximately corresponding to the point of intersection between an average linear sloping foreshore and an equilibrium profile for a given sediment diameter or the location of a seawall.

87. Wave height calculations are not carried out using the exact topography of the profile; instead, a smoothed profile is used. The reason for this is that the response of waves to bottom topography takes place over a certain distance, suggesting that shoaling and refraction do not occur instantaneously. For example, a very small hump (a rock) on the bottom would not cause a wave to shoal, which the equations would predict if no profile smoothing were applied. The smoothed profile is used only to compute wave properties; the actual calculated profile is maintained to compute transport rates and beach profile change.

88. The number of calculation cells over which the smoothing is performed (a moving average scheme) is determined based on the breaking wave height as $3H_b$. The averaging distance $3H_b$ is somewhat arbitrary and is based on numerous comparisons of model predictions made in Report 1. The distance over which a wave changes markedly in shoaling to the break point is not known; Smith and Kraus (in preparation) have recently suggested use of the distance $L/3$, where L is the average local wavelength, a qualitative observation made from their physical model tests of wave breaking over bars. A simple predictive formula is used to estimate the breaking wave height at each time step prior to determining the wave height distribution (Larson and Kraus 1989a) as

$$H_b = 0.53\ H_o \left[\frac{H_o}{L_o}\right]^{-0.24} \tag{34}$$

PART IV: NUMERICAL MODEL OF STORM-INDUCED BEACH CHANGE

89. The model SBEACH consists of three calculation modules that are executed consecutively at each time step in a simulation. The modules calculate wave height across-shore, net cross-shore sand transport rate, and profile change, respectively. Wave height is used to calculate the transport rate from which profile change is calculated. The bathymetry is then revised, and these modules are stepped through successively to calculate profile change for the simulation period.

90. Part III described the theoretical background and numerical solution scheme of the wave module. Relationships used to determine the net cross-shore sand transport rate were given in Part II. In this chapter, an overview of the capabilities and limitations of the profile change model is given with a discussion of the input data requirements and types of output produced by the model. Finally, the numerical solution scheme for calculating profile change, boundary conditions, model stability, and typical time interval and length step is described.

Model Capabilities and Limitations

91. A fundamental assumption of the numerical model is that breaking waves are the major cause of profile change, and thus the major part of cross-shore sand transport takes place in the surf zone. The volume of sand transported is determined by the wave energy dissipation per unit water volume in the surf zone (dependent upon wave conditions and profile shape) and by empirical functional relationships obtained from the large wave tank data in other zones along the profile. The direction of transport is given by an empirical predictive criterion (Equation 1), and calculation of the fluid velocity field in the surf zone is not required.

92. Wave height, wave period, and water level can be specified at each time step to account for variable forcing conditions. Water level change appears in the computations as a translation of the origin of the vertical coordinate axis; the water level is shifted back to the original level prior to entering the mass conservation equation.

93. The numerical model incorporates the principle of superposition in the sense that random waves, as exist in the field, are represented by consecutive individual waves appearing in a time series of monochromatic waves. This assumption is appropriate with respect to the engineering utility of the model where a macroscopic quasi-stationary approach is taken in calculating the cross-shore wave height distribution. Also, the time interval should be sufficiently short to represent the many different waves in a time series of random waves.

94. For the large wave tank data, choice of input wave height and period for the computations is unambiguous because waves of constant height and period were used. On a natural beach, the forcing parameters show appreciable variation in time. By trial calculations using field data, it was concluded that significant wave height gives the best result regarding the transport rate and corresponding profile change as compared with mean or root-mean-square wave height (Report 1). An intuitive explanation for using significant wave height is that energy dissipation, which determines the transport rate, increases with the square of the wave height implying that higher waves give a relatively larger contribution. Thus, as a representative wave height, a larger measure should be used rather than the mean wave height.

95. Mimura, Otsuka, Watanabe (1986) conducted small-scale laboratory experiments using irregular waves in order to determine the representative monochromatic wave height for describing various cross-shore transport phenomena. They found that the overall profile response as erosional or accretionary was best described by the mean wave height. This finding is in agreement with the results in Report 1 as displayed by the criterion separating erosion and accretion (Equation 1 and Figures 1 and 2). The study by Mimura, Otsuka, and Watanabe did not provide clear guidance concerning choice of a representative wave for calculating the net cross-shore transport rate, but both the mean and significant wave height appeared to be applicable. Their transport relationship (Watanabe 1982) is based on the Shields parameter, which is conceptually and functionally different from the wave energy dissipation approach used in Report 1.

96. Median grain diameter for the studied profile is a key parameter in calculating the net cross-shore transport rate and resulting profile change. This representative sand size determines the equilibrium energy dissipation

which appears in the transport rate formula in the zones of broken waves (Equation 4). Moore (1982) presented a relationship between D_{eq} and D_{50} in graphical form based on field profiles, and Dean (1987, 1990) re-expressed the relationship in terms of fall speed. As described in Report 1, the numerical model gave the best overall fit for large wave tank data if 0.75 D_{eq} was used in the simulations rather than D_{eq} . This proved satisfactory for field data as well.

97. In the numerical model it is possible, in principle, to specify a different grain size and thus equilibrium energy dissipation in every calculation cell. However, since the movement of individual grains is not tracked, the median grain diameter will remain the same throughout the simulation in a specific cell, which is unrealistic considering grain movement. Some beach profiles exhibit grain size characteristics with distinctly different regions across-shore. If, for instance, the dune region has a median grain diameter different from the subaqueous part of the profile, it may be permissible to schematically represent these conditions. In this case, every cell located in the dune region is assigned one grain size, whereas the cells located seaward are given a different grain size. Using this technique, it is implicitly assumed that as grains pass from the dune region to the seaward region, the transported amount exchanged between regions is so small that it does not alter the original distribution of grain size.

98. Development of the numerical model was directed towards predicting profile change during erosional and accretionary events. Two main areas of application of the model are estimation of profile erosion and shoreline retreat during storm or hurricane events and initial adjustment of beach fills to changes in water level and waves. Useful descriptive quantities are eroded volume above a certain contour and retreat distance of that contour. The program calculates these quantities for an arbitrarily specified contour and selected time step. These applications, together with the properties of the large wave tank experiments, emphasized model development focusing on erosional processes.

Profile Change Model

99. Profile change is calculated from the mass conservation equation using the net transport rate distribution determined from Equations 2 through 5. If sand sources or sinks are absent, the mass conservation equation is

$$\frac{\partial h}{\partial t} = \frac{\partial q}{\partial x} \tag{35}$$

The boundary conditions are zero sand transport rate at the runup limit and at the seaward depth signifying the onset of significant sand movement. The seaward boundary of the calculation grid (limiting depth for sand motion) is effectively determined by the exponential decay in Zone I, taken to be a point where the transport rate has decreased to a small value.

100. As the wave height distribution is calculated across-shore for a given time step, the location of the boundaries between the different sand transport zones is determined. The location of the break point is given directly from the wave height calculations, and the plunge point is computed as $3H_b$ based on findings by Galvin (1969) and Svendsen (1987). The landward boundary of the surf zone is defined as the point of tangency between a linearly sloping beach face and an equilibrium profile for a given median grain diameter, whereas the runup limit is given by a formula for predicting the active profile height developed from the large wave tank data (Report 1). The expression for active profile height is similar to the formula provided by Hunt (1959), where the runup height normalized with the incident wave height is a function of the surf similarity parameter.

101. The active subaerial profile height Z_R is given by

$$Z_R = 1.47\ \xi^{0.79} \tag{36}$$

The surf similarity parameter ξ is defined in Equation 25, and the slope to be used in Equation 36 is the average beach slope in the surf zone. Originally Equation 36 was based on the initial slope in the large wave tank tests, but application of the model to field data showed that using the average surf zone slope gave satisfactory results. The runup height has little influence

on bar size and movement, but it does define the shoreward limit for cross-shore sand movement (Report 1). The amount of erosion on the foreshore is similar even for significant variations in the runup height, but the shape of the foreshore is quite different. Transport at the landward end of the surf zone determines how much material is transported from or to the foreshore. Higher runup implies a larger area from which material can be taken and thus a different resulting foreshore shape compared with that given by a smaller runup height.

102. From knowledge of the locations defining the various transport zones, the transport rate distribution can be calculated from Equations 2 through 5. Several break points may occur along a profile if wave reformation takes place, leading to several zones of Type II and III transport. To determine the transport rate distribution, sand transport is first calculated in zones of fully broken waves (Zone III) according to Equation 4, written in difference form

$$q_i = K \left[\frac{(D_i + D_{i-1})}{2} - D_{eq} + \frac{\varepsilon}{K\Delta x} (h_i - h_{i-1}) \right] \tag{37}$$

The definition of the calculation grid is given in Figure 5. Energy dissipation per unit water volume is taken at h-points (in the middle of a calculation cell) making it necessary to average D when calculating the transport rate.

103. Calculation of the transport rate in zones of fully broken waves defines the boundaries of Zone III, from which the transport rate may be calculated in the other zones. After these values are determined at the plunge point and at the end of the surf zone, Equations 2, 3, and 5 are applied to completely define the transport rate distribution. In discretizing the mass conservation equation, transport rate distributions from two time levels are used. The superscript k is used to denote a specific time level, and the difference equation is expressed as

$$\frac{h_i^{k+1} - h_i^k}{\Delta t} = \frac{1}{2} \left[\frac{q_{i+1}^{k+1} - q_i^{k+1}}{\Delta x} + \frac{q_{i+1}^k - q_i^k}{\Delta x} \right] \tag{38}$$

where Δt is the time step (sec). Since the transport rate distribution is determined from different relationships depending on the zone of transport, its spatial derivative will generally be discontinuous at the boundaries between the zones. To obtain a smoother, more realistic transport distribution, a 3-point filter is applied to the calculated transport rates on grid cells away from boundaries by

$$q'_i = 0.25\ q_{i-1} + 0.50\ q_i + 0.25\ q_{i+1} \tag{39}$$

where the prime (') denotes the smoothed transport rate.

104. In some large wave tank cases, the local beach slope exceeded the angle of repose due to constant waves and water level. Monochromatic waves caused erosion and accumulation to occur at the same locations along the profile for a sufficiently long duration to produce excessive profile steepening. Steepest profile slopes occurred during erosional conditions on the shoreward side of the bar just seaward of the berm crest. Local profile slopes exceeding the angle of repose rarely develop on a natural beach because wave height, wave period, and water level are continuously varying.

105. The concept of avalanching, as discussed by Allen (1970), was incorporated in the numerical model, and a routine was included to account for transport induced by slope failure. Allen recognized two different limiting profile slopes, the angle of initial yield (angle of repose) and the residual angle after shearing. If the local slope exceeds the angle of initial yield ψ_{iy}, material is redistributed along the slope, and a new stable slope is attained, known as the residual angle after shearing ψ_{ra}. From analysis of maximum local profile slopes from the large wave tank data, considerably lower values were obtained for ψ_{iy} and ψ_{ra} than reported by Allen. From his experiments with natural sands (diameters ranging from 0.27 to 3.17 mm), he noted an angle of about 48 deg* caused avalanching, whereas an angle of 33 deg seemed to be the stable slope after avalanching had ceased.

106. Analysis of the large wave tank data (Report 1) showed smaller values of the maximum slope, inferred to be the angle of initial yield, with a

---

* A table of factors for converting non-SI units of measurement to SI (metric) units is presented on page 5.

mean value of 28 deg. The average value for the residual angle after shearing was determined to be 22 deg; however, this conclusion is not firm since some profile steepening undoubtedly occurred between the time of avalanching and the next profile survey. Allen determined from experiments that the difference between ψ_{iy} and ψ_{ra} (dilatation angle) is in the range of 10 to 15 deg for sand. Therefore, in the numerical model, if ψ_{iy} is set to 28 deg and ψ_{ra} is set to 18 deg, a dilatation angle of 10 deg is used.

107. If the local slope exceeds ψ_{iy} in the model, material will be redistributed in the neighboring cells so that the slope everywhere is less than or equal to ψ_{ra}. Computationally this is performed by checking the local slope ψ at each time step along the grid, and, if $\psi > \psi_{iy}$, avalanching is initiated. Two conditions determine the redistribution of material: mass should be conserved and the residual angle after shearing is ψ_{ra}. Figure 6 is a definition sketch for avalanching where the local slope between cells 1 and 2 exceeds ψ_{iy}. Depths before avalanching are denoted with h, whereas new depths after sand redistribution are indicated with a prime.

108. The number of cells N over which avalanching occurs is not known *a priori* and has to be found iteratively. Initially, it is assumed that the avalanching takes place between cells 1 and 2. Material is moved from cell 1 to 2 in order to obtain the slope ψ_{ra} between the cells, and the new slope between cells 2 and 3 is checked to see if it exceeds ψ_{yi}. If this is the case, the calculation is repeated, now incorporating cells 1 to 3, using the mass conservation equation and assigning the slope ψ_{ra} to all slopes between cells. This procedure is continued until the slope between cells N and $N+1$ is less than ψ_{ra}.

109. For the general case where sand is redistributed in N calculation cells included in avalanching, the mass conservation equation is written

$$\sum_{i=1}^{N} \Delta h_i = 0 \tag{40}$$

where

$$\Delta h_i = h_i' - h_i \tag{41}$$

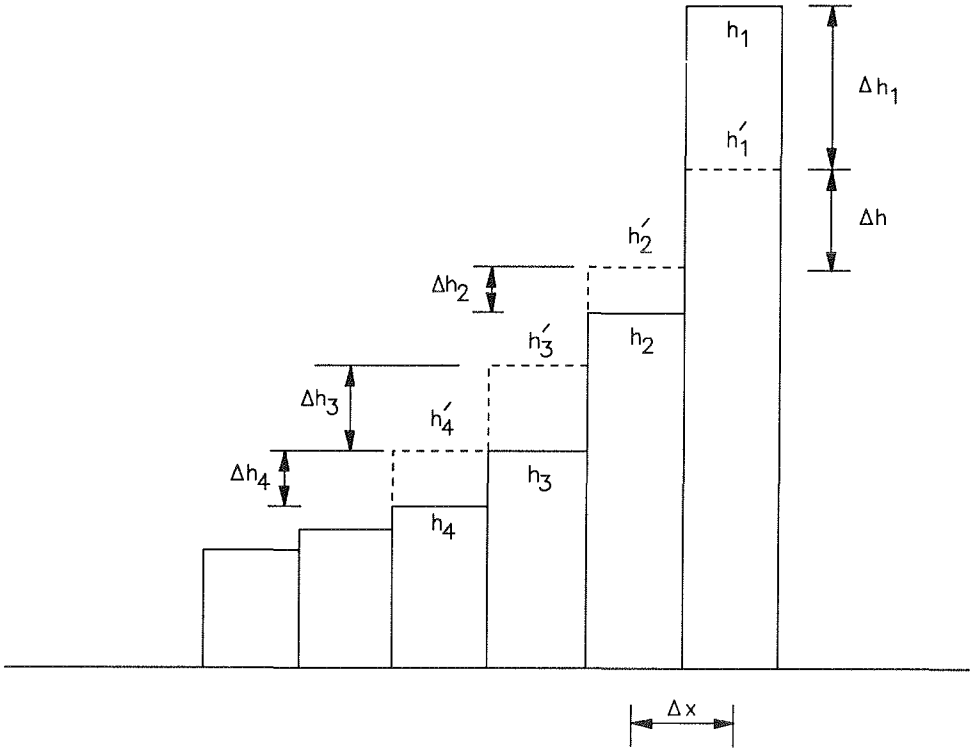

Figure 6. Definition sketch for avalanching calculation

Here the cell numbering, denoted by i, starts from the cell where avalanching is initiated and is taken in the direction of sand redistribution. Also, depth changes have to be taken with the proper sign. The other criterion necessary to obtain the solution is that after avalanching, the slope between calculation cells must be ψ_{ra}. If the length of the calculation cell is Δx, the residual angle after shearing is expressed as

$$\psi_{ra} = \frac{h_i - h_{i+1}}{\Delta x} \tag{42}$$

Since ψ_{ra} is constant, the difference in depth between neighboring cells Δh has to be a constant given by

$$\Delta h = \psi_{ra} \Delta x \tag{43}$$

110. The requirement on the difference in depth between cells, as given by Equation 43, may be written for $N-1$ pairs of cells included in the avalanching as

$$\begin{aligned} \Delta h &= (h_1 + \Delta h_1) - (h_2 + \Delta h_2) \\ \Delta h &= (h_2 + \Delta h_2) - (h_3 + \Delta h_3) \\ \Delta h &= (h_i + \Delta h_i) - (h_{i+1} + \Delta h_{i+1}) \\ \Delta h &= (h_{N-1} + \Delta h_{N-1}) - (h_N + \Delta h_N) \end{aligned} \tag{44}$$

This system of equations may be rewritten by consecutively eliminating the first part of the right-hand side of each equation by adding the previous equation. The result is

$$\begin{aligned} \Delta h &= (h_1 + \Delta h_1) - (h_2 + \Delta h_2) \\ 2\Delta h &= (h_1 + \Delta h_1) - (h_3 + \Delta h_3) \\ i\Delta h &= (h_1 + \Delta h_1) - (h_{i+1} + \Delta h_{i+1}) \\ (N-1)\Delta h &= (h_1 + \Delta h_1) - (h_N + \Delta h_N) \end{aligned} \tag{45}$$

111. From Equation 45, the unknown depth changes Δh_i may be explicitly identified as

$$\begin{aligned} \Delta h_2 &= (h_1 + \Delta h_1) - h_2 - \Delta h \\ \Delta h_3 &= (h_1 + \Delta h_1) - h_3 - 2\Delta h \\ \Delta h_{i+1} &= (h_1 + \Delta h_1) - h_{i+1} - i\Delta h \\ \Delta h_N &= (h_1 + \Delta h_1) - h_N - (N-1)\Delta h \end{aligned} \tag{46}$$

From Equation 46, it is possible to compute all the depth changes once the depth change in the first cell is known. To determine the depth change in the first cell, the mass conservation equation (Equation 40) is used. The sum of all changes in depth must be zero

$$\sum_{i=1}^{N} \Delta h_i = \Delta h_1 + \sum_{i=2}^{N} \Delta h_i = 0 \tag{47}$$

Replacing the summation over the depth changes from cell 2 to N using Equation 46 yields

$$\Delta h_1 + \sum_{i=2}^{N} (h_1 + \Delta h_1) - \sum_{i=2}^{N} h_i - \sum_{i=2}^{N} \Delta h = 0 \tag{48}$$

112. From Equation 48, it is possible to explicitly solve for the depth change in cell 1.

$$\Delta h_1 = - \frac{(N-1)}{N} h_1 + \frac{1}{N} \sum_{i=2}^{N} h_i + \frac{1}{2} (N-1) \Delta h \tag{49}$$

Depth changes in cells 2 to N are then given by

$$\Delta h_i = h_1 + \Delta h_1 - h_i - (i-1) \Delta h \tag{50}$$

113. The time interval in the numerical model typically varies between 5 and 20 min, whereas the length step is typically 1 to 5 m. The time interval and length step are not independent because they both govern the stability of the numerical solution scheme. Generally, a shorter length step requires a smaller time interval. An explicit criterion for the relation between time and length step for numerical stability could not be determined due to the nonlinearity of the equations and the smoothing of the transport rate. However, it was empirically found that use of the slope-dependent term in the transport equation in the broken wave zone (Equation 4) greatly improves stability of the solution. If this term is omitted, numerical oscillations may originate from the shoreward side of the bar as the profile slope steepens under constant waves and water level.

PART V: MODEL TESTS

114. Although the numerical model successfully reproduced beach profile change generated in large wave tanks, including bar formation, bar movement, and foreshore erosion, the ultimate test is to verify model performance for field beaches. This chapter reviews previous field simulations (Report 1) that concentrated on bar formation and movement and discusses recent field simulations where the objective was to test the model for reproducing foreshore erosion as well as accretion. In the field tests, documented storm erosion events from both the US east and west coasts were simulated. The chapter begins with a summary of sensitivity analyses performed to investigate predictions of bar features to changes in model parameters.

Sensitivity Analyses and Previous Model Tests

115. The objective of a sensitivity analysis is to establish the influence of model parameters on simulation results. Report 1 describes simulations performed to quantify the effect of variations in model parameters on the prediction. The investigation focused on bar properties such as volume, maximum height, and location of the center of mass. Parameters investigated were the transport rate coefficients K and ε, breaker decay model coefficients κ and Γ, and equilibrium energy dissipation D_{eq}. The influence of wave height, wave period, and runup height were also explored.

116. Grain size is a critical input parameter that determines the equilibrium energy dissipation and thus the amount of material that is moved by the waves in the course of reaching an equilibrium beach shape. Figure 7 displays the time evolution of bar volume for various grain sizes in a hypothetical erosional case. The equilibrium beach profile, defined as the profile shape for which no net transport occurs and bar growth ceases for a given wave condition, is approached more rapidly for coarser grain sizes. This is expected since less material has to be redistributed by waves for a larger value of D_{eq}. Grain size is one of the few model parameters that significantly affects the movement of the bar center of mass. Figure 7 is typical of the results from the sensitivity analysis, and similar curves are presented in Report 1 for all model parameters discussed here.

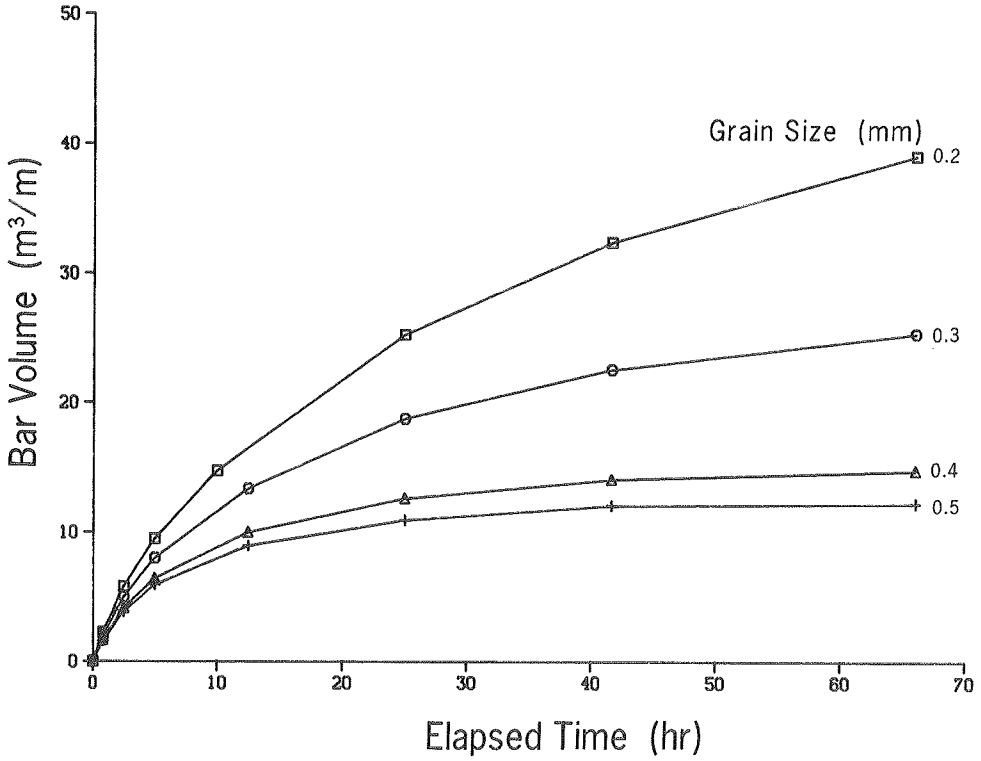

Figure 7. Evolution of bar volume for different grain sizes for hypothetical simulations

117. The transport rate coefficient K mainly governs the time response of the profile and has much less influence on bar volume and eroded foreshore sand volume. A large value of K implies rapid profile response with rapid attainment of equilibrium. The coefficient ε, controlling the strength of the slope-dependent term in Equation 4, does not greatly influence the time response, particularly at the initial phase of a simulation, and mainly contributes to reduce the depth of the trough landward of the bar. Bar volume, however, is affected by a change in ε, where a larger value implies a larger bar volume.

118. The empirical coefficients in the breaker decay model have a marked influence on profile evolution with regard to bar volume. A decrease in κ causes an increase in bar volume that may be physically explained by the resultant larger wave energy dissipation in the inner part of the surf zone. A smaller κ-value produces more gradual energy dissipation, allowing waves to retain more energy to be dissipated farther inshore. A large value of the stable wave height coefficient Γ implies a flatter equilibrium beach

profile, requiring more material to be moved before equilibrium is attained and thus more foreshore erosion.

119. The effect of changing wave height and wave period is obvious, where an increase in either quantity implies greater incident wave energy and more erosion. Runup height has little influence on bar development since about the same amount of sand is eroded along the profile independent of runup height. However, the shape of the foreshore can be substantially different depending on runup height. Smaller runup height causes erosion to occur over a narrower portion of the foreshore in comparison to larger runup; a more pronounced scarp develops with a smaller runup height.

120. In Report 1, the numerical model was used to simulate profile change measured at the FRF, located on a barrier island beach facing the Atlantic Ocean at Duck, NC. High-quality beach profile surveys from the dune to the depth of significant sand transport have been made at approximately 2-week intervals for more than 4 years. Four different shore-normal lines were monitored together with more frequent wave and water level measurements. Gage measurements of wave height and period were made at 6-hr intervals, and water level is recorded every 6 min but available at hourly intervals. A portion of the profile data set is given in Howd and Birkemeier (1987).

121. Five beach profile sets were chosen for supplying simulation data for model verification. Each set contained two profile surveys with a time history of waves and water levels between surveys. Erosion predominated for all five events, including significant offshore movement of one or two bars, but shoreline position showed little or no movement. Shoreline stability is characteristic at the FRF beach and may be caused in part by an abundance of coarse material on the foreshore. The data set from Duck was thus unsuitable for testing predictability of the numerical model regarding shoreline retreat and subaerial beach erosion, but the data were considered appropriate for evaluating bar movement.

122. Potential three-dimensionality of changes on a natural beach must be considered in simulating profile change. Even though simulation time periods were chosen such that neighboring profile surveys most nearly displayed similar development, some three-dimensional effects were present. The degree of three-dimensionality was quantified by applying the mass conservation equation to calculate the loss or gain of sand between consecutive

profiles. A survey line located southeast of the FRF pier was used in the simulation because it is beyond major influence of the pier, and the bottom contours are essentially straight and parallel (Howd and Birkemeier 1987).

123. Four of the five events were used for calibration, where the calibration criterion comprised minimizing the sum squares of the difference between measured and calculated profile change. The fifth event was used for model verification (Report 1). The energy-based significant wave height (H_{mo} from gage 620 located in 18 m of water) was used to calculate the transport rate distribution together with the peak period of the spectra. Since the measurement intervals of waves and water level were longer than the model time step, required intermediate values were obtained by cubic spline interpolation. A typical simulation time step was 20 min, and the length step was 5 m.

124. Essentially the same parameter values obtained from the large wave tank simulations were used, although some modifications had to be made for field simulations. The most important difference was that the transport coefficient K had to be decreased to obtain optimal agreement for field simulations. The optimal value of K for field simulations was about half the value for the large wave tank data. Two different median grain diameters were used to represent sediment characteristics of the FRF beach along transect 188 (Howd and Birkemeier 1987). A median grain size of 2.0 mm was used on the foreshore, and 0.15 mm was used for points seaward of the foreshore.

125. Figure 8a shows the measured wave height, wave period, and water level for the simulation period, developed as a spline fit through measured values at 1-hr intervals. Figure 8b illustrates one of the calibration runs for 3-6 April 1984 when a single bar was present that moved about 60 m offshore during a minor storm event. Measured initial and final profiles are given together with the final calculated profile. Bar location was rather well predicted, whereas bar volume was underestimated and the trough was not sufficiently pronounced. Also, some shoreline retreat was calculated in spite of the larger grain size on the foreshore.

126. Model verification gave reasonable agreement between measured and calculated profiles, although the selected event encompassed profiles exhibiting two bar features, which was not the case in the calibration events. As with the calibration cases, direction of bar movement and location were

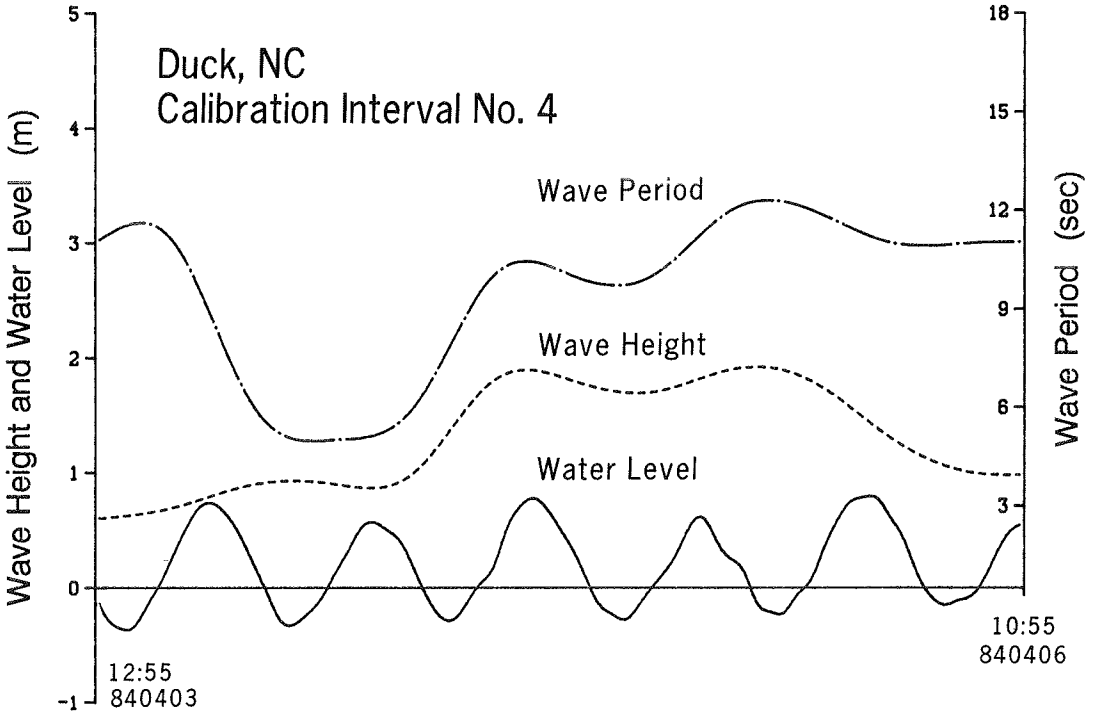

a. Input wave height, wave period, and water level

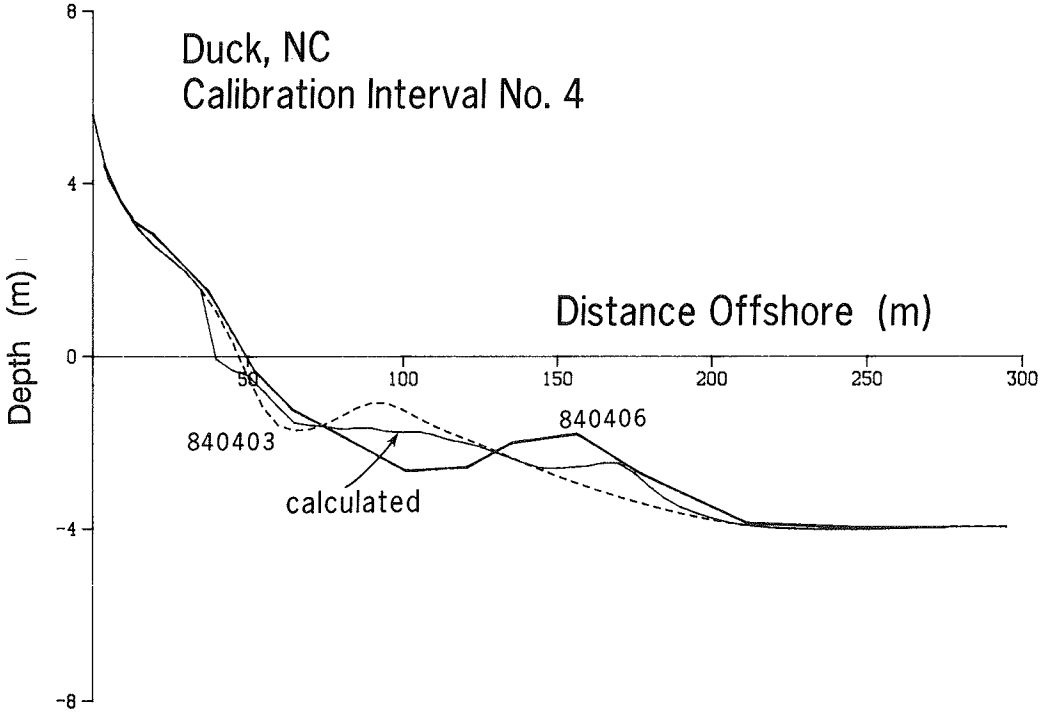

b. Beach profile change simulation result

Figure 8. Calibration of numerical model against field data from Duck, NC

correctly predicted, whereas the size of the bars was smaller than measured (Figure 9). Simulations performed subsequent to these early field tests indicate that a probable reason for the smaller calculated bar size is insufficient variability in the imposed wave input. Greater variability would tend to shift the break point back and forth to produce a wider bar. Some variability in wave and water level conditions is reproduced through use of a time series of different regular waves, but it is believed that introduction of random fluctuations around these values would give more realistic predictions. The absence of randomness in the wave description is probably one of the factors requiring use of a lower transport rate coefficient in field simulations as compared with large wave tank simulations. A random variation in wave height, for example, would reduce the tendency for a steady trend in profile evolution, thereby requiring a larger value of the transport rate coefficient K to achieve optimal agreement.

127. Summarizing experience from modeling beach profile evolution at Duck, prediction of the direction of bar movement and bar location was successful, although calculated bar size showed less agreement with observed profile development. Profile response was best reproduced using as much information as possible on wave height, wave period, and water level (as opposed to using average values for the simulation period), lending credibility to the predictive capabilities of the numerical model. The success of the model in predicting observed bar movement supports the hypothesis that breaking waves are the main agent for cross-shore sand movement, at least in the outer surf zone. The steep bar and foreshore slopes appearing in the large wave tank simulations were not encountered in field simulations because measured changing forcing conditions were used. Reproduction of milder bar features validates the concept of simulating profile change by random waves through a summation of transport events produced by different regular waves acting over short time intervals.

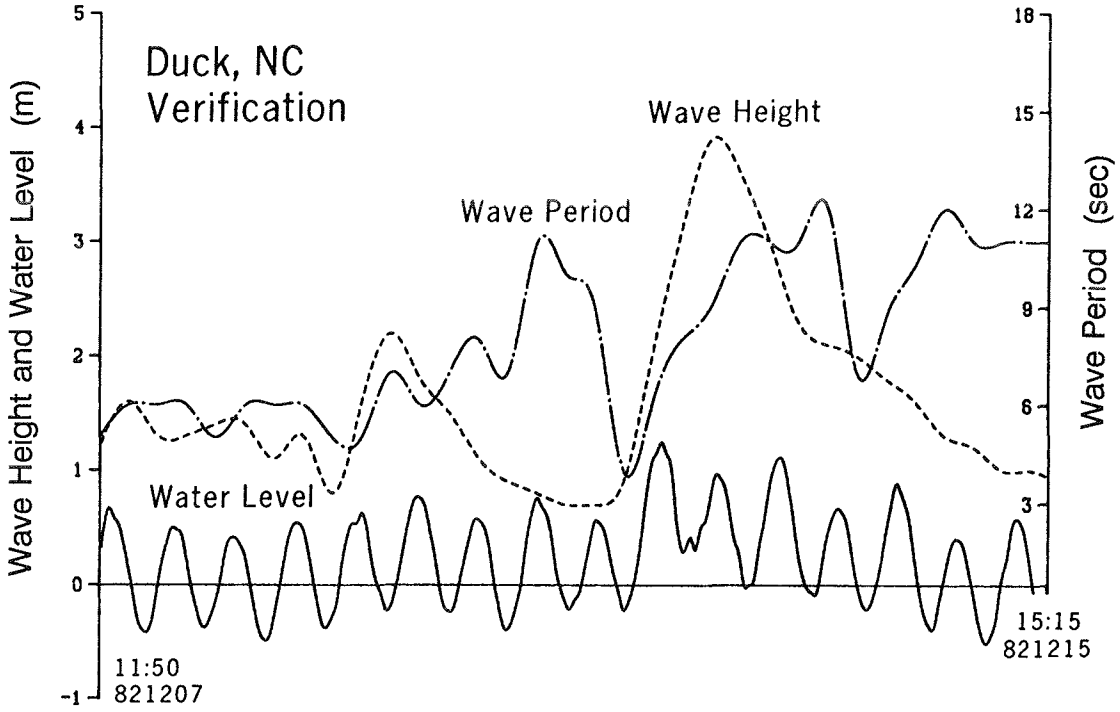

a. Variation of wave height, wave period, and water level

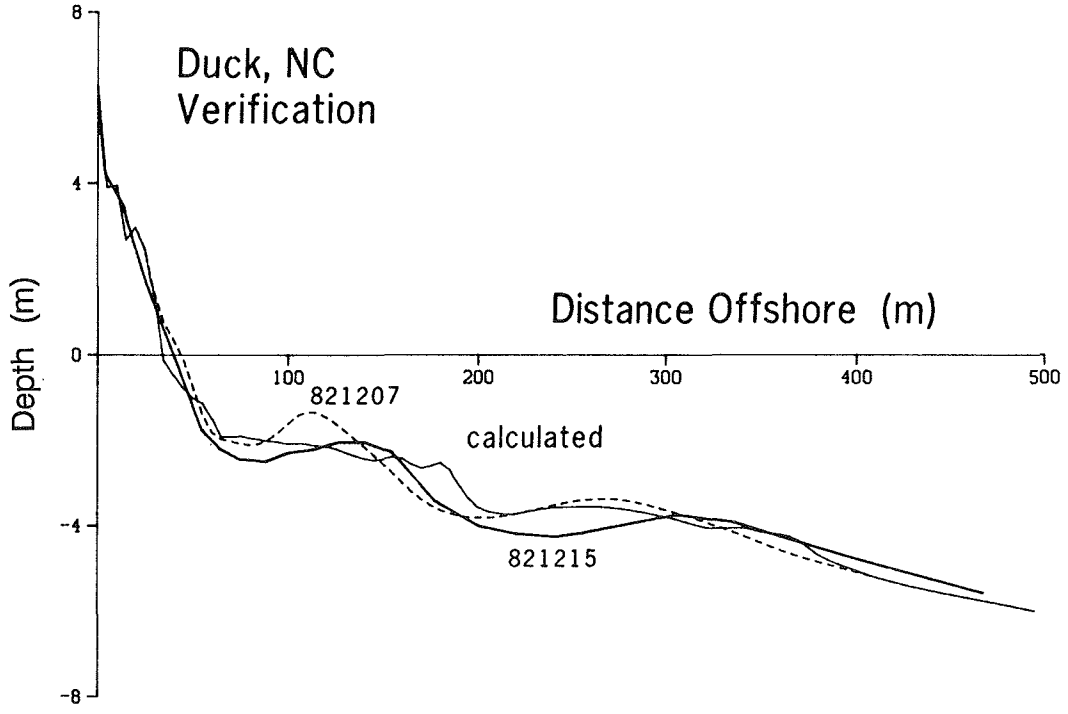

b. Beach profile change simulation result

Figure 9. Verification of numerical model against field data from Duck, NC

Storm Event on the US East Coast

128. Several profile lines, located north and south of Manasquan Inlet, NJ, were surveyed by the US Army Engineer District (USAED), Philadelphia, over a period that encompassed the 27 to 29 March 1984 northeaster (Gebert, Watson, and Hemsley, in preparation). The data set includes profile surveys of the subaerial beach taken 1 to 2 days prior to arrival of the storm and 3 to 4 days after the storm. Prestorm subaqueous profile data used for simulations were collected in early January 1984 and poststorm nearshore surveys were made approximately 2 weeks after the event. A time series of wave height and period was recorded by a wave rider buoy located directly offshore in 15.2-m water depth, and water level at Manasquan Inlet was also available.

129. Profile measurements were made along eight beach transects at Manasquan to the north of the Manasquan Inlet jetties and along nine transects at Point Pleasant Beach to the south of the jetties (Figure 10). Point Pleasant Beach is relatively wide and sandy with no coastal structures in the surf zone south of the 678-m-long south jetty at Manasquan Inlet, whereas Manasquan has a narrow sandy beach with short groins located at approximately 200- to 300-m intervals.

130. Regular profile surveys were carried out at Manasquan and Point Pleasant Beach from 1982 to 1984 under the auspices of the CE Monitoring Completed Coastal Projects (MCCP) Program. The main purpose of the project was to monitor the structural stability of the jetties after rehabilitation with 16-ton dolosse armor units. Two secondary concerns dealt with maintenance of inlet cross-sectional area and potential change on adjacent beaches caused by the jetties (Gebert, Watson, and Hemsley, in preparation). Figure 10 gives the locations of the survey lines and the numbering convention. The lines are numbered consecutively from 1 starting at the jetties and increasing north and south, where the symbols M and PP are used to denote Manasquan and Point Pleasant Beach, respectively. A tide gage, operated by the National Oceanographic Service (NOS), is located on the bay side of Manasquan Inlet. At the time, a wave rider buoy was operated by MCCP and located in 15.2 m of water seaward of Manasquan. Wave conditions generally were measured every 6 hr for a 20-min period, and the sampling interval was automatically decreased to 1 or 2 hr when the wave height exceeded 3 m.

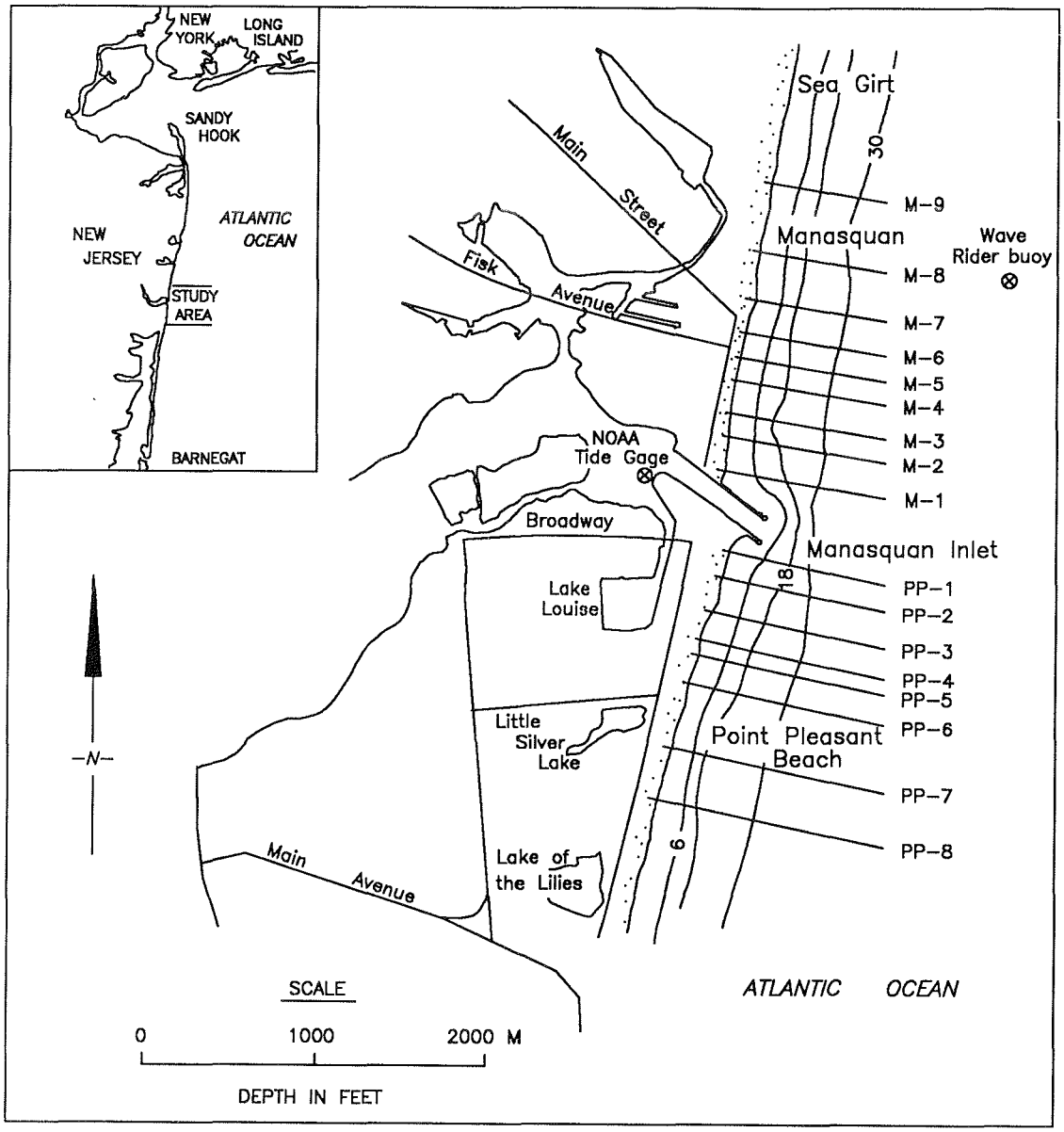

Figure 10. Location map showing profile survey lines and the tide gage and wave rider buoy positions at the Manasquan and Point Pleasant Beach study area

131. Toward the end of March 1984, a northeaster passed the area causing severe erosion of the beaches. The time-history of measured significant wave height and peak spectral wave period for the storm is displayed in Figure 11, and water level is shown in Figure 12. Water surface elevation is given with respect to mean sea level (MSL) and comprises both storm surge and tidal variations. Wave height began to increase in the morning on 28 March

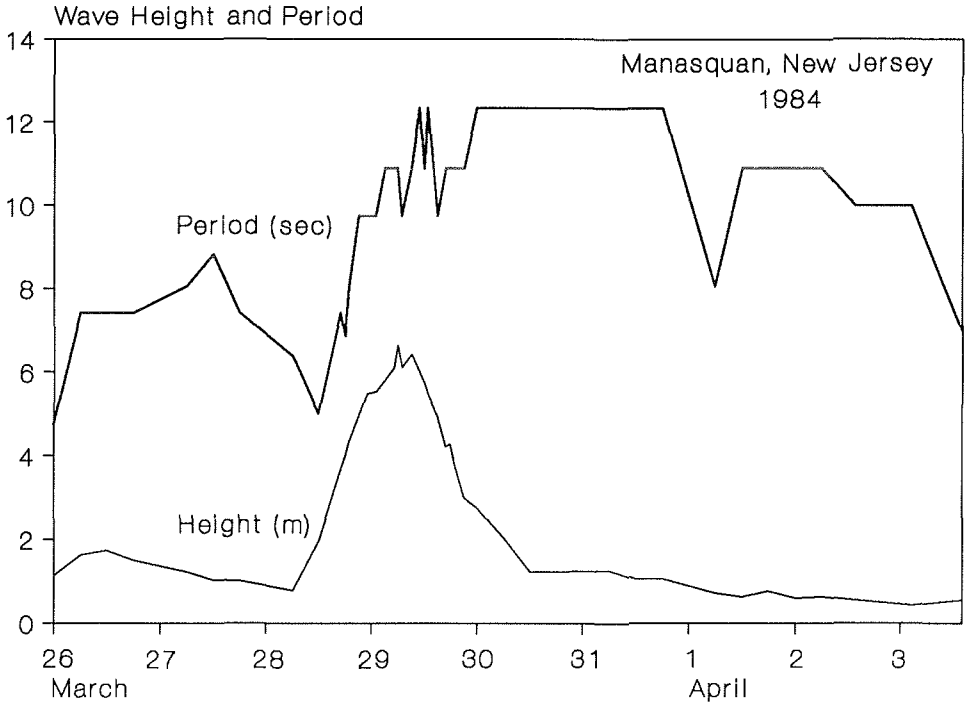

Figure 11. Wave height and period measured northeast of Manasquan Inlet

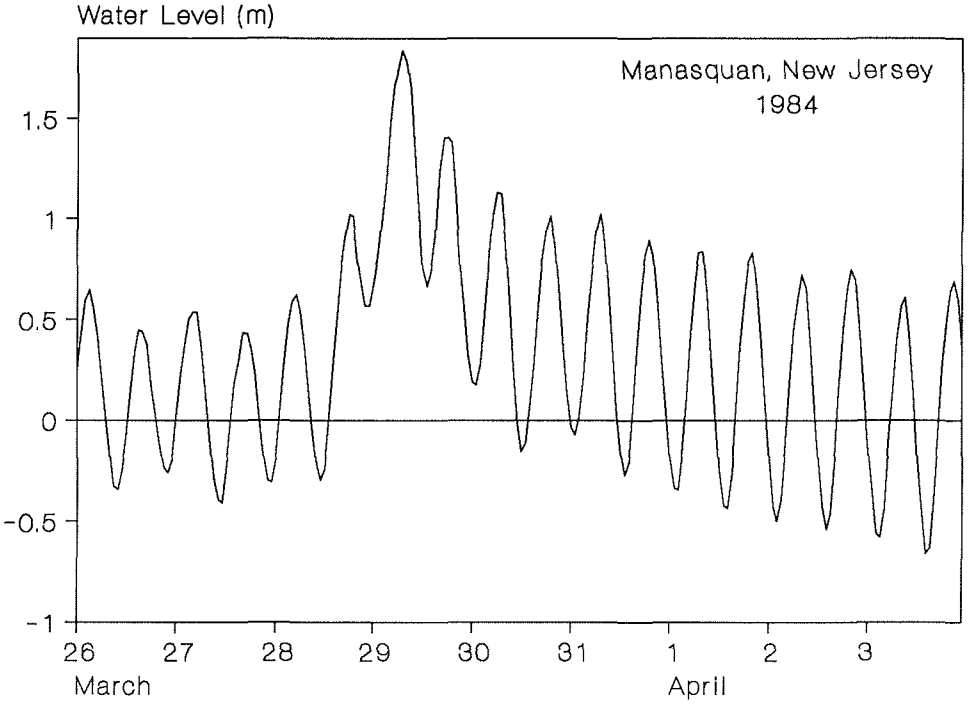

Figure 12. Water level measured on the landward side of Manasquan Inlet

and peaked about 24 hr later on 29 March with a maximum height of 6.6 m. By noon on 30 March, the storm had passed, and more typical wave heights were recorded. Wave period increased sharply with arrival of the storm, similar to the behavior of wave height, but long periods persisted after the storm, creating mild-steepness waves and strongly accretionary conditions.

132. The water level record displayed a pronounced peak for the middle of the storm, approximately coinciding with the maximum wave height. The tidal variation at Manasquan Inlet is semidiurnal, with two high and two low waters in a tidal day, and the mean tidal range is 1.2 m. Maximum surface elevation measured during the storm event was 1.90 m at about 0600 on 29 March.

Profile measurements

133. Prestorm beach profile surveys were taken on 26 and 27 March for Manasquan and Point Pleasant Beach, respectively. However, when the storm arrived, the scheduled Fathometer surveys had to be halted due to high waves, and only wading depth profiles were obtained for these dates. Subaqueous profile measurements obtained from the previous profile survey (28 December 1983 at Manasquan and 29 December 1983 at Point Pleasant Beach) were used to construct complete prestorm profiles. Poststorm profiles were recorded on 3 April at Manasquan and 2 April at Point Pleasant Beach. Profile survey elevations were made with respect to the National Geodetic Vertical Datum (NGVD), and were converted to MSL in this report by the relationship MSL(m) = NGVD(m) + 0.24 m.

134. Profile survey data were analyzed to yield representative profiles to be used in numerical simulations. Also, longshore variability in eroded volume was investigated to evaluate the applicability of a two-dimensional approach. Since the shoreline was curved close to the jetties, especially at Point Pleasant Beach, profiles at the respective beaches were shifted across-shore and aligned with reference to MSL. A single representative profile for each beach was determined by averaging profile elevations at fixed intervals.

135. Figure 13 shows plots of the eight prestorm profiles measured at Point Pleasant Beach. The shapes of the profiles are surprisingly similar, indicating relatively good two-dimensionality. However, the two profiles located closest to the jetty (PP-1 and PP-2) show depths that are significantly less than those associated with the other profiles. This shallower subaqueous portion of the profile is probably a result of impoundment of sand

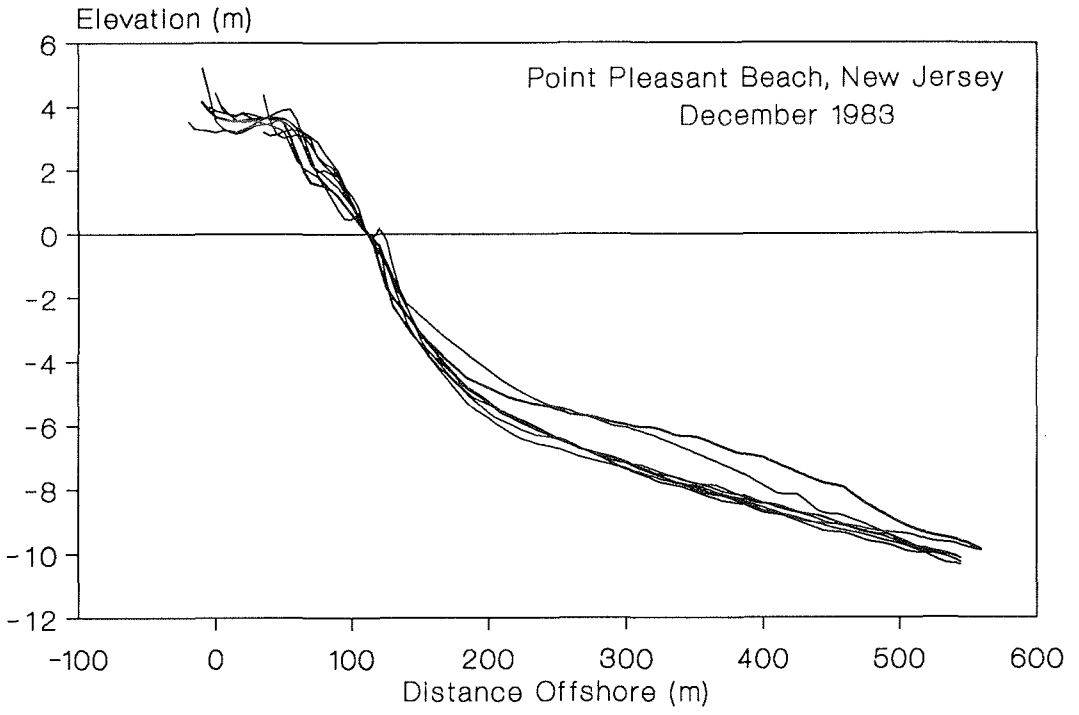

Figure 13. Profiles measured at Point Pleasant Beach during December 1983 aligned with respect to MSL

transported alongshore. The two profiles closest to the jetty were therefore excluded when determining the generic profile for simulation. These two profiles also exhibited markedly less erosion during the storm as compared with the other profiles.

136. In a manner similar to the analysis for Point Pleasant Beach, two profiles were removed from the analysis at Manasquan; seven profiles were used for determining a generic profile for the simulation. The transect closest to the jetty (M-1) was not used along with the profile farthest to the north (M-9). Their exclusion was motivated by the significantly different response of the two profiles to the storm, for which substantial accumulation took place at their seaward ends. This is attributed to longshore effects and the influence of structures.

137. A generic prestorm profile was created using the average profile from the immediate prestorm subaerial surveys matched with an average

subaqueous profile developed from December 1983 survey data. In the same manner, a poststorm profile was developed based on the surveys of 2 and 3 April 1984.

138. Representative prestorm and poststorm profiles determined for Manasquan and Point Pleasant Beach (Figures 14 and 15) differ in two characteristics. First, the dune is higher and narrower at Manasquan as compared with Point Pleasant Beach. Second, a wide subaqueous bar exists in the profile at Manasquan, extending approximately 300 m seaward of the baseline, out to the end of the groins. It appears as if the groin field is effective in trapping sand on the nearshore portion of the profile.

Beach grain size

139. Grain size is a principal parameter in the numerical model and can be difficult to quantify for use in SBEACH since a wide range of grain sizes is normally present on a natural beach. In the study area, investigations have been made on the temporal and spatial distribution of grain size (USAED, New York 1954; Gorman, Stauble, and Reed, in preparation). However, because of inconvenient sample location and lack of measurements in the dune region, available grain size information was supplemented with sampling from the subaerial portion of the beach for specific use for modeling with SBEACH.

140. The additional sediment sampling, performed by Mr. Jeffrey Gebert, USAED, Philadelphia, in April 1989, showed a uniform median grain size of approximately 0.5 mm in the dune region. Median grain size varied more on other portions of the subaerial profile with coarser material typically present at the berm crest. Sand samples were taken at four cross-shore locations on the dry portion of the beach and at four alongshore sites. Table 1 gives a summary of median grain size data available for the Manasquan and Point Pleasant Beach study sites.

141. Two sampling sites south of the jetties and one to the north were used in defining median grain size in the dune region, together with data from previous investigations. Samples collected adjacent to the jetties were excluded from the analysis by reasoning similar to that used in determining a representative profile. An average median grain size for the dune region was determined to be 0.49 mm for Manasquan and 0.54 mm for Point Pleasant Beach. On the foreshore, coarser material was found near the berm crest with median grain sizes around 0.3 to 1.5 mm. For the subaqueous portion of the profile,

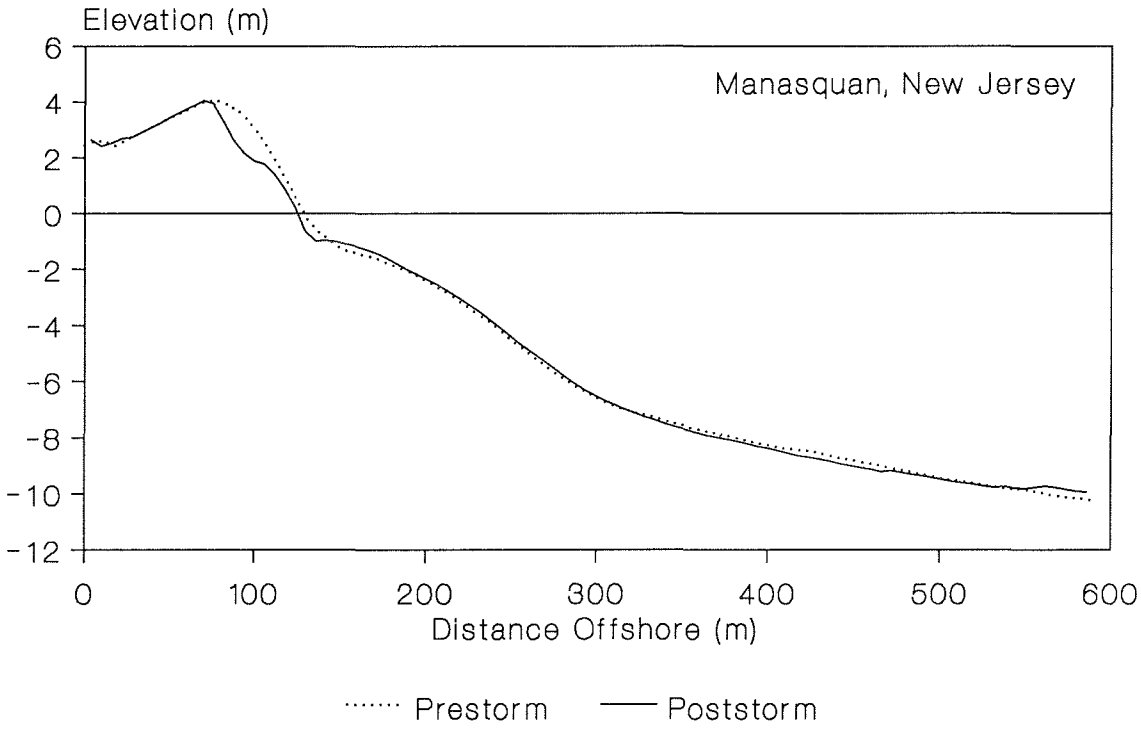

Figure 14. Generic prestorm and poststorm profile for Manasquan

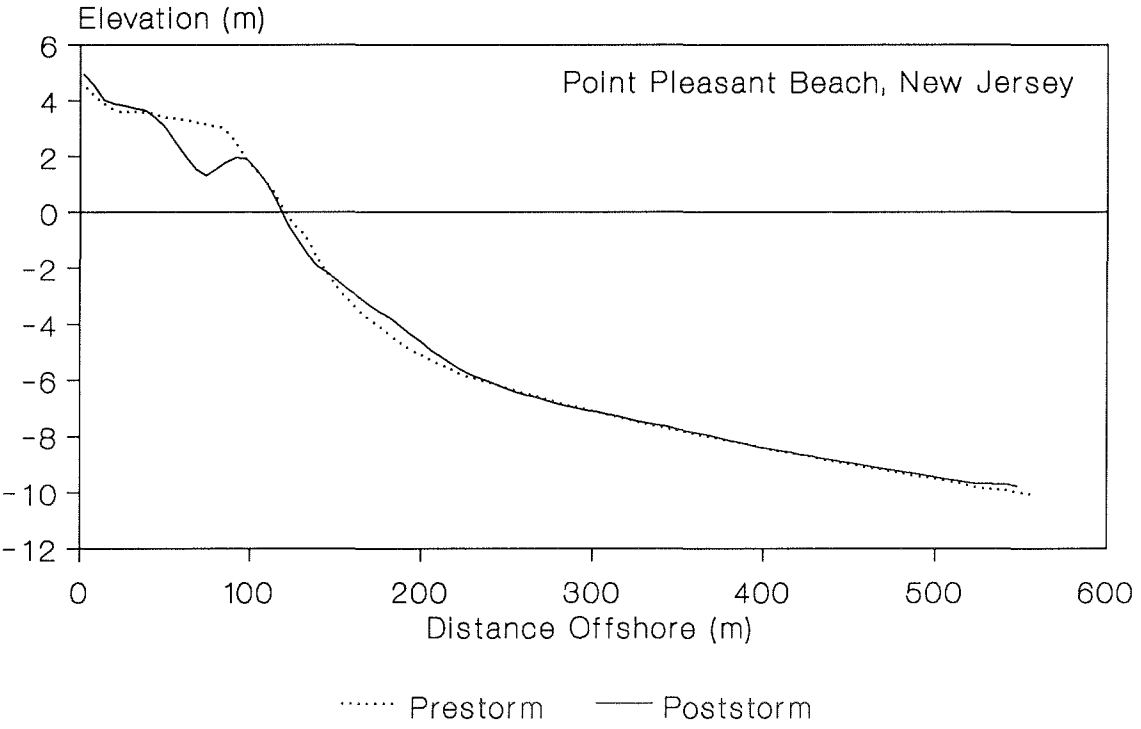

Figure 15. Generic prestorm and poststorm profile for Point Pleasant Beach

Table 1

Median Grain Size (mm) for Manasquan and Point Pleasant Beach

Profile	Landward Limit of Dune	Dune Crest	Berm Crest	Mid-Tide	Nearshore*
		Manasquan			
M-1**	--	--	0.38	0.43	0.20
M-2++	--	0.47	0.56	0.86	--
M-9**	--	--	0.44	0.38	0.16
M-9+	--	0.51	0.60	1.31	0.21
		Point Pleasant Beach			
PP-1**	--	--	0.28	0.34	0.21
PP-1+	--	0.53	--	0.36	0.29
PP-1++	0.54	0.55	1.51	0.51	--
PP-3++	0.47	0.53	1.13	0.82	--
PP-6++	0.48	--	1.05	0.68	--
PP-8**	--	--	0.53	0.64	0.19
PP-8+	--	0.66	0.41	0.47	0.18

* Average D_{50} on subaqueous profile.
** June 1953.
+ May 1987.
++ April 1989.

median grain diameter from previously collected sand samples showed an overall trend of decreasing grain size with distance offshore. The average median grain size for all subaqueous samples showed D_{50} = 0.19 mm for Manasquan and D_{50} = 0.22 mm for Point Pleasant Beach.

142. An indirect method of obtaining a representative grain size for the subaqueous portion of the profile is to approximate the beach profile with the equation proposed by Dean (1977) and solve for the shape parameter A . From the shape parameter, it is possible to determine the corresponding grain size based on curves presented by Moore (1982) and Dean (1987, 1990). This equation ($h = Ax^{2/3}$) was least-square fitted to the prestorm profile from the January surveys to indirectly determine a representative grain size for the

January surveys to indirectly determine a representative grain size for the subaqueous portion of the profile. In this equation, the shape parameter A is an empirical function of grain size. The effective median grain diameter calculated for profiles M-2 to M-8 was 0.47 mm, and for profiles PP-3 to PP-8 the effective grain size was 0.51 mm. In the least-square fit, both the shape parameter and the horizontal location of the still-water shoreline were estimated to minimize the sum of squares between measured profiles and the profile equation.

143. The profile equation could in general explain a large portion of the variation in the measurements, but visual inspection showed some deficiencies in the description. To illustrate this point, Figure 16 shows the representative prestorm profile at Point Pleasant Beach and the least-square fitted profile. For an average median grain size of 0.5 mm, the fitted profile gives an overall reasonable description relative to the representative profile. Directly seaward of the shoreline, however, the representative profile is steeper than the fitted profile, whereas the opposite occurs in the offshore region. The actual profile shape is probably sensitive to varying median grain size, resulting in a shape that locally deviates from a fit involving a 2/3 power for a single grain size.

Alongshore variability in storm erosion

144. The numerical model simulates cross-shore sand transport only; longshore effects are not represented. In order to evaluate this approximation for the target storm event, the amount of erosion was determined for each profile survey. Equal amounts of erosion would suggest that the forcing conditions were similar during the storm event and differentials in longshore transport were small. It is important to note that significant recovery occurred before the poststorm profile was surveyed. Figure 17 illustrates the recorded volume difference above the 1-m contour between the prestorm and poststorm profile. Profile location is referenced to the profile closest to the jetties, going north and south at Manasquan and Point Pleasant Beach, respectively. Table 2 lists measured volumes of erosion above the 1 and 0 (MSL shoreline) contours.

145. Significantly less erosion is indicated for the two profile lines closest to the jetties at Point Pleasant Beach. South of profile line PP-2, the eroded volume is fairly constant (50 to 65 m^3/m) except for line PP-6.

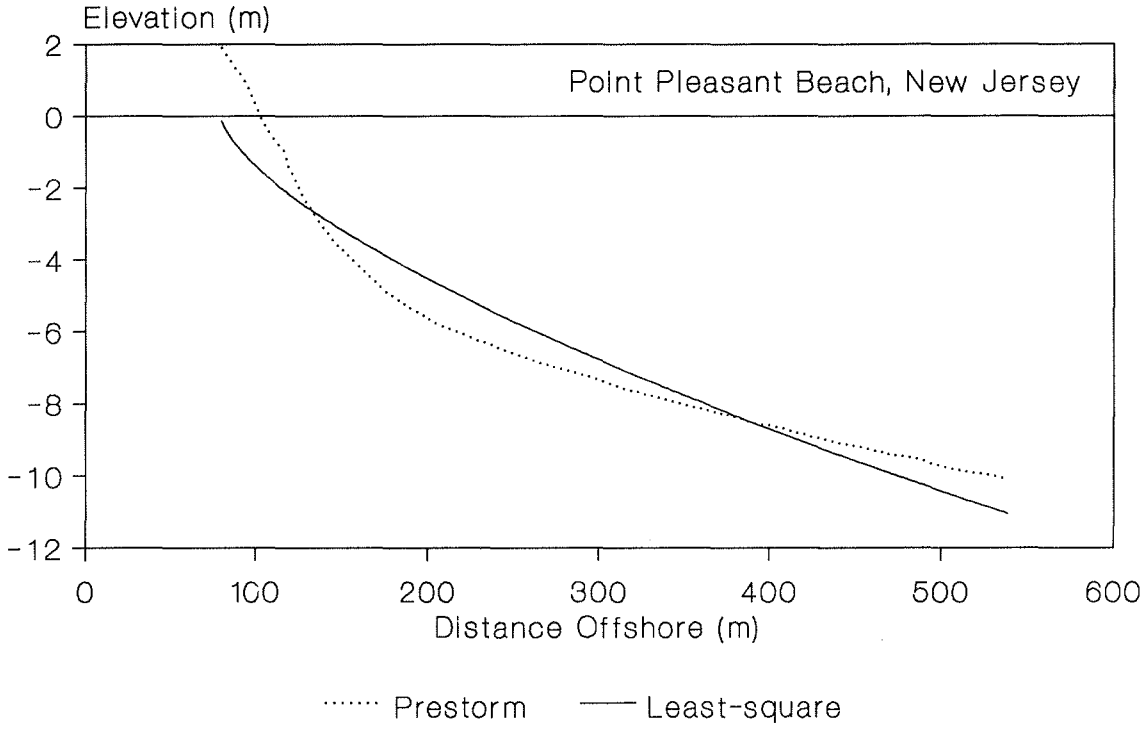

Figure 16. Generic prestorm profile at Point Pleasant Beach and least-square fitted equilibrium profile

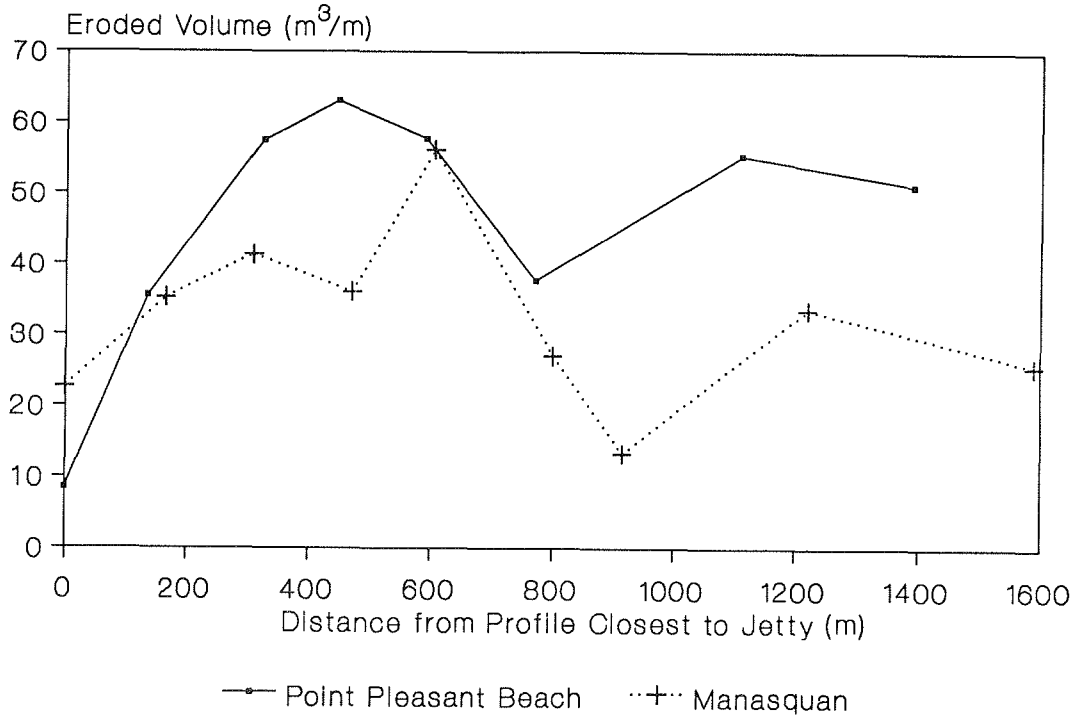

Figure 17. Volume difference above the 1-m contour between prestorm and poststorm profiles at Manasquan and Point Pleasant Beach

Table 2

Eroded Profile Volumes at Manasquan and Point Pleasant Beach for the March 1984 Storm Event (m^3/m)

Contour	Group Average	Average of Selected Profiles	Minimum	Maximum
		Manasquan		
0	36.3	39.3	14.7	62.6
1-m	32.4	34.7	13.4	56.2
		Point Pleasant Beach		
0	48.9	55.8	9.6	66.0
1-m	45.8	53.8	8.5	56.2

Examination of the poststorm profile survey at line PP-6 shows considerable deposition on top of the dune. As previously noted, the eroded volume calculation interval includes a period of recovery or accretion that contaminates the data set with respect to storm-induced erosion modeling. The average volume eroded above the 1-m contour for all profile lines at Point Pleasant Beach is 45.8 m^3/m, and for profiles PP-3 to PP-8 the average eroded volume is 53.8 m^3/m. To gage the intensity of storm activity and resultant magnitude of beach profile change, data from this event were compared with similar parameters from 13 other east coast storms (Birkemeier, Savage, and Leffler 1988). Comparison of peak wave and water level conditions, and associated changes in beach profile volume, with data from the 27 to 29 March 1984 event at Manasquan and Point Pleasant Beach indicates that dynamic characteristics associated with this storm and resultant volume changes were more extreme than any of the 13 previously recorded events. Analysis of extreme wave statistics for this area suggests that this major storm event has a frequency of occurrence of about 30 years (Jensen 1983, Corson and Tracy 1985).

146. The profiles at Manasquan experienced less erosion than those at Point Pleasant, with an average eroded volume for all profile lines of 32.4 m^3/m. Survey line M-1 closest to the jetty experienced somewhat less erosion than all but one of the other profiles. The average volume eroded above the 1-m contour for profiles M-2 to M-8 was 34.7 m^3/m.

147. Variability in volume of erosion is greater for Manasquan than for Point Pleasant if the profile lines closest to the jetty are neglected (Figure 17). This is probably due to localized processes associated with the groin field, giving rise to longshore variability in sand transport. The lower average eroded volume for Manasquan is also partially attributed to the groins, which evidently caused a large subaqueous bar to develop. This feature increases energy dissipation on the seaward portion of the profile and reduces wave energy reaching the dune face. Expressed differently, the bar is a sand reservoir that must first be depleted by erosive waves before they can fully attack the subaerial beach.

148. In summary, it appears that longshore variability in eroded volume was relatively small for Point Pleasant Beach because structures were not present to create differentials in longshore transport. At Manasquan, larger volume differences are noted due to the presence of structures and the location of profile lines with respect to the groins. Applying the numerical model to a representative generic profile should be acceptable both at Manasquan and Point Pleasant Beach in terms of longshore variability in eroded volume. However, if only one profile survey were available for modeling, significant variability or deviation in calculated and measured results could be expected.

Numerical simulations

149. Average representative profiles were used in the numerical simulations. Since median grain diameter did not differ significantly between the two sites, the same value was specified. A schematized description of cross-shore variation in grain size was specified based on sampling results, with a diameter of 0.5 mm shoreward of the MSL shoreline and 0.3 mm seaward of the MSL shoreline. Model parameters were initially set at the same values as for the large wave tank studies, but some modifications were made in the calibration process.

150. Simulation periods for the two beaches corresponded with different survey times at the respective sites. The exact time of day of the surveys was not known and was assumed to be 1200. For Manasquan the simulation interval was 26 March to 3 April, and for Point Pleasant Beach it was 27 March to 2 April. Wave and water level conditions for the calculation periods are given in Figures 11 and 12, for which cubic spline interpolation was used to

obtain intermediate values between measurement points. The model time step was 5 min, and the length step was 2 m.

151. Simulation results are shown in Figure 18 for Manasquan and in Figure 19 for Point Pleasant Beach. The initial and poststorm representative profiles are plotted with the calculated profiles. Calculated erosion was defined as the time at which the model switched from calculating erosion to accretion by Equation 1, and recovery was defined as the time at which the poststorm survey was taken. Since poststorm profile measurements were made after several days of recovery waves, the final measured profile includes a period of potentially significant beach recovery. In particular, at Point Pleasant the recovery was very strong with a wide gentle ridge evolving with a crest 2 m above the MSL shoreline. Beach recovery at Manasquan was considerable but not as pronounced as at Point Pleasant Beach, probably due in part to a steeper dune face and a narrower foreshore, conditions that tend to retard the recovery process.

152. Manasquan. Simulated profile retreat at the top of the dune is close to the measured retreat for Manasquan, and the dune slope is reproduced well. Also, the poststorm eroded volume is considered to be in good agreement with what probably occurred as inferred from the profile taken on 3 April by extrapolating the slope of the dune face to MSL and neglecting the accretionary berm feature. Model simulation of recovery is limited to qualitative and not quantitative agreement with the measurements, showing berm buildup but with a smaller volume. Another aspect of profile development that differs between calculated and measured is the evolution of the bar located near the seaward terminus of the groins. The numerical model predicts that the upper part of the terrace is transported farther offshore, whereas measurements indicated that this feature was stable during the event. This shortcoming of the model may be partially attributed to neglect of longshore processes.

153. Point Pleasant Beach. The model simulation for Point Pleasant Beach shows much the same characteristics as for Manasquan, although predicted dune retreat was smaller as compared with measured retreat. Poststorm eroded volume is again considered to be in good agreement with the actual amount through examination of the 2 April profile and disregarding the large ridge assumed to have been formed during the recovery phase. Simulated recovery is stronger at Point Pleasant compared with Manasquan, which is qualitatively in

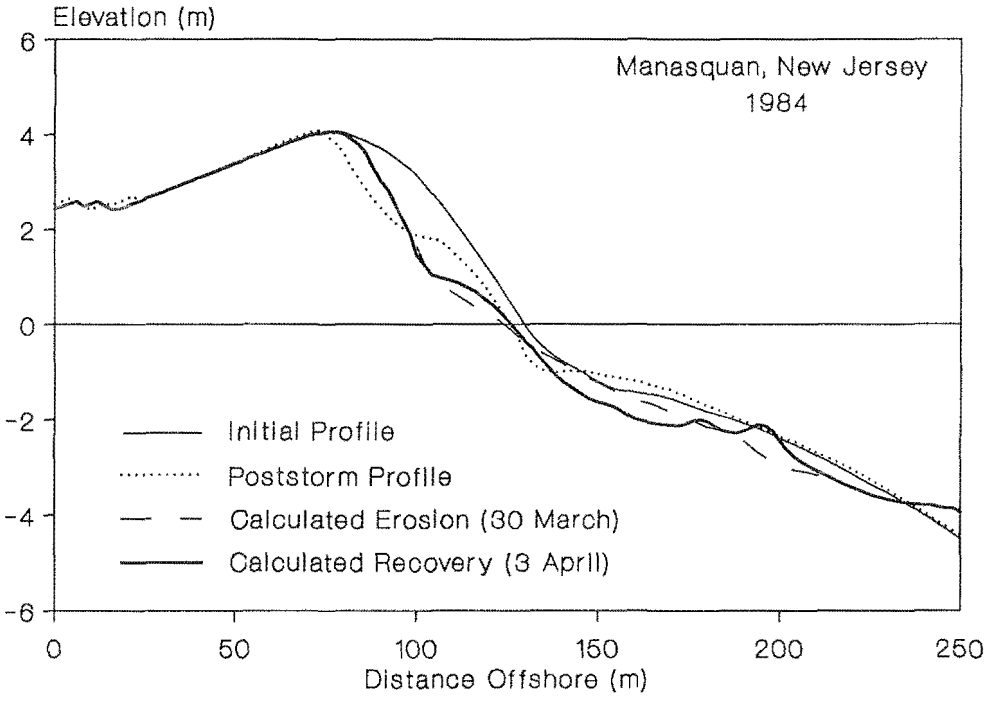

Figure 18. Measured and calculated profile change at Manasquan

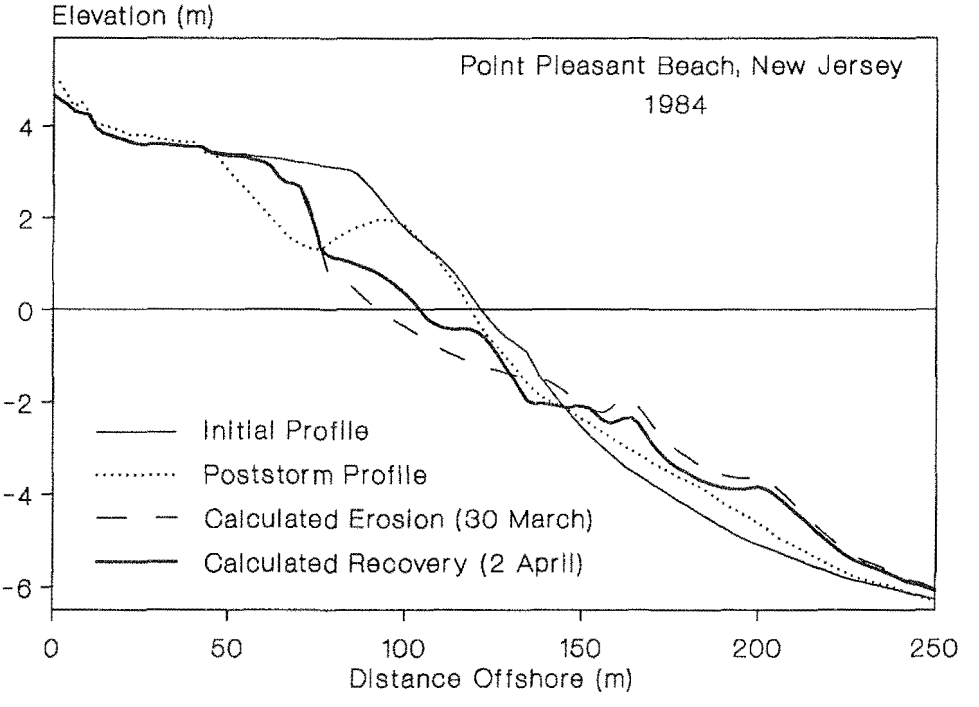

Figure 19. Measured and calculated profile change at Point Pleasant Beach

accordance with observations, although the predicted berm volume is smaller. The numerical model also indicates development of bar-like features in the seaward portion of the profile that were not present in the measured profile.

Discussion

154. In the simulations for both beaches, the transport rate coefficient K was changed to obtain optimal agreement between model results and the measured profile. The coefficient value determined for both sites was $K = 2.0 \times 10^{-6}$ m^4/N , compared with the value from the large wave tank simulations of $K = 1.6 \times 10^{-6}$ m^4/N and from the Duck, NC, simulations of $K = 0.7 \times 10^{-6}$ m^4/N . The Manasquan and Point Pleasant Beach profile change simulations used an optimal K-value similar to the large wave tank simulation, whereas the coefficient for the Duck data was considerably lower, probably due to the unusual stability of the shoreline at Duck that hindered erosion.

155. To better account for naturally variable wave conditions, wave heights used in model simulations were randomly varied a certain percentage around the values interpolated from the measured wave heights. This technique simulates variability in the location of the break point and development of profile features. The method for randomly varying wave height consisted of choosing a height from a rectangular distribution with its center as the interpolated height and its width as a predefined percentage of the interpolated height. Different distribution widths were tested, and 10 to 20 percent proved to give a good qualitative description of profile evolution. For the calibration runs displayed in Figures 17 and 18, a 20-percent variation was employed. Although this technique was not performed in simulations for the case at Duck, a larger K-value and smoother, more realistic profile features would be expected.

156. In order to obtain a qualitatively improved description of the accretion process, adjustments to the transport rate distribution were made. For the large wave tank data simulations, the transport rate distribution was calculated the same way, independent of whether onshore or offshore transport occurred. However, for a natural beach with a variable wave climate, unusual conditions arise that must be dealt with in a special way. For example, some accretionary-type waves are small enough that breaking will not occur until they arrive almost at the shoreline. The transport rate distribution in this case is very narrow and peaked, producing large accretion in the cells around

the shoreline. This local accumulation steepens the lower foreshore slope, making more waves break at the shoreline. To take care of this condition, if at any time-step the surf zone was calculated to be less than four cells wide, the transport rate was specified as linearly decreasing from the plunge point to the runup limit. The transport rate at the plunge point was determined from the wave energy dissipation according to Equation 4, as usual.

157. If onshore transport is high, berm buildup is rapid, and the foreshore beach slope may become unrealistically steep, limited only by the angle of initial yield. Such slopes predicted by the numerical model are in contradiction with observations from the large wave tank data (Takeda and Sunamura 1983, Larson and Kraus 1989a) and much steeper than what is found on a natural beach (Bascom 1951, Wiegel 1964, Thomas and Baba 1986, Hughes and Cowell 1987). To limit steepening of the foreshore, the cross-shore sand transport rate was reduced with respect to the local slope when transport was directed onshore. This introduced a second dependence on beach slope because Equation 4 already contains a term dependent on dh/dx, but was necessary to achieve a smoother, more realistic approach to equilibrium.

158. Eroded volumes for the predicted poststorm profile and profile after recovery were calculated above the 0 and 1-m contour and are displayed in Table 3. These values can be compared with eroded volumes based on measured profile evolution listed in Table 2. As previously discussed, eroded

Table 3

Calculated Eroded Profile Volumes at Manasquan and Point Pleasant Beach (m^3/m)

Contour	Maximum Erosion	With Recovery
	Manasquan	
0	51.5	44.2
1-m	37.2	37.2
	Point Pleasant Beach	
0	86.4	73.9
1-m	54.6	54.2

volume determined from the measured profiles includes a period of recovery as the immediate poststorm profile was not surveyed. Since model prediction of recovery was only in qualitative agreement with measurements, calculated eroded volumes at the end of the simulation period were too large in comparison with measured changes. Calculated eroded volume at Manasquan agrees well with measurements, although the shape of the profile differs, with the measured profile exhibiting less foreshore erosion and greater dune retreat. Poststorm erosion is probably well predicted at Point Pleasant Beach, but berm buildup is underestimated. Little or no recovery is produced by the numerical model above the 1-m contour, which differs from what occurred in the field.

159. In conclusion, the numerical model was successful in reproducing the erosional portion of the studied storm event, but predicted profile evolution during the recovery stage was only in qualitative agreement with measurements. Parameter values obtained for model calibration were similar to those found for simulations of the large wave tank data, particularly the transport rate coefficient K. A two-dimensional approach to estimate profile evolution during a storm event was justified based on the small measured alongshore variability in eroded volume. However, if nearshore structures such as groins exist in a study area, care should be taken in choosing a representative profile, and, if possible, averages of several profiles should be used.

Storm Event on the US West Coast

160. A mission-support project performed by CERC for the Coast of California Storm and Tidal Waves Study conducted by USAED, Los Angeles, provided an opportunity to apply SBEACH to storm-erosion events on the southern coast of California (Kadib, Fine, and Ryan 1989). This application involved considerably different environmental conditions than east coast field tests of the model. West coast conditions of note include small storm surge, typically less than 0.3 m, longer period waves than on the east coast, and broad, low-relief bars if bars are present.

161. Documentation of storm-induced beach erosion suitable for model testing and calibration is relatively scarce for the west coast, and no publications relating to numerical modeling of dune erosion were found in a literature review. As of late 1988, after a search of the literature and

inquiry to leading coastal investigators, only the data collected by Aubrey (1978) were considered to be adequate. The measurements of interest were made at Torrey Pines Beach, California, located approximately 2 miles north of Scripps Institution of Oceanography (Aubrey, Inman, and Nordstrom 1976; Aubrey 1978; Gable 1979), between December 1975 and January 1977.

162. Figure 20 shows the locations of three range lines along Torrey Pines Beach referred to as North Range, Indian Canyon Range, and South Range. Onshore and offshore portions of the profiles were measured periodically between 1972 and 1978, together with the associated wave climate and water level. All elevations were measured relative to NGVD; MSL is 4.3 cm above NGVD in this region. Time series of wave height, wave period, and water level for the periods 29 December 1975 to 9 January 1976 and 21 December 1976 to 4 January 1977 were available for defining short-term beach profile change produced by storms. Wave measurements were made along Indian Canyon Range with an array of pressure sensors located at a depth of approximately 9.1 m (Figure 20). Examination of the Torrey Pines data shows these events to be less significant than most storms producing notable beach change in southern California. However, this information provides the only comprehensive data base on storm conditions and associated beach profile response for the region that could be found during this study.

163. Beach profile data were collected three times during the first storm event (12/29/75, 12/31/75, and 1/9/76) and twice during the second event (12/21/76 and 1/4/77). All surveys were carried out near the time of predicted low water. The offshore bathymetry indicated very little longshore variation, implying only minor differences in wave properties at the three range lines. Therefore, an average profile shape was constructed for each date by matching the zero crossings (referenced to NGVD) for each of the three profiles and averaging the elevations at known positions relative to $z = 0$. Use of an average profile should reduce changes associated with longshore variability caused by local differences in nearshore bottom topography, sediment size, and waves (Savage and Birkemeier 1987, Birkemeier et al. 1988). These composite data were used for simulating beach profile response to both storm events. The recorded time series of waves and water level between surveys were input to the beach profile change model SBEACH, and data quality checks were made on all process and response measurements before model runs proceeded.

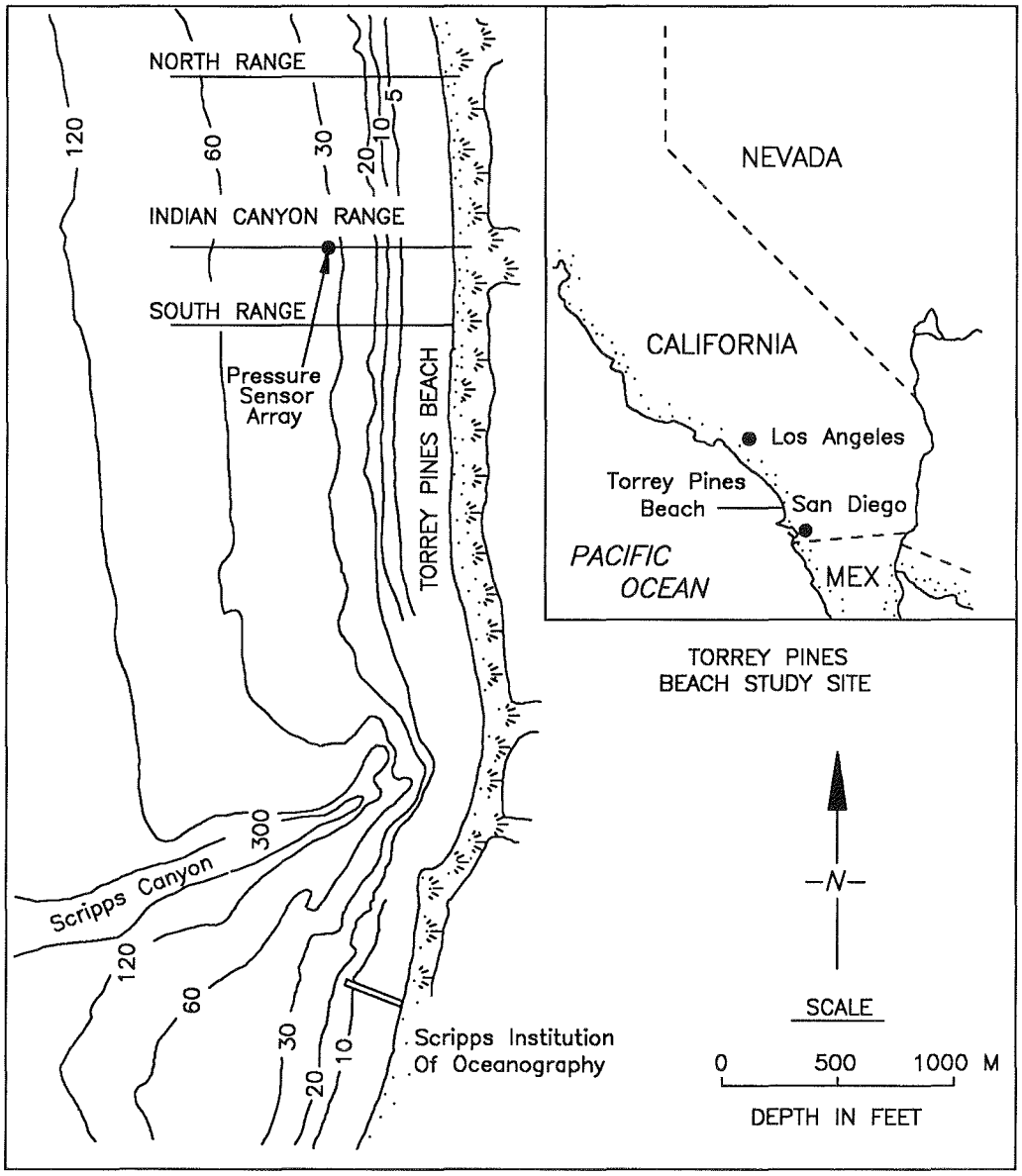

Figure 20. Location map of Torrey Pines Beach showing position of range lines and pressure sensor array (after Aubrey 1978)

164. Model parameter values resulting from calibration with the large-scale laboratory data sets (Report 1) were initially used to simulate field beach profile response. It became apparent, however, that values of the two principal empirical coefficients would have to be modified to achieve optimal agreement between measured and calculated profiles. The sand transport rate coefficient K in Equation 4 obtained from these two west coast storm events

was slightly smaller than that obtained from the laboratory experiments (1.4×10^{-6} m^4/N versus 1.6×10^{-6} m^4/N), and the transport rate coefficient ε for the slope-dependent term of the transport rate equation (Equation 37) was increased from 0.001 to 0.002. In addition, to account for time-varying, random wave height fluctuations that tend to create relatively smooth macro-scale features observed on the subaqueous profile in nature, a 30-percent random variation in recorded wave height, representing one standard deviation of the measured wave height for each 6-hr time interval, was imposed on the entire time series. A time step of 5 min and a length step of 2 m were used for all simulations.

165. Finally, it was inferred that water level measured at the gage (located approximately 1 km offshore) was not entirely representative of water elevations at the shoreline influencing profile change. Calculated beach profile response best matched measured profile change when water level at the gage was increased by approximately 0.3 m during the storm event. This is consistent with onshore- and offshore-directed wind stress associated with storms affecting the southern California coast that typically create fluctuations in water surface elevation at the shoreline, producing setup as a storm approaches and setdown as a storm passes.

Storm Event 1

166. Figure 21 shows the time series of wave height, peak wave period, and water level for the period 29 December 1975 through 9 January 1976. These measured quantities were available at 6-hr intervals. Pressure data from the array of sensors were depth-corrected and converted to sea-surface elevation, yielding the significant wave height. Since the time step used in the numerical model (typically 5 min) was shorter than the wave and water level measurement interval, input values for time steps between measurements were interpolated.

167. A 2-day period near the beginning of the record illustrates storm energy resulting from a relatively weak North Pacific low pressure system. Maximum wave heights were approximately 1.8 m with a peak period of 11.1 sec. Elevated water levels associated with storm surge, coincident with high tide, produced a measured water level at the gage of 1.2 m at the time of maximum wave height. Poststorm wave height decreased to less than 0.9 m, and peak wave period increased as swell wave energy became dominant.

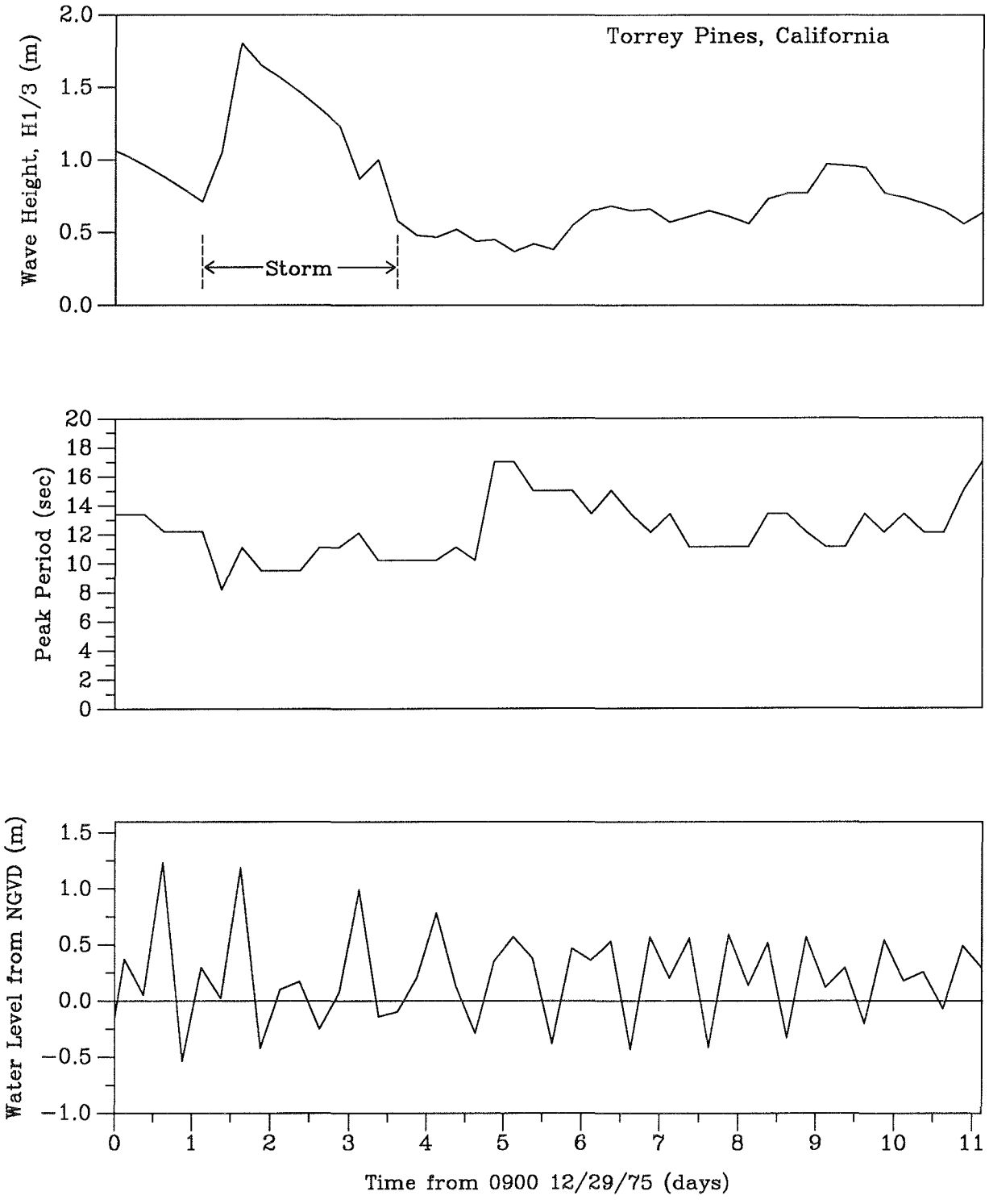

Figure 21. Time series of wave and water level characteristics, winter 1975 storm

168. The distribution of median grain diameter along the profile is required to run SBEACH. Grain size data were not available for this period, but median grain diameter recorded near the site in October 1983 showed little variation between the 1- and -1-m contours (USAED, Los Angeles 1984). Therefore, an average median grain diameter of 0.17 mm was used for model calibration.

169. Since this storm was of minimal intensity, recorded beach profile erosion was relatively minor. Figure 22 illustrates measured and calculated profile shape for the 11-day period. Calculated profile change from 29 December to 31 December 1975 was concentrated on the upper half of the foreshore and was related to locally elevated water levels. Generally, calculated profile response above NGVD was slightly less than measured adjustments; the 2-m contour retreated approximately 4.6 m, and profile volume change above the mean shoreline ($z = 0$) was -8 m^3/m. Only small adjustments in bar elevation were recorded.

170. Measured profile response between 29 December 1975 and 9 January 1976 includes effects of the 2-day storm event as well as approximately 8 days of poststorm recovery wave action. After 31 December 1975, most profile changes occurred below NGVD, where two new bar features developed. However, cumulative retreat of the 2-m contour increased to 10 m, and associated subaerial volume change increased to -15 m^3/m. The calculated profile for 9 January 1976 shows a small bar located at about the 0.6-m depth contour, in close proximity to the innermost measured bar. Although the measured bar immediately seaward of this position is not represented on the calculated profile, the broad, low-relief deposit at about the -2.4-m contour is fairly well represented by the simulation. Calculated profile change above NGVD showed increased retreat of the 2-m contour between 31 December 1975 and 9 January 1976, resulting in a cumulative retreat of about 6.4 m. Simulated profile volume adjustments gave a cumulative loss of 14.8 m^3/m. A comparison of measured and calculated profile changes shows good agreement for this storm.

Storm Event 2

171. Verification of SBEACH simulations was accomplished using process and response data from a second small storm event that occurred at Torrey Pines Beach approximately 1 year after Storm Event 1. Data were analyzed and prepared for model application in a manner identical to that for the winter

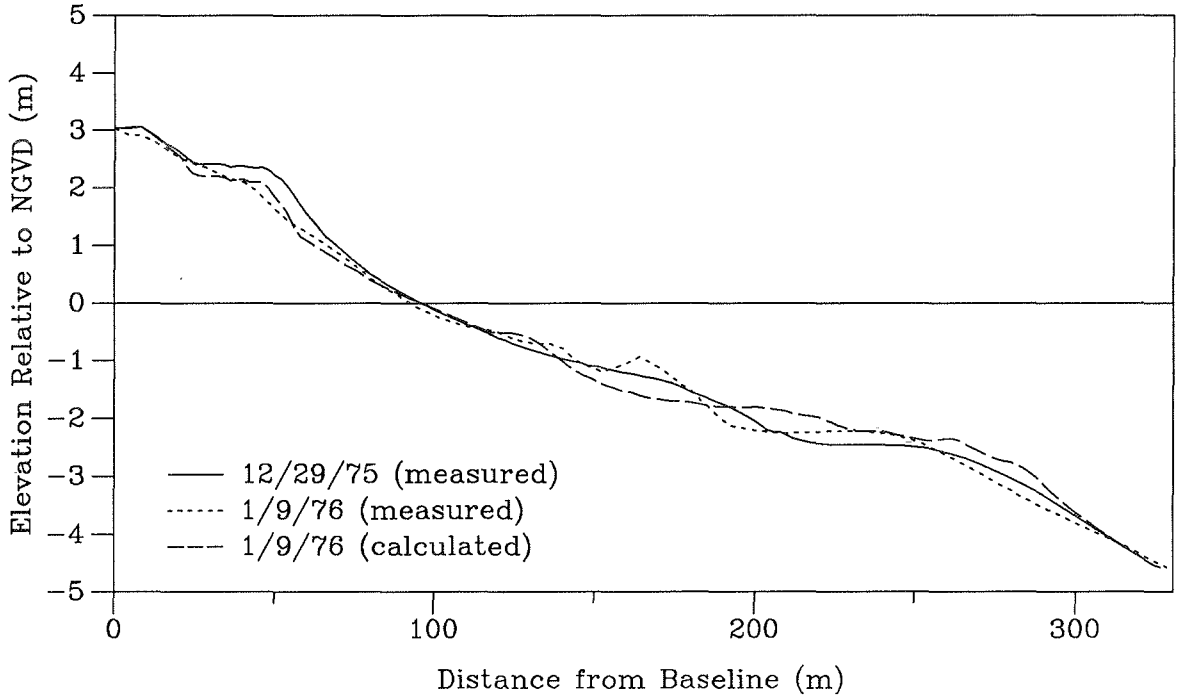

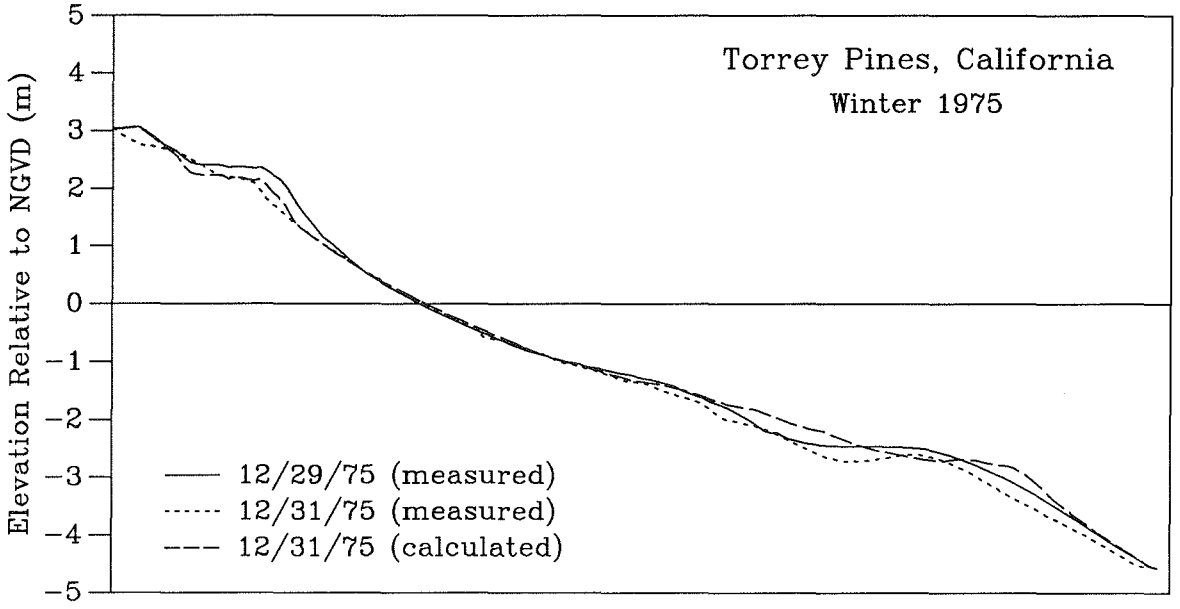

Figure 22. Measured and calculated beach profile change, Torrey Pines, winter 1975

1975 storm. Figure 23 shows the time series of wave and water level parameters for the period 21 December 1976 to 4 January 1977. In this case, the record covers 14 days with an increase in wave height occurring toward the middle portion of the time series. Small variations in wave period suggest that locally generated winds likely were not the main source of energy for this event. Consequently, an increase in water level due to wind setup at the shoreline was not imposed, and only direct measurements of water level at the gage were used for simulations. All other previously determined model parameters were held constant.

172. A maximum wave height of 1.6 m was recorded on 27 December 1976 associated with a 15.1-sec wave period. For the next 4.5 days, wave height averaged about 1.1 m. Fluctuations in water level were at a minimum during this time; however, water surface elevation remained above NGVD while wave heights were greatest. This feature was not present in Storm Event 1 and likely contributed to an increase in eroded volume above NGVD during Storm Event 2. Wave energy associated with North Pacific swell was dominant in the 14-day record.

173. This second event exhibited lower wave energy than the first storm; however, changes in profile volume and contour position above NGVD were slightly greater. This can be attributed to the duration of water level above the mean water line during higher wave conditions. Figure 24 illustrates measured and calculated profile change for the period 21 December 1976 to 4 January 1977. Unlike responses recorded during the first storm event, a relatively thin veneer of sand was eroded from the original profile between the berm crest (approximately 2.3-m contour) and the -2.1-m contour. This volume of sand was not conserved along the profile since deposits of near-equal volume were not recorded at a seaward position. Redistribution of sand by longshore processes is a likely cause for the lack of cross-shore conservation of mass during this period of dominant swell energy. Measurements of beach profile change above NGVD showed a maximum retreat associated with the 0-depth contour (12.8-m recession) and a steady decrease in contour retreat at higher elevations. The 1-m contour receded 8.8 m, and the 2-m contour receded 4 m. Measured changes in profile volume above NGVD were approximately -16.3 m^3/m.

174. Calculated profile change satisfactorily verified predictive capabilities of the model. Changes in position of the 1- and 2-m contours

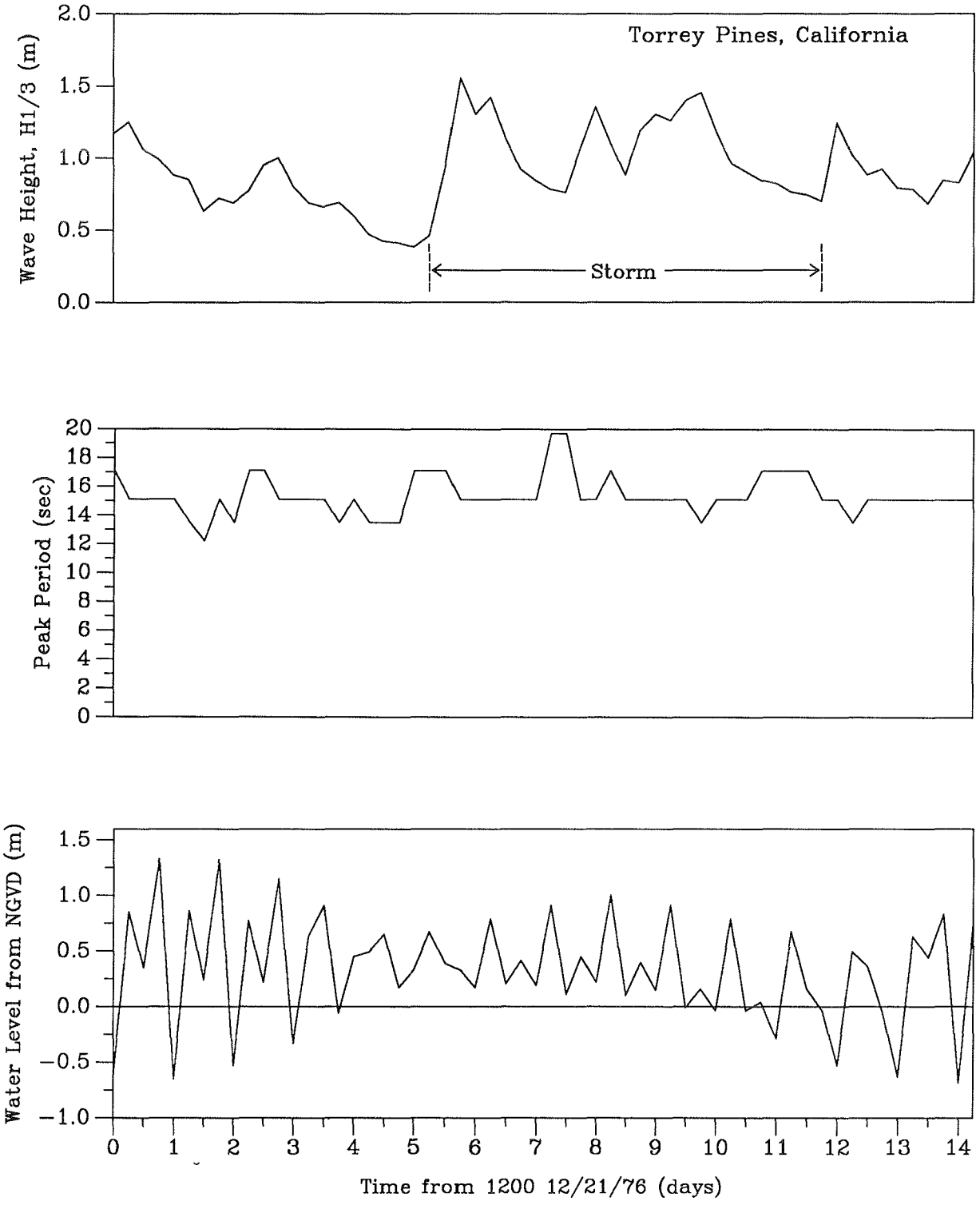

Figure 23. Time series of wave and water level characteristics, winter 1976 storm

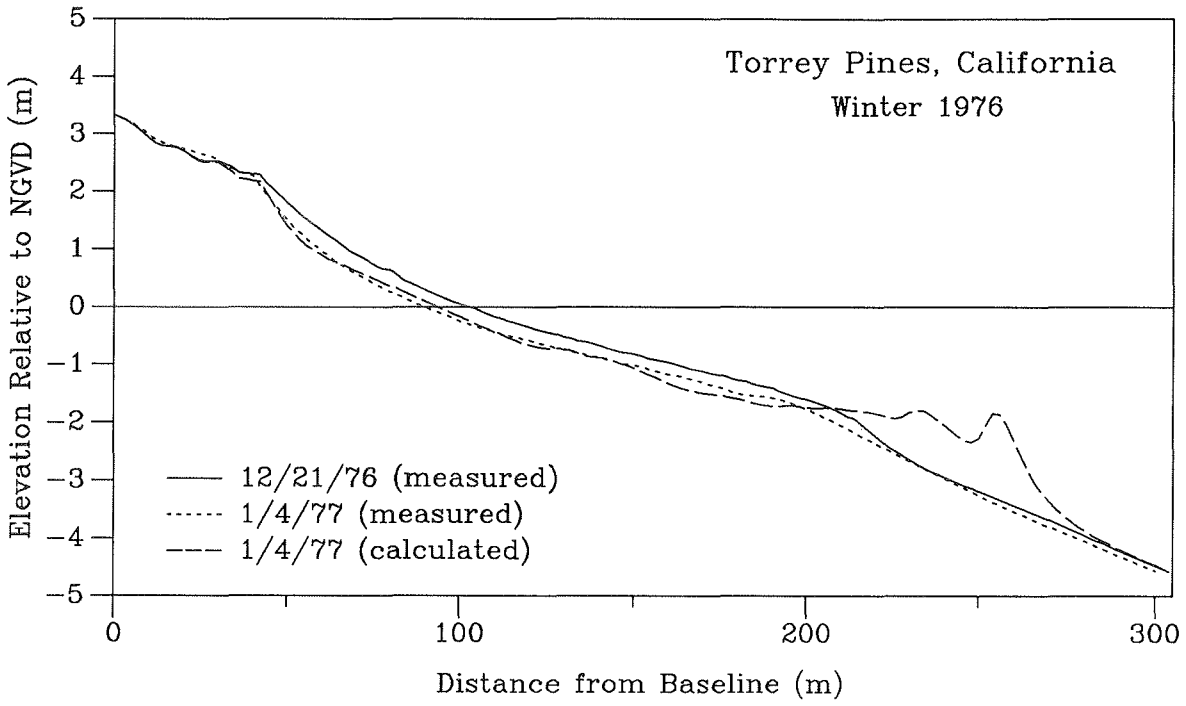

Figure 24. Measured and calculated beach profile change, Torrey Pines, winter 1976

were nearly identical to measured changes (-10.4 and -4 m), and the 0-depth contour was slightly underpredicted. Therefore, profile volume change above NGVD was consistent with measured changes (-17.6 m^3/m). However, calculated profile shape on the seawardmost portion of the active profile was significantly different from measured change. This apparent inconsistency is explained by examining the way in which profile change is calculated. At the shoreward end of the profile, the runup limit constitutes a boundary where cross-shore sand transport becomes zero. The seaward boundary is determined by the depth at which no significant sediment motion occurs. Once the distribution of the sand transport rate is known, profile change is calculated from the mass conservation equation. If the assumption of conservation of mass in a two-dimensional sense is not approximated by a three-dimensional natural process, either an excess or deficit of sand volume will be predicted. In this case, calculated profile change shows an excess of sand volume deposited as a bar, suggesting that longshore processes may have been important in redistributing nearshore sand deposits. Verification of calculated profile response for this region was otherwise good.

PART VI: MODEL APPLICATION TO BEACH-FILL DESIGN

175. Beach nourishment is becoming a preferred shore protection measure because it is often the least expensive solution, is flexible and can augment existing shore protection structures, and provides a natural and enjoyable coastal environment. Prediction of beach-fill behavior is required to determine the benefits of a nourishment project in relation to other shore protection alternatives as well as to estimate its longevity and functionality. A realistic description of coastal sediment transport processes and beach-fill change involves numerous hydrodynamic, sediment, and morphologic characteristics that vary in space and time. Numerical modeling of beach profile and fill change provides a general and quantitative means of representing the combined and simultaneous effects of these variables. Application to beach-fill design was one of the objectives in developing SBEACH.

176. Figure 25 is a definition sketch of a nearshore region containing a beach fill. The fill is acted on by ordinary cross-shore wave processes, such as those associated with episodic and potentially catastrophic storms, which mold it from an initial shape to a dynamic equilibrium shape. The fill

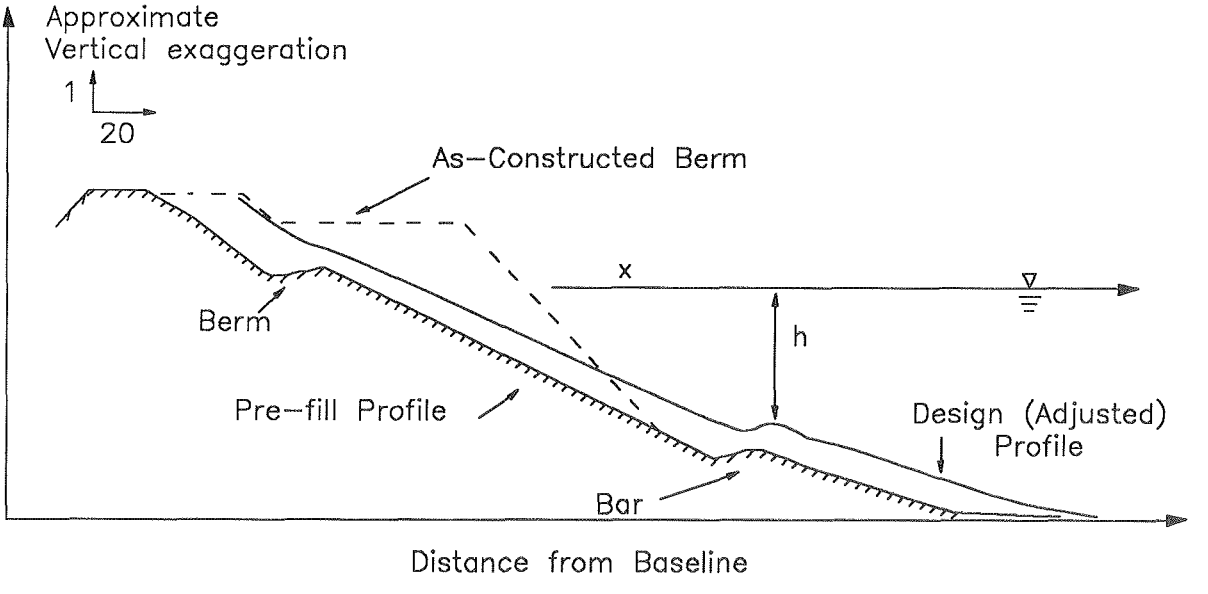

Figure 25. Definition sketch categorizing a beach fill

is also exposed to longshore currents induced by waves and wind, which move sand alongshore and deplete the fill when updrift sand source is inadequate or maintenance nourishment is not provided. Longshore transport does not enter in SBEACH; therefore, the model is most appropriately applied to the internal region of a long fill and far from coastal structures and boundaries where differentials in longshore transport may be large.

177. This chapter describes hypothetical applications of SBEACH to predict the initial adjustment of beach fill to wave action by storms. Initially, simulations are made for two types of storms occurring on the US east coast. One synthetic tropical storm (hurricane) and one synthetic extratropical storm (northeaster) representing mid-Atlantic events with approximate 2- to 5-year return periods are used to predict erosion associated with two hypothetical beach-fill configurations and subsequent poststorm recovery. Eroded sand volume and contour movement are evaluated as a function of storm type, fill cross section, grain size, and time.

178. In the second half of the chapter, simulations are made of the response of two different fill cross sections of two different grain sizes to a tropical storm with a return period of about 10 years. Comparisons are made to a beach without a fill to evaluate the effectiveness of artificial nourishment as a means of shore protection. A seawall is included in the simulations to illustrate model capabilities to predict profile evolution in situations involving a vertical wall. Poststorm recovery is also simulated for this case making it feasible to assess the possibility for the eroded fill sand to contribute material in the beach recovery process. Some general guidelines are provided concerning the design of beach nourishment schemes based on the numerical simulations.

179. Finally, a concluding discussion is given regarding capabilities and limitations of the numerical model as a tool for predicting beach-fill evolution. Much of the material presented in this chapter may be found in Kraus and Larson (1989) and Larson and Kraus (in press).

Fill Response to Moderate Storms

180. A verified model enables examination of the shore protection functioning of alternative fill cross sections or fill templates at a beach

nourishment project impacted by storms. Such calculations must be made to perform cost-benefit analysis and to estimate the minimum fill volume needed to provide a specified level of storm protection against erosion and inundation. In an overall evaluation, longshore variability of the protective beach complex as well as storms must be considered (van de Graaff 1983, Savage and Birkemeier 1987).

181. Two approaches can be taken to estimate storm impact on a beach-fill complex: the design-storm approach and the storm-ensemble approach. The design storm is either a hypothetical or a historical event that produces a specified storm surge hydrograph and wave condition at the project site. Surge is a water level rise caused by wind stress and atmospheric pressure variation; waves also produce a rise in mean water level through setup. The time average (on the order of an hour) of surge, wave setup, and tide is called the stage. In a stage-frequency analysis, the design storm may have a certain frequency of occurrence or return period (for example, a 100-year storm).

182. The design-storm approach is problematic for use in beach erosion modeling because profile change is sensitive to storm duration, surge shape, and wave height and period, in addition to peak stage. The maximum water level associated with the surge of a design storm may produce less erosion than a storm of lower surge but longer duration, or a storm of lower surge but higher waves. However, in the absence of an extensive storm data base, use of several large historical storms (large in the sense of having caused significant erosion) to drive the model is considered acceptable. In this approach, it is recommended that the phasing of the peak tide be varied with the peak surge because model results are sensitive to water level. For example, arrival of the peak surge during low tide on a mesotidal or macrotidal coast may produce little or no erosion, whereas arrival of the peak surge at high tide could bring disaster.

183. The most satisfactory solution to the problem of the many-to-one relation between beach erosion and stage frequency is to use the storm-ensemble approach, i.e., calculating erosion for a large number of storms and keying the erosion to the frequency of storm occurrence (Kriebel 1982; Scheffner 1988, 1989). This method yields an erosion or recession frequency of occurrence curve. In this method, tropical and extratropical storms must

be treated independently because they have different physical characteristics. Tropical storms are infrequent events of short duration and high intensity, whereas extratropical storms are more frequent and usually of longer duration and lower intensity. The storm-ensemble approach is recommended for project design, although it requires a storm data base and is much more computationally intensive than the design-storm approach.

184. In this section, the response of nourished beaches to a representative tropical storm and an extratropical storm is calculated to examine predictions of the model to storms of differing waves and water levels (surge and duration). The two storms were synthesized to produce erosion resulting from a 2- to 5-year storm surge for the mid-Atlantic Ocean coast of the United States. The amount of eroded volume for such events is on the order of 20 to 30 m^3/m (Savage and Birkemeier 1987).

Design storms

185. Surge hydrographs developed for the hypothetical storms are shown in Figure 26. The hurricane surge has a duration of approximately 12 hr, with

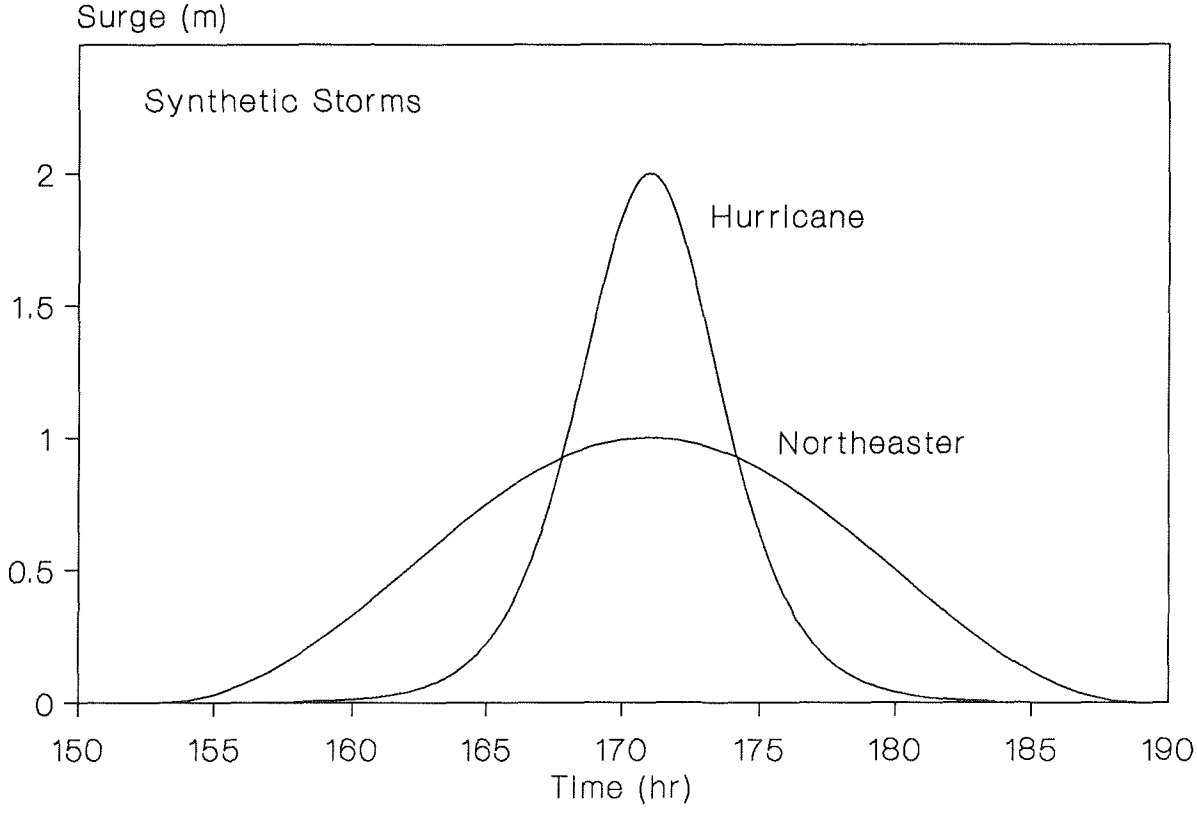

Figure 26. Surge hydrographs for the synthetic storms

a peak surge of 2 m, and a duration above half the peak surge (1 m) of 6 hr. The shape of the hydrograph follows an inverse hyperbolic cosine squared. The surge of the northeaster has a duration of 36 hr, with a peak surge of 1 m, and a duration above half the peak surge (0.5 m) of 18 hr. A cosine-squared function was used to generate the shape of the northeaster surge. The peak surge of the hurricane is higher because wind speeds in hurricanes are on average greater than those in northeasters.

186. The time-histories of wave height and period assigned to the storms are shown in Figure 27. Both have peak deepwater wave heights of 5 m, which occur during the time when the respective surges are greater than half the maximum. The duration of high waves for the northeaster is thus three times that of the hurricane. Since the radius of a northeaster is typically several times greater than that of a hurricane, the fetch is longer, resulting in longer wave periods. Wave height and period of 1 m and 7 sec were applied for 6.5 days before the start of the storms to mold the profiles into a realistic shape under ordinary waves. As the storm passed, wave height and period were changed to 0.5 m and 10 sec to simulate long-period recovery swell wave conditions. A sinusoidal tide was applied with a 12-hr period and 0.5-m amplitude; a peak in the tide occurred during the peak surge of each storm.

Beach-fill shapes

187. Following the procedure of Kraus and Larson (1989), two different beach-fill cross sections or templates were designed for exposure to storms. The artificial berm had most of the fill placed on the beach and above MSL. The as-constructed berm extended horizontally for a distance of 16 m at an elevation of 3 m and then tapered with a 1:20 slope to join the original beach profile at a depth of 1.4 m (Figure 28). This is a common beach-fill design in the United States (e.g., Jarrett and Hemsley 1988). The other fill template is termed profile nourishment, a concept advocated by Bruun (1988). In the example, the material was placed over the profile from an elevation of 1 to -2 m (Figure 29) in an approximation of the existing profile shape. The fill volume was the same for each template (140 m^3/m).

188. Initially, all simulations were made assuming a 0.2-mm sand beach, with the fills and the natural beach having the same grain size. However, simulations were also made for fill grain sizes in 0.1-mm increments from 0.2 to 1.0 mm. In these cases, the grain size was specified as that of the

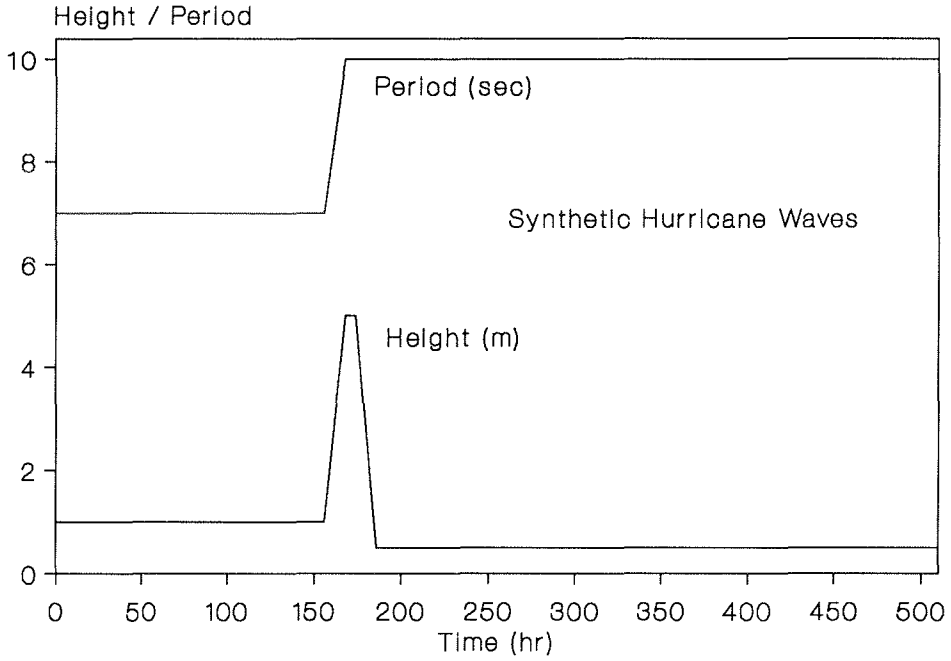

a. Hurricane

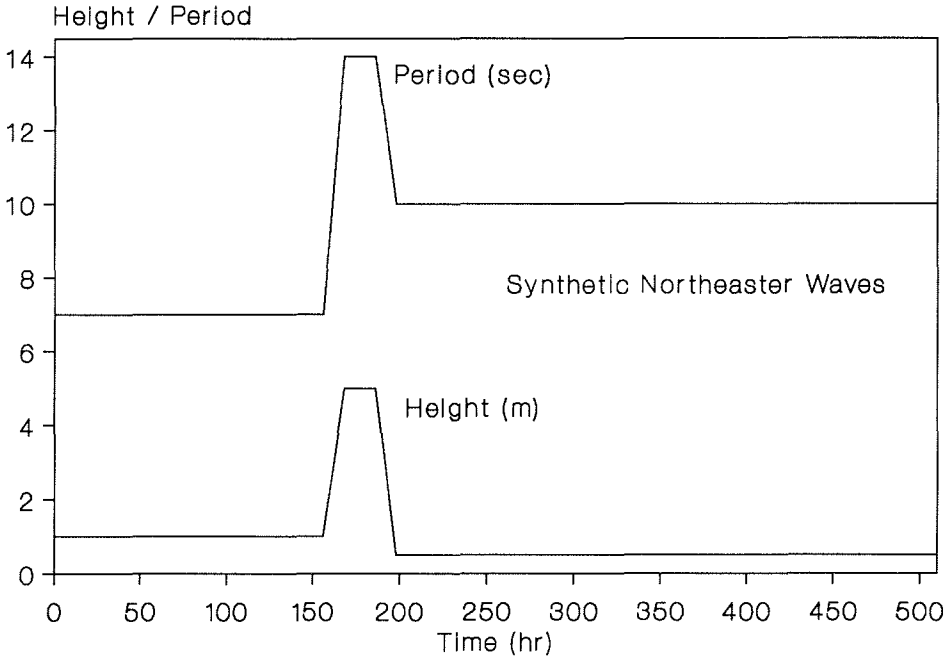

b. Northeaster

Figure 27. Time-history of wave height and period for synthetic storms

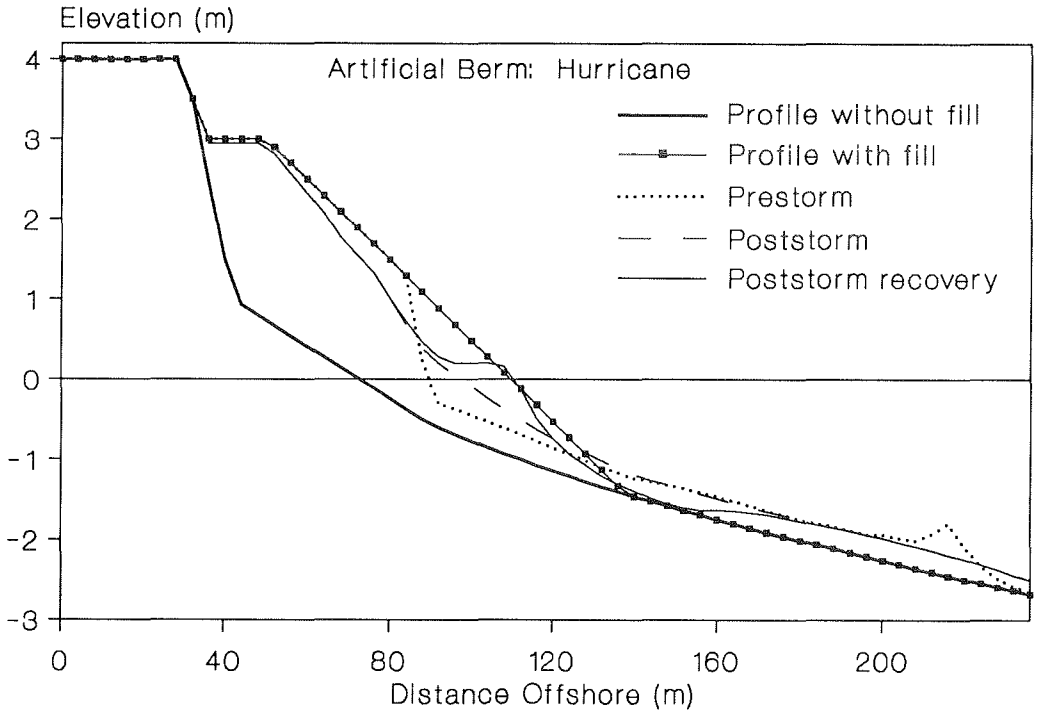

Figure 28. Response of artificial berm to hurricane impact

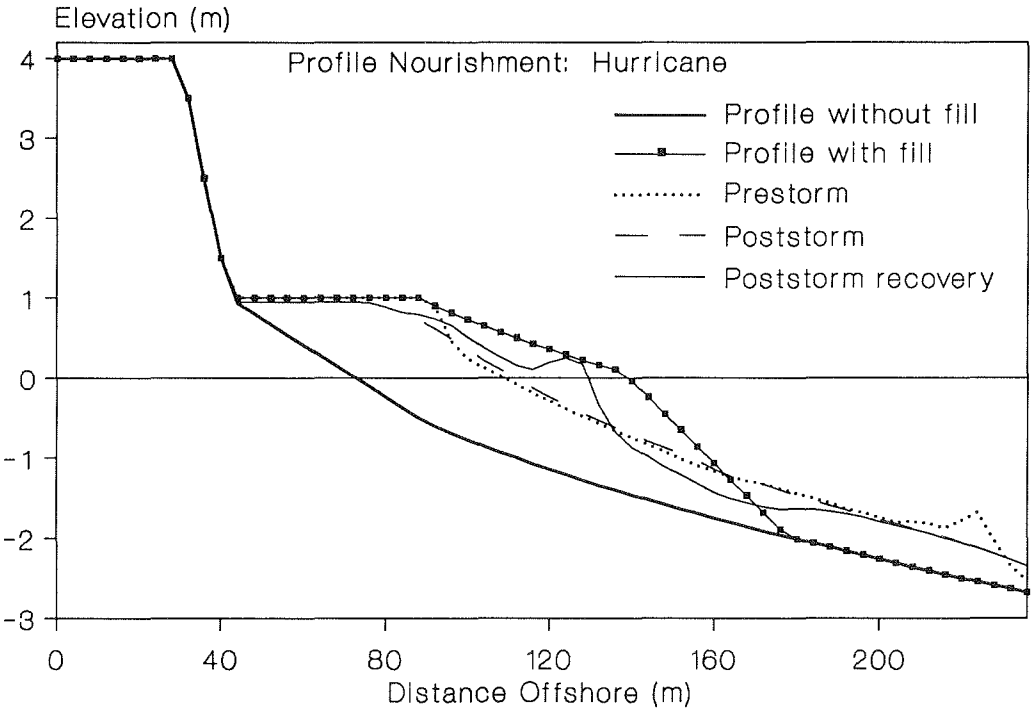

Figure 29. Response of nourished profile to hurricane impact

fill over the portion of the profile originally occupied by the fill and 0.2 mm elsewhere. Profile elevations are given with respect to MSL, and a water temperature of 20° C was specified in the model for computation of the sand fall speed.

Profile change

189. Figures 28 through 31 illustrate predicted impacts of the two storms on the two nourishment schemes. The curve labeled "profile without fill" gives a hypothetical dune, beach, and subaqueous equilibrium profile for reference. The construction profile configuration is denoted as "profile with fill," whereas the "prestorm profile" shows the profile after 6.5 days of ordinary waves. The "poststorm profile" represents the shape prior to the recovery wave period and the "poststorm recovery" profile displays the profile after experiencing approximately 2 weeks of recovery waves. The following paragraphs discuss prestorm and poststorm profile development.

190. Prestorm. Prestorm profiles ("design profile" of Figure 25) of the artificial berm and nourished profile differ significantly in the inner surf zone. A pronounced scarp is produced with the artificial berm, whereas the nourished profile experiences more subtle changes because it was placed in a near-equilibrium configuration. For both cross sections, a small breakpoint bar formed at about the 210- to 220-m mark (measured from an arbitrary baseline). Sand was removed from the foreshore and distributed along the profile just beyond the 2-m-depth contour. Thus, regardless of the initial fill configuration, the model predicts that fill material will be transported a considerable distance offshore to the point of incipient wave breaking in the process of molding the surf zone profile to an equilibrium shape.

191. Poststorm. Subaqueous portions of the poststorm profiles are quite similar in shape, being reworked by storm waves to the same equilibrium shape independent of initial profile configuration and type of storm. The shoreline position (0-depth contour) actually moved seaward of its prestorm location, with the accreted material supplied from the ordinarily subaerial portion of the profile that was inundated due to storm surge. A small bar formed at approximately the 5-m-depth contour under the high storm waves, but it is not shown here to better display changes near the beach.

192. An important outcome of the predictions is that, under the action of simulated hurricane and northeaster events, resultant profile change was

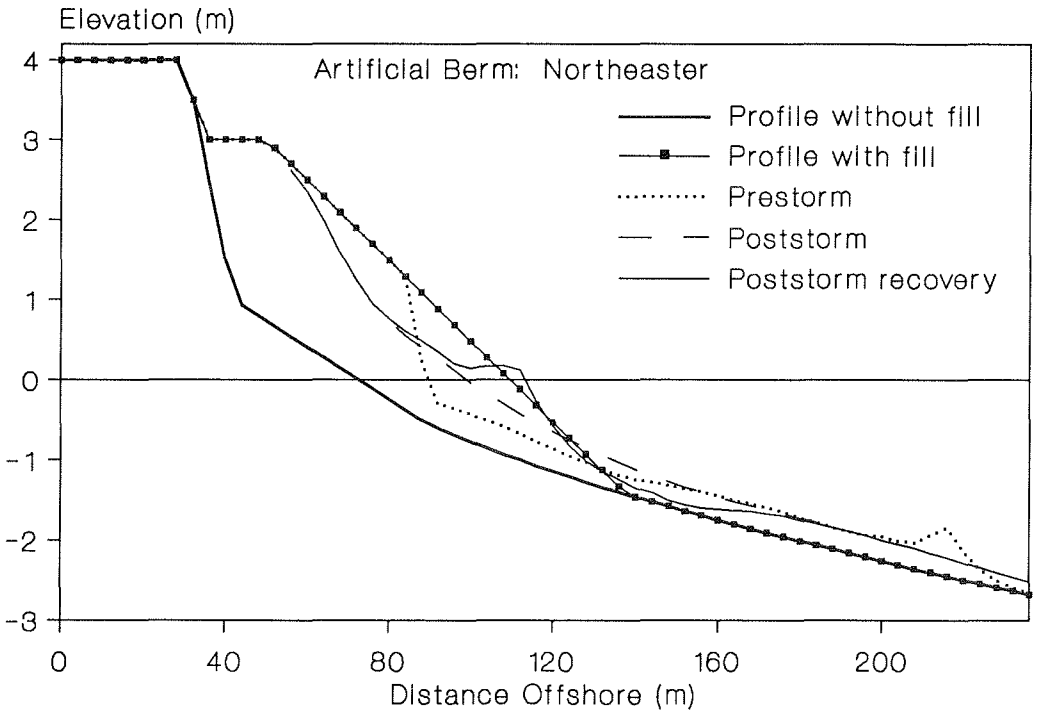

Figure 30. Response of artificial berm to northeaster impact

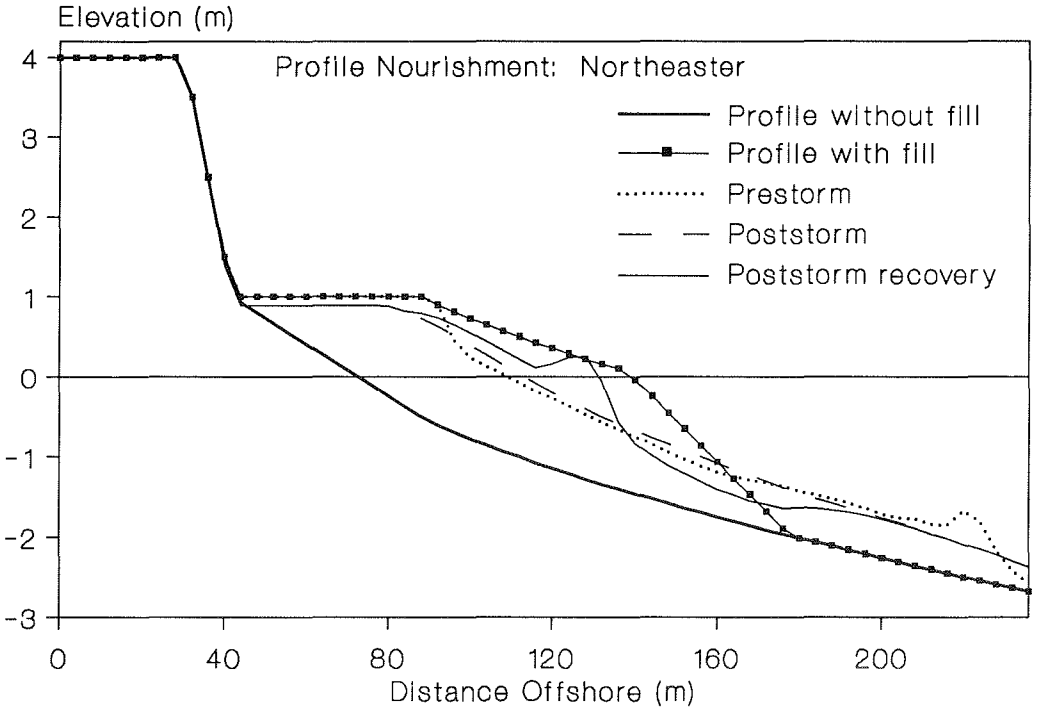

Figure 31. Response of nourished profile to northeaster impact

very similar. The use of one typical storm descriptor (e.g. maximum stage) to estimate shoreline recession or eroded volume would have predicted greater changes associated with the hurricane, thus producing misleading results.

193. Poststorm recovery. In all cases, substantial accretion occurred near MSL during the poststorm recovery phase. The upper foreshore of the nourished profile experienced more accretion than the artificial berm cases. These results are consistent with the concept that a beach profile with a natural shape can best respond to changes in incident waves.

Eroded volume and contour change

194. Figure 32 shows the evolution of eroded volume above the 0- and 1-m contours (and 0.5-m contour for the profile nourishment case). Eroded volume above the 0-depth contour increases rapidly at the beginning of pre-storm ("ordinary") wave action, describing the behavior of fill material during initial profile adjustment. In contrast, eroded volume above the 1-m contour shows a much slower increase. The profile nourishment case illustrates greater initial erosion during the early stage of wave action, but also greater recovery during the poststorm period. It should be emphasized that longshore processes are omitted from the present discussion; however, profile nourishment places a greater amount of material into the active littoral zone, thereby increasing its potential for transport alongshore and out of the project reach.

195. The volume of eroded material above the 0-depth contour does not show a significant increase during the storms, changing from about 22 to 27 m^3/m for erosion of the artificial berm during the northeaster. Eroded volume above the 1-m contour abruptly increases at the start of the storms from about 3 to 17 m^3/m for the artificial berm impacted by the northeaster. The volume of erosion above the 0-depth contour is relatively unchanged because these moderate storms primarily remove material from the upper portion of the profile and redistribute it over the shallow nearshore region.

196. The hurricane and the northeaster produce nearly the same amount of erosion, 25 to 30 m^3/m above the 0-depth contour and 13 to 16 m^3/m above the 1-m contour. Therefore, the longer surge duration of the northeaster was approximately equivalent in erosion capacity to the higher surge of the shorter duration hurricane. Eroded volumes above the 0-depth contour are comparable with those associated with 2- to 5-year return period storms

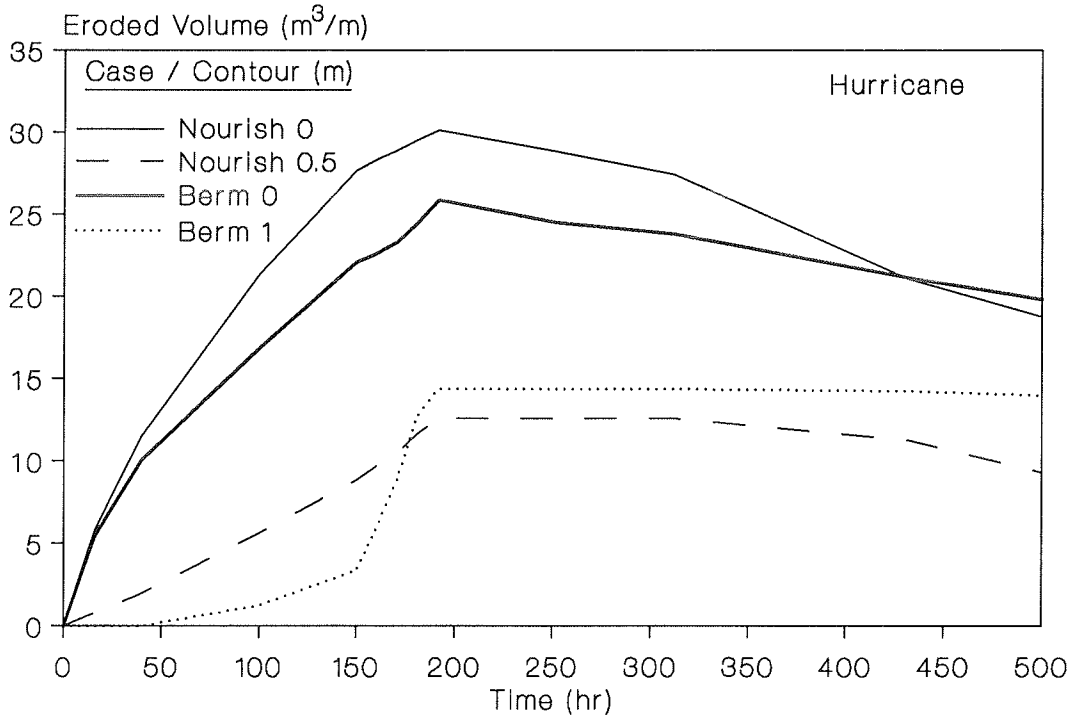

a. Hurricane

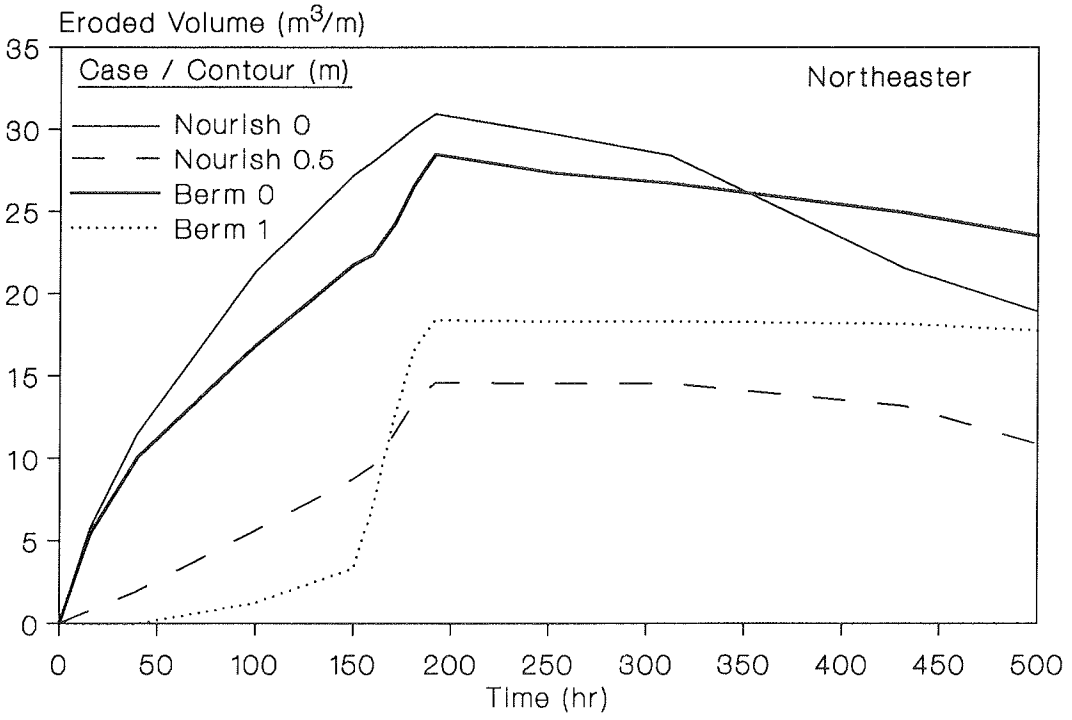

b. Northeaster

Figure 32. Eroded volume above specific contours

impacting the mid-Atlantic coast (Savage and Birkemeier 1987). Evolution of the eroded volumes above MSL shows an approximate exponential approach to an equilibrium value. These trends are in general agreement with those obtained by Kriebel and Dean (1985), who numerically examined eroded volume and berm recession as a function of wave height, surge level, and other parameters.

197. It is interesting that there is a tendency for the hurricane-impacted beach to recover more rapidly than the northeaster-impacted beach (Figure 32). This is in agreement with qualitative observations of poststorm recovery along the Florida coast. An explanation lies in the nature of the storm hydrograph; material is not removed as far offshore during hurricanes as in the case of the longer duration and lower surge extratropical storms. This material is deposited closer to shore and can be moved back on the beach more rapidly under recovery wave action.

198. Figure 33 displays the evolution of the position of the 0 and 1-m contours. A decrease in contour position indicates recession of the beach at that contour. The 0-depth contour for both fill types and both storm types shows recession during prestorm and storm periods, but begins to advance before the end of the storms and prior to arrival of recovery waves, as the surge subsides and the wave height decreases. The 1-m contour shows no recovery for the artificial berm because the foreshore is relatively steep, whereas the 0.5-m contour for the nourished profile does show some recovery since the gentler slope allows poststorm wave runup to build a berm. In SBEACH, berm formation and growth are largely controlled by the elevation reached by wave runup (Larson 1988, Larson and Kraus 1989a), and accretionary processes are diminished on steeper slopes.

199. Figure 34 illustrates eroded volume at the end of the storm (prior to recovery wave action) as a function of beach-fill grain size. As previously mentioned, median grain diameter of the native beach was set at 0.2 mm, and the area in which the fill was placed was assigned the grain size of the fill. This procedure does not allow tracking of movement of the different grain sizes. However, because surf zone sediment is usually sorted with coarser material located higher on the active profile, this simple procedure is considered to provide a reasonable first approximation of the response of a natural beach of varying grain size.

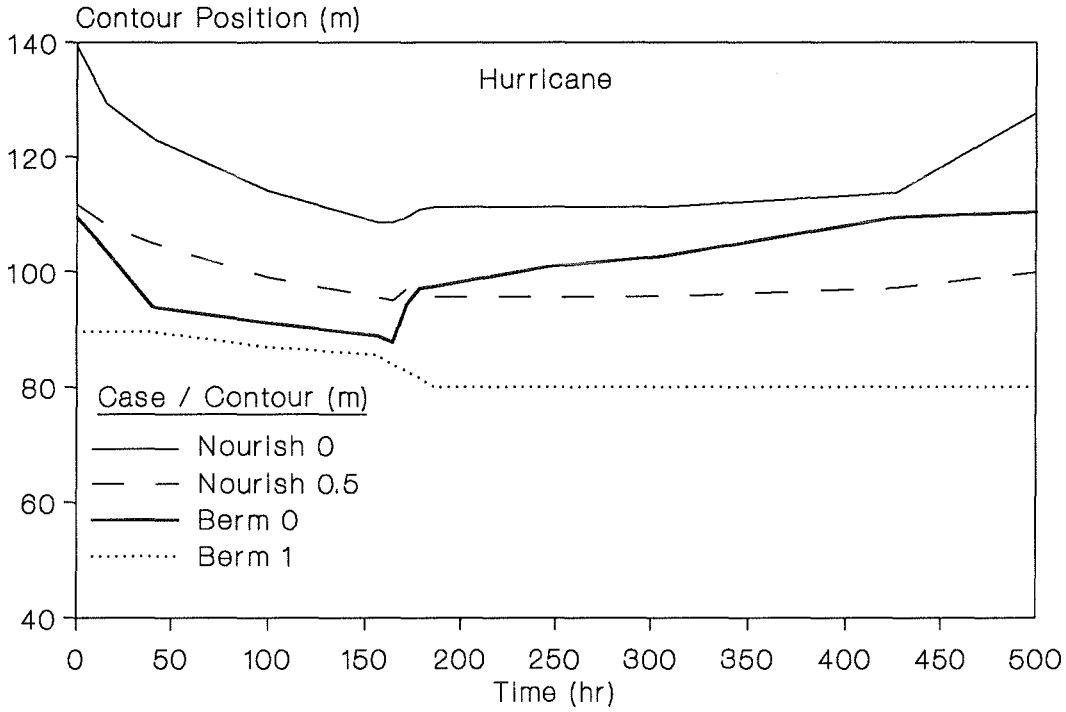

a. Hurricane

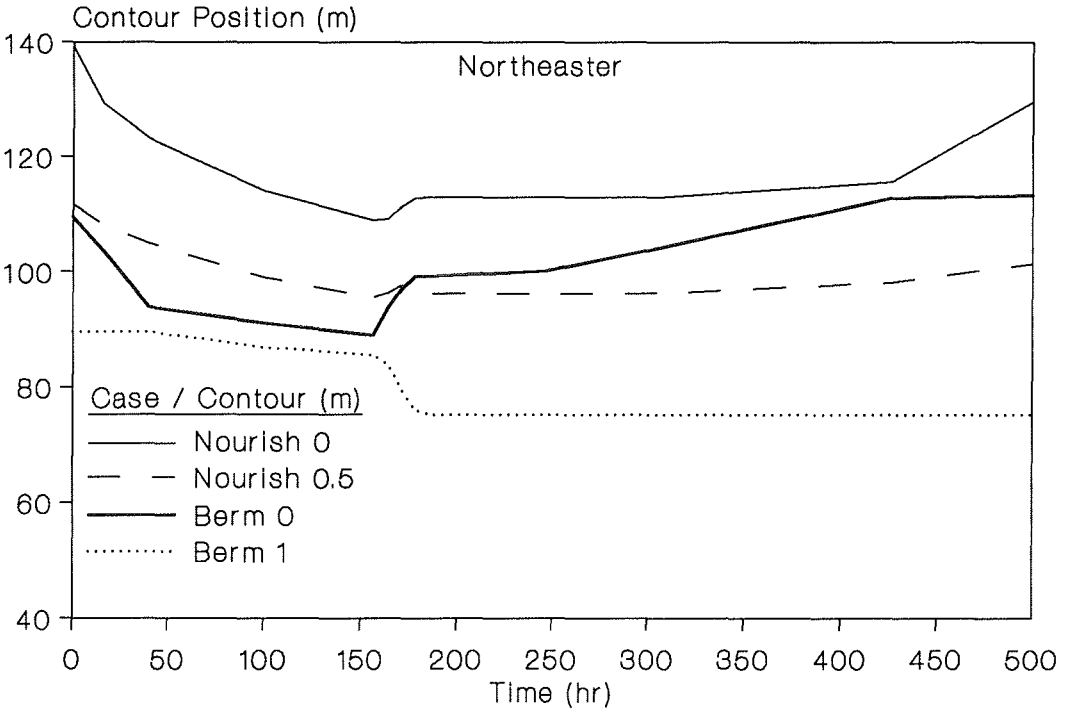

b. Northeaster

Figure 33. Movement of selected contours

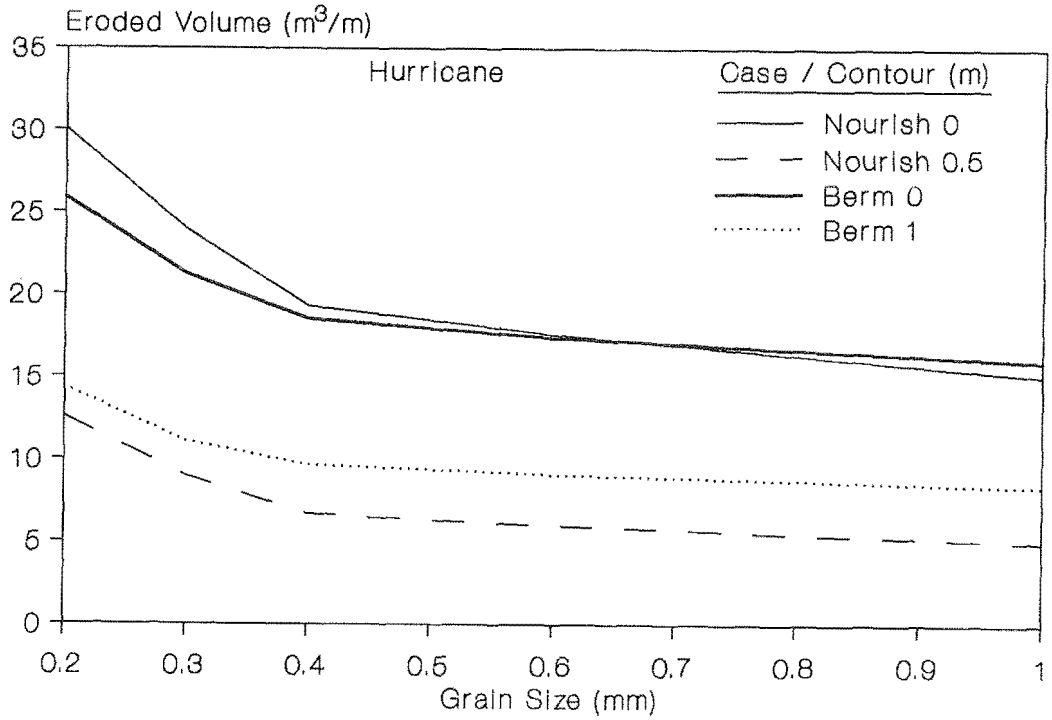

a. Hurricane

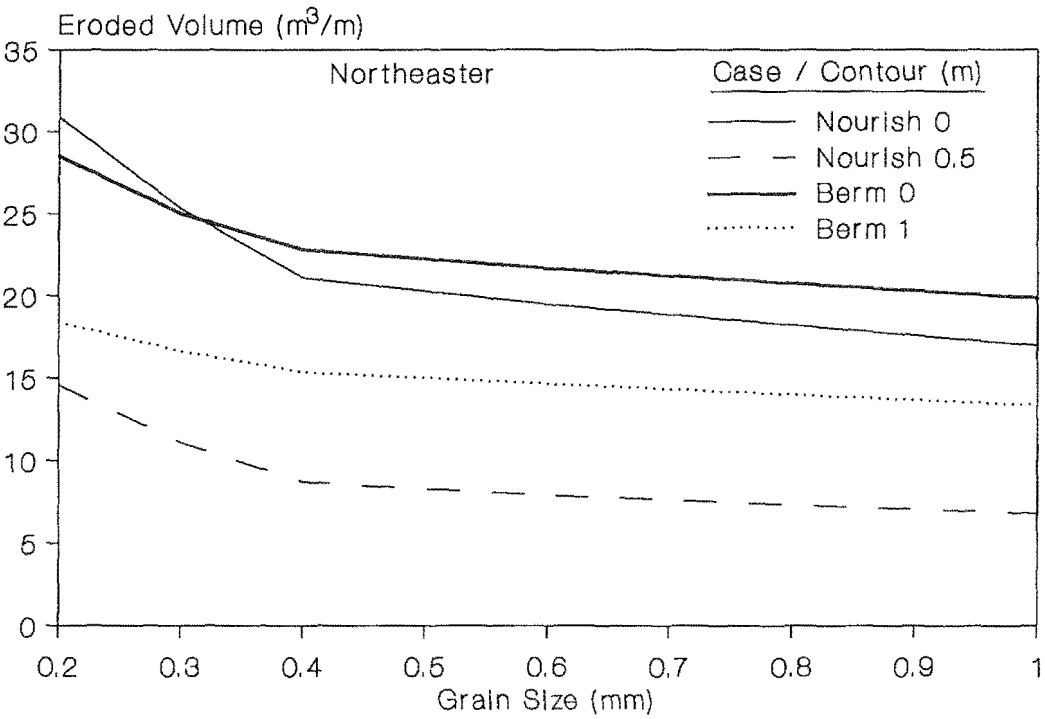

b. Northeaster

Figure 34. Effect of grain size on eroded volume

200. For the particular synthetic storms used, Figure 34 shows a relatively steep decrease in eroded volume as grain size increases from 0.2 to 0.4 mm, with a gentle decrease thereafter. This behavior results from the property of the empirically determined functional dependence of wave energy dissipation needed to generate an equilibrium profile of a given grain size. The property is manifested by computed dissipation rates that rise steeply in the range of 0.1 to 0.4 mm and then increase at a lower rate with increasing grain size (Moore 1982). Since the rate of decrease in erosion is small beyond 0.4 mm and the cost of beach fill typically increases substantially for larger size material, calculations such as those illustrated in Figure 34 allow an evaluation to be made of initial nourishment volume and subsequent fill maintenance costs. In project planning, curves similar to those in Figure 34 should be developed with consideration of the design profile and the storm characteristics of the area, using the storm-ensemble approach.

Beach-Fill Response with a Seawall

201. Another aspect of the simulation was to display the capabilities of the model to predict profile evolution of a fill fronting a seawall. A schematic storm event was developed similar to the previous two synthetic storms and consisted of a period of low waves when profile adjustment took place, a 3-day storm event, and a period of recovery waves. The total simulation time was 30 days, and comparisons were made for a beach with and without fill. The two fill types studied were again an artificial berm and profile nourishment, with cases examined using median grain diameters of 0.25 and 0.40 mm. Although wave reflection from the seawall is not considered in the simulations, it is recognized that this process alters surf zone hydrodynamics and may affect profile development.

202. The first 21 days of the simulation consisted of constant waves and water level, with a wave height of 0.5 m and a wave period of 8 sec. These values were assumed to represent typical wave conditions on an open-ocean Atlantic coast and were used to produce a realistic equilibrium profile. Under these conditions, beach change can be mildly erosional or accretionary, depending on the grain size and initial profile shape. At day 21 ("Prestorm" in Figure 35) a storm was imposed that lasted for 3 days. The average surge

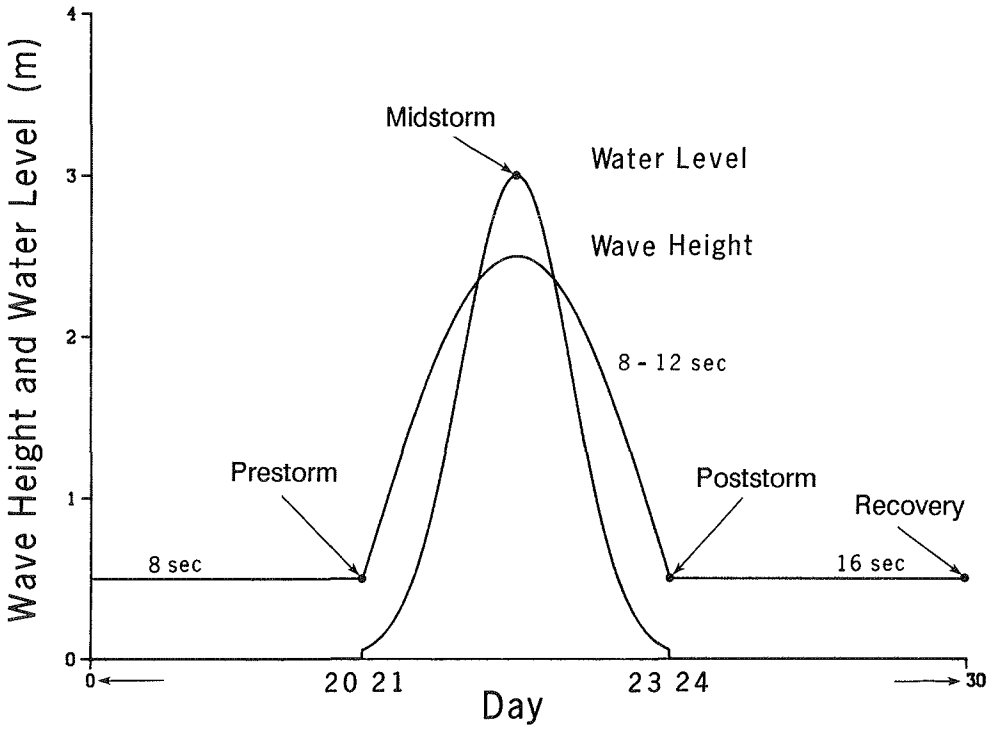

Figure 35. Time-history of waves and water level

water level during the storm followed a Gaussian form and reached a maximum elevation of 3 m above MSL. The average wave height was given a sinusoidal variation during the storm, having a peak of 2.5 m at the peak of the surge ("Midstorm"). Wave period during the 3-day event varied between 8 and 12 sec, with 12-sec waves occurring at the time of the maximum wave height. At the end of the storm ("Poststorm"), the surge was considered nonexistent, and waves arrived as swell with a height of 0.5 m and a period of 16 sec.

203. In the following sections, adjustment of the profile to the 30-day design sea conditions is examined with SBEACH for three situations: an original (existing) condition, a fill of artificial berm-type, and a fill carried out using the profile nourishment technique. The simulations were done using parameters from the calibrated model with a time-step of 20 min and a space step of 5 m.

Existing conditions

204. The profile configuration representing the beach prior to nourishment activity is shown in Figure 36. A 2-m-high foreshore is backed by an infinitely high seawall, although its crown is truncated at a 2-m elevation in

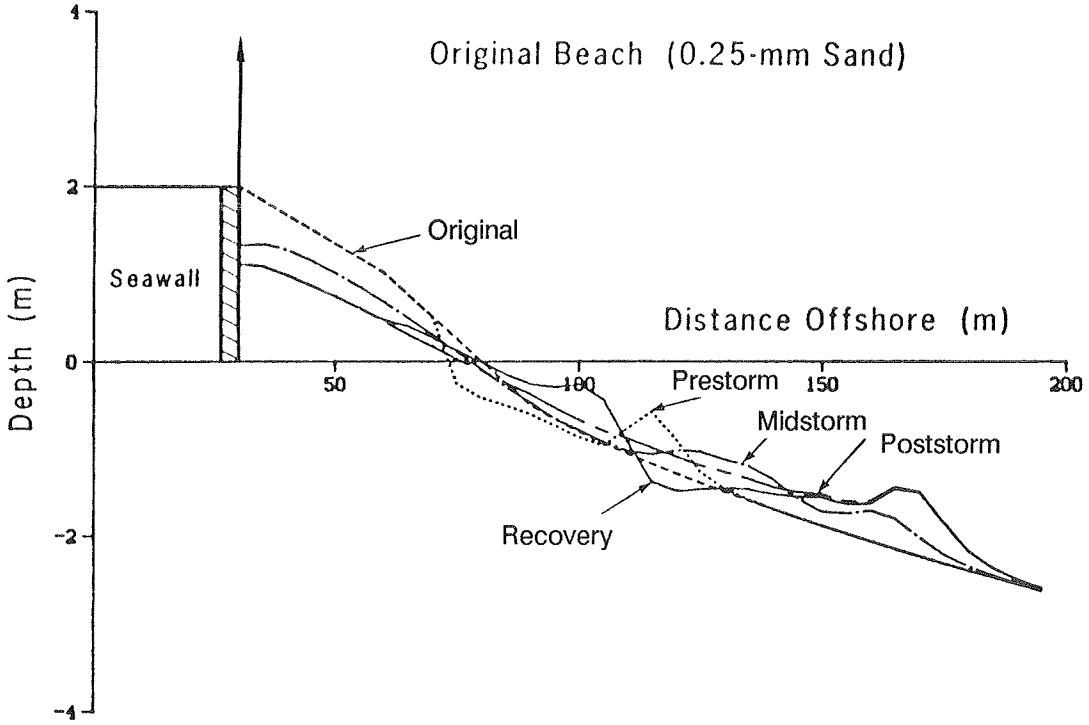

a. 0.25-mm-sand beach

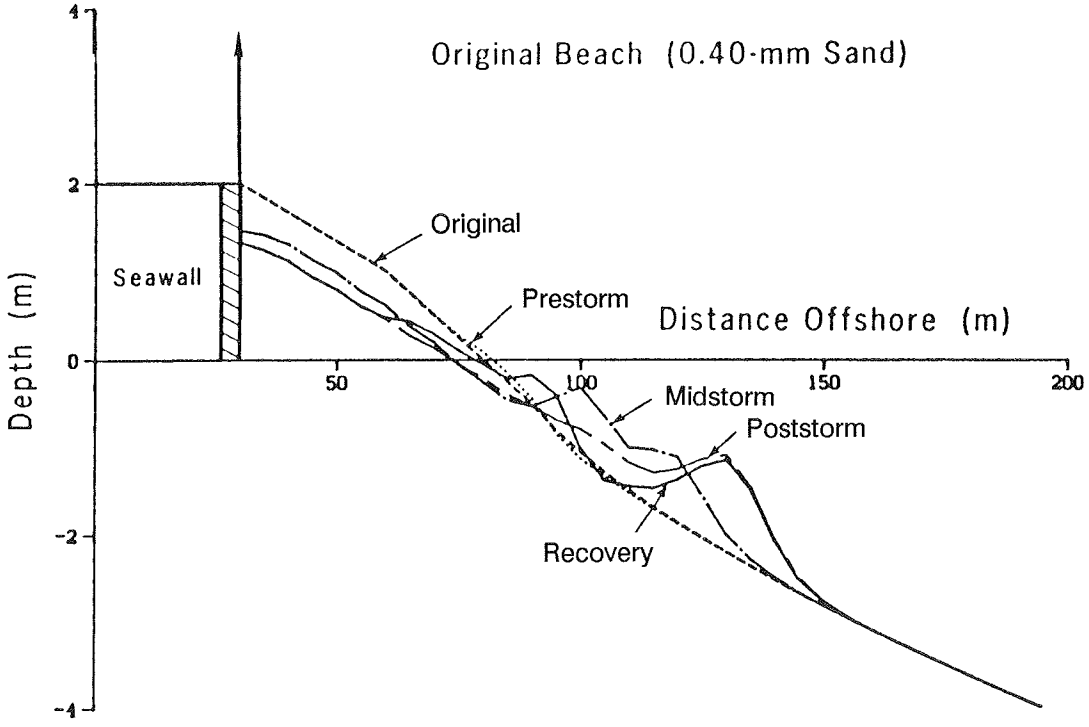

b. 0.40-mm-sand beach

Figure 36. Simulation of profile evolution for existing beach

this and subsequent figures. The original profile decreases linearly to the 0.5-m-depth contour with two different slopes; the break in slope is located at an elevation of 1 m. Seaward of the segmented linear profile, an equilibrium shape is used into deeper water.

205. Simulations showed that the 0.25-mm-sand beach eroded on the foreshore during the first 21 days of low waves, and a small bar formed with a crest located about 120 m from the baseline. In contrast, the 0.40-mm-sand beach accreted slightly on the foreshore, indicating that the transport was directed onshore. At midstorm, two bars formed offshore, the berm was completely submerged, and the beach eroded considerably at the seawall for both sand sizes. The inner bar was created at the beginning of the surge, whereas formation of the outer bar corresponded to the peak surge and maximum wave height. Poststorm profile shape showed that the berm had eroded further at the seawall, slightly more so for the 0.25-mm-sand beach than for the 0.40-mm sand beach, and a single large bar appeared on both profiles. The bar on the finer sand beach is broader and lower in elevation with respect to the initial profile than the coarser sand bar. It is interesting to note that the position of the poststorm shoreline is at about the same location (approximately 75 m from baseline) for both beaches; however, sand moved farther offshore on the finer sand beach, and its subaerial section is more deflated.

206. Lower steepness waves arriving during the 7-day recovery period passed over the storm bars on both beaches, causing little change in bar shape. During the recovery phase, swell broke in shallower water, creating a small secondary bar inshore on both profiles. The inner bar was formed by onshore transport, producing a deep trough between the storm bar and inshore bar. Both beaches accreted to the limit of runup.

Artificial berm fill

207. Simulation results for the artificial 3-m-high berm are given in Figure 37. A beach fill of volume 85 m^3/m with the same grain size as the existing beach was placed mainly on the subaerial portion of the profile. The fill extended horizontally from the seawall for 20 m, tapered down for several meters, and then extended offshore with slope 1:10 to meet the equilibrium profile at a depth of approximately 1 m.

208. Twenty-one days of prestorm waves eroded the toe of the 0.25-mm artificial sand berm and created a small bar, whereas the 0.40-mm-sand beach

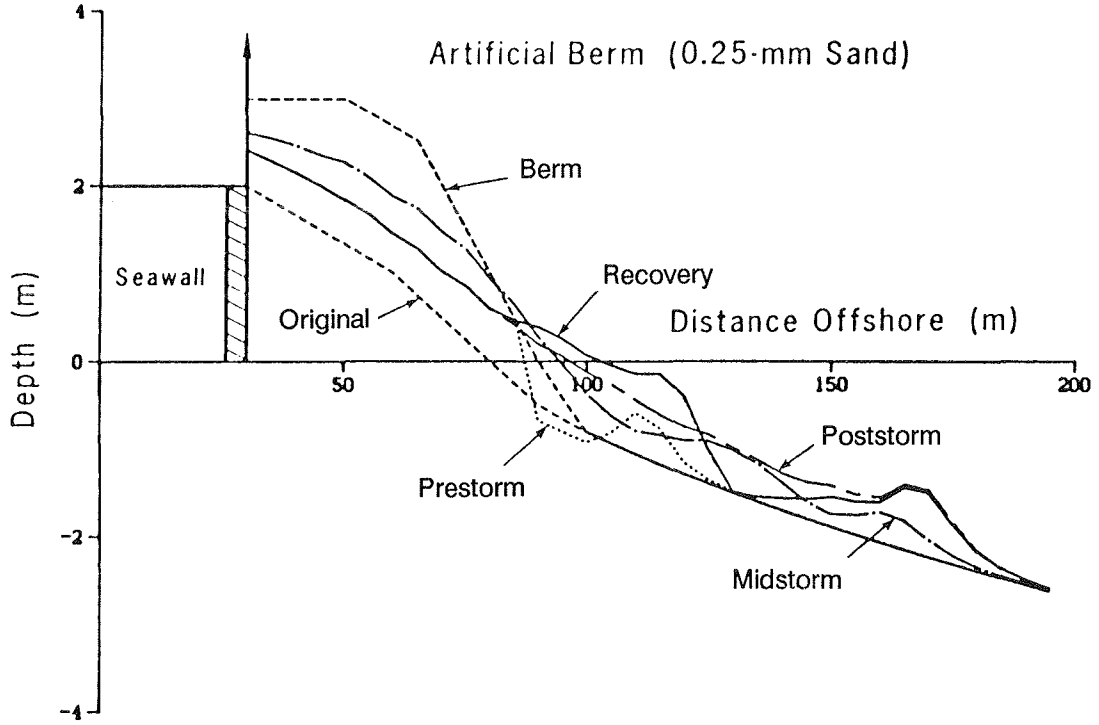

a. 0.25-mm-sand beach

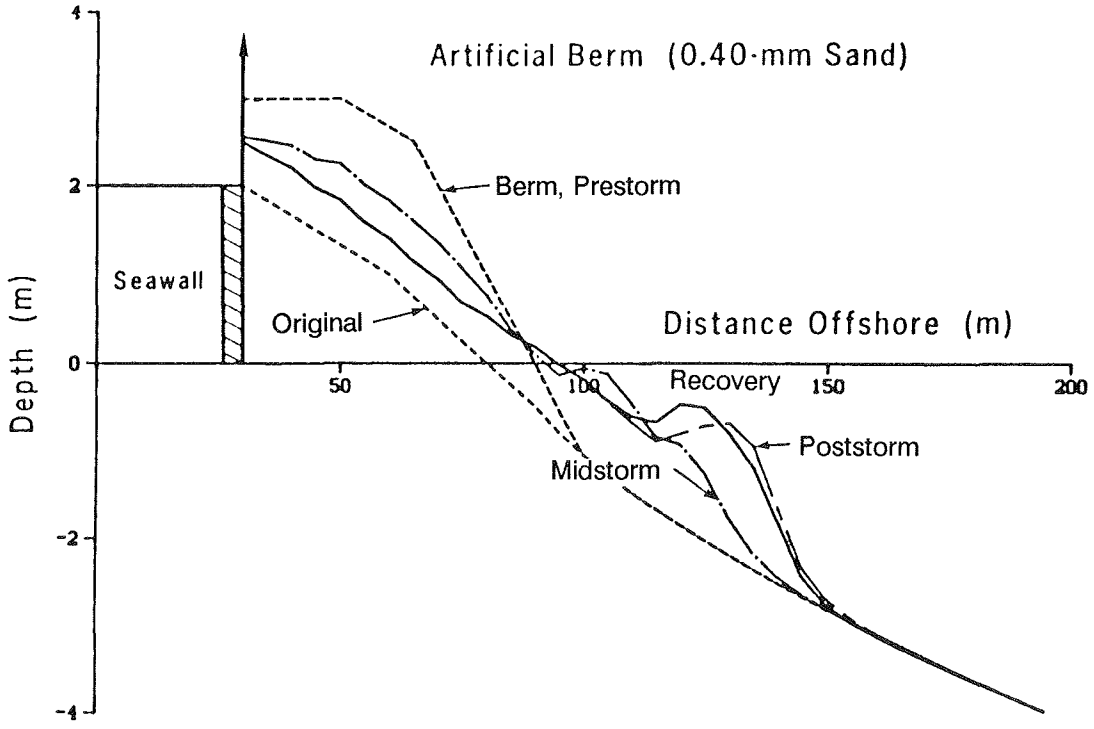

b. 0.40-mm-sand beach

Figure 37. Artificial berm simulations

configuration was effectively stable under the mild waves. Berm elevation for both sand sizes was lowered during the storm, but not to the extent of the original beach case (Figure 36). The artificial berm provided substantial protection, but should have been higher to prevent waves from reaching the seawall for this extreme storm surge. The prestorm bar was located closer to shore than in the existing case simulation. Poststorm bars for both sand sizes were located in essentially the same position as for the corresponding existing beach cases.

209. The recovery cross sections for both sand sizes were considerably different from the original beach cases because of the greater amount of sand in the system. Although significant recovery took place for the 0.25-mm-sand beach, sand was effectively trapped in the storm bar and could not contribute to poststorm beach recovery. Eroded material for the coarser sand beach was deposited closer to shore and, during the recovery phase, the entire storm profile translated shoreward. Although a limited amount of foreshore recovery took place with the 0.40-mm sand, a significant volume of material remained near to shore.

Profile nourishment

210. The profile nourishment case is depicted in Figure 38, where the major amount of material is placed along the nearshore portion of the profile in accordance with the concept that a beach can best protect itself if in a natural shape. The same volume of fill as in the artificial berm case (85 m^3/m) was placed over the profile in an equilibrium shape and tapered at the seaward end. This fill template resulted in positioning of the shoreline approximately 10 m seaward of the artificial berm case.

211. Simulation results show that subaerial erosion was reduced significantly as compared with existing conditions, even though the entire profile was submerged for much of the storm. Two bars developed again, but the inner bar ("Midstorm") for the 0.25-mm sand generated during the rising surge was located shoreward of the prestorm bar. Bar development (with respect to the initial profile) for this grain size was more pronounced than that for the artificial berm case, whereas profile evolution with 0.40-mm sand showed less bar development. The profile nourishment template showed greater retention of sand above MSL than the artificial berm case, and less material was redistributed along the profile. However, because of its low elevation,

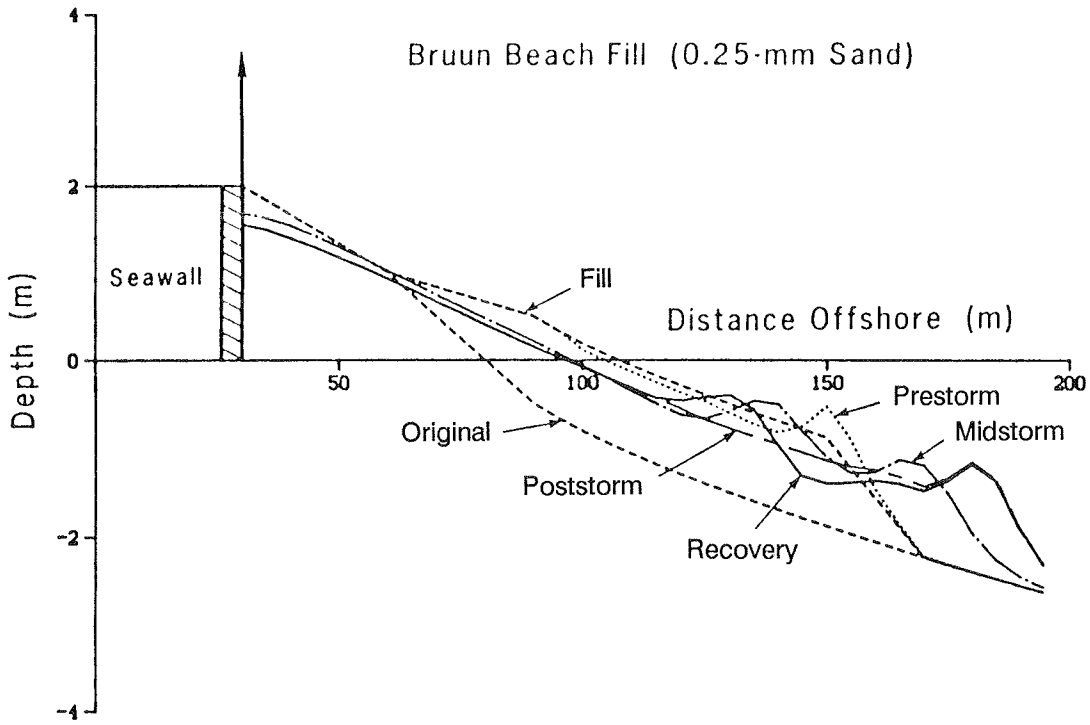

a. 0.25-mm-sand beach

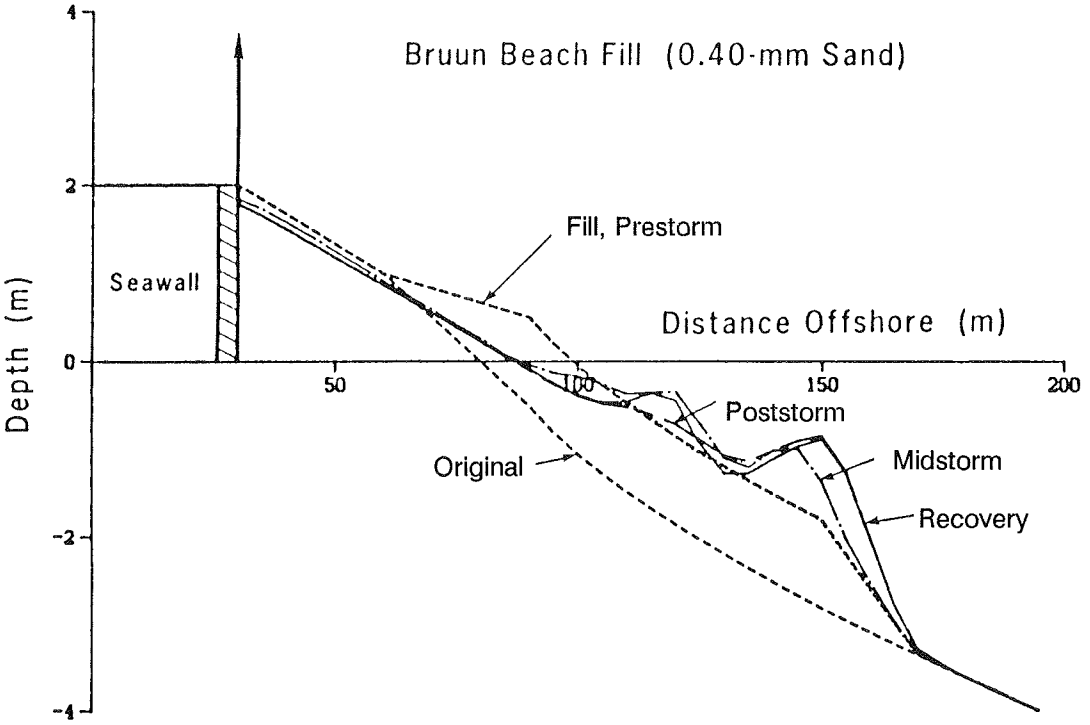

b. 0.40-mm-sand beach

Figure 38. Profile nourishment simulations

the profile nourishment template exposed the wall to more wave action during the surge than did the artificial berm of the same volume.

Discussion of Beach-Fill Simulations

212. The numerical model allowed realistic time-dependent calculations to be made of beach-fill change in terms of readily available engineering data. Model performance was realistic regarding storm-induced beach erosion, showing correct dependencies on surge and wave input, as well as initial profile shape. Storm-induced beach and dune erosion cannot be uniquely specified through a single storm-related parameter such as maximum stage. This result demonstrates the limited usefulness of the design storm approach. Qualitative features of the poststorm recovery phase were also reproduced, but further work is required to accurately simulate recovery.

213. The model can be used to judge the relative behavior of various beach-fill cross sections exposed to ordinary and extreme waves for time intervals on the order of days to weeks. Fill placed on the upper beach was calculated to move offshore to the region of incipient wave breaking, in general agreement with the initial movement of beach-fill material (Hansen, in preparation). Also, a limited number of calculations indicated that it may not be cost-effective to use beach fill with a median grain diameter much greater than 0.4 mm for storm protection, owing to the typically greatly increased cost and the declining benefit in decreased volume of eroded material. Design alternatives for specific situations (fill grain size, fill cross section, and storm climate) could be evaluated with the model.

214. The model is based on relationships for cross-shore sand transport produced by breaking waves, implying that longshore sand transport is considered negligible. Thus, caution must be exercised in applying the model and interpreting results if gradients in longshore transport exist. Longshore transport is expected to be a major contributing process to beach change over long periods, for example, seasons to a year. For such time frames, the present model should be combined with other predictive methodologies, such as a shoreline change model (e.g. Kraus 1983; Kraus, Hanson, and Harikai 1984; Hanson 1989; Kraus 1989), which compute the time rate of change of shoreline position based on estimates of wave-induced longshore sand transport.

PART VII: CONCLUSIONS AND RECOMMENDATIONS FOR FURTHER STUDY

215. The numerical model of beach profile change SBEACH was developed using large wave tank data and was verified with field data, as reported in previous work (Larson 1988, Larson and Kraus 1989a). In the present report, additional model verification was made using field data on berm and dune erosion from the US east and west coasts. Overall model performance for simulating the erosional phase of a storm event was satisfactory, whereas the recovery phase following a storm event was less well described and essentially only in qualitative agreement with the measured profile evolution.

216. A high-quality data set describing storm-induced erosion off the coast of New Jersey was used to investigate the capability of the model to simulate berm and dune erosion. SBEACH predicted eroded volumes and contour retreat in agreement with what could be confidently inferred to occur during the erosional part of the storm event. When the storm waned and waves became accretionary, a large sand ridge formed on the foreshore of a size that was not predicted by the model. However, qualitative features of the recovery were reproduced by the model, including development of profiles with different shapes according to initial conditions.

217. The capability of the model to describe profile change on the US west coast was evaluated with data available from minor storms at Torrey Pines Beach, California. Contour retreat on the foreshore was well simulated along the general profile shape. The amount of erosion predicted by the model was also in good agreement with field measurements. Similar quantities of calculated and measured erosion were obtained by increasing the water level by 0.3 m over that measured at the gage located offshore in 9.1 m of water. This increase can be ascribed to a number of factors such as locally generated wind setup landward of the gage, wave setup, and differences in atmospheric pressure. Further theoretical, laboratory, and field research is needed to better quantify hydrodynamic and sand transport processes in the swash zone, as model predictions are sensitive to changes in water level nearshore.

218. SBEACH was applied to simulate the short-term fate of beach fill by examining initial adjustment of the fill and its response to storms. In these hypothetical cases, beach-fill cross section and grain size were varied, and the response of the fill to synthetic storm events was investigated. Synthetic

storms corresponding to tropical (hurricane) and extratropical (northeasters) events were chosen as being typical for the US east coast. Two fill cross sections were evaluated, the artificial berm and profile nourishment.

219. Simulations of fill response to storm events showed the importance of peak surge level, surge duration, and wave conditions. For example, a high surge with a low duration produced as much erosion as a low-surge storm with a longer duration. The profile nourishment fill design showed less change for the design storm than the artificial berm of the same volume, suggesting that the nourished profile was more in accordance with the natural equilibrium profile and minimized profile change as the wave and water level conditions changed. This assumption was further substantiated by the stronger recovery shown by the profile-nourished beach. Model simulation also indicated that little gain in fill stability (erosion protection) was achieved during a storm if the fill grain size exceeded 0.40 mm. Overall, the numerical model provided reasonable results for simulating the response of beach fills and could be used in a cost-benefit analysis for determining the optimal fill design and protection level. However, it is recommended that the model be verified prior to use in planning and design with data from the project site or a neighboring representative site.

220. Conditions under which the numerical model is expected to give reliable results may be summarized as follows:

a. Variations in water level and breaking waves are the main causes of sand transport and thus profile change.

b. Longshore effects are negligible; that is, the incident waves approach normal to the shoreline, or differentials in longshore transport are minor (influence of structures blocking longshore transport is small, and the shoreline is straight).

c. Median grain diameter on the profile is in the interval 0.1 to 2.0 mm and reasonably uniform across-shore.

221. Experience in simulating field situations has identified several areas requiring basic research and model refinement. The most important area for further research is the description of onshore sand transport and berm development. The poststorm recovery phase must be reproduced to properly estimate storm impacts, since field surveys may be made after some recovery has already taken place.

222. SBEACH and similar beach erosion models are sensitive to changes in water level. Considerable effort is required to make progress in predicting water levels at the coast in an economical and complete fashion. Phenomena to be studied and incorporated into a coastal engineering methodology compatible with profile change modeling include wind setup, infragravity wave motion, and contributions from differentials in atmospheric pressure.

223. In the present version of SBEACH, the same transport formula is used independent of transport direction. This description is probably acceptable in the initial stage of beach recovery when waves break offshore and a well-established surf zone exists. However, as material is transported onshore and waves break closer to shore, the width of the surf zone is reduced, and the character of wave breaking might change abruptly from plunging to surging. This development during the recovery phase is not described satisfactorily by the model. Also, onshore transport in deeper water outside the break point, which takes place over long periods, lacks a good description in the model. Finally, regarding the transport rate formulation, only two types of cross-shore distributions are presently allowed, purely onshore or purely offshore transport. During times of changing wave conditions and mixed waves, more complex transport rate distributions occur, particularly if the profile is nearly in equilibrium with the waves.

224. It is possible to specify different grain sizes (equilibrium energy dissipation) according to location along the profile in the model, but since no tracking of individual grains is performed, the description is rather crude. Thus, it is only realistic in the present model to simulate beach conditions involving a few distinct grain sizes. By keeping track of the grain movement and assigning a probability distribution to the grains in each calculation cell, it would be possible to improve this aspect of the model.

225. Future research for refining and extending the capabilities of SBEACH will be directed toward improved understanding and modeling of sand transport associated with wave runup, dune overtopping, and accretionary processes on the foreshore; study of the representation and action of irregular waves; and collection of high-quality field data. At present, model reliability is limited by necessity to calibrate the model at the project site or neighboring sites. Field data collected immediately before, during, and

after storm events causing significant change in beach profile shape will allow examination and improvement of individual model algorithms.

226. Values of the calibration parameters determined for the east and west coast case studies can be viewed as nominal values used in model applications. Sensitivity tests and variation of input parameters must be made to obtain a range of predictions in which the actual storm-induced beach change may be expected to fall.

REFERENCES

Allen, J. R. L. 1970. "The Avalanching of Granular Solids on Dune and Similar Slopes," Journal of Geology, Vol 78, No. 3, pp 326-351.

Aubrey, D. G. 1978. "Statistical and Dynamical Predictions of Changes in Natural Sand Beaches," Ph.D. Dissertation, University of California, San Diego, CA.

Aubrey, D. G., Inman, D. L., and Nordstrom, C. E. 1976. "Beach Profiles at Torrey Pines, California," Proceedings of the 15th Coastal Engineering Conference, American Society of Civil Engineers, pp 1297-1311.

Basco, D. R. 1985. "A Qualitative Description of Wave Breaking," Journal of Waterway, Port, Coastal and Ocean Engineering, Vol 111, No. 2, pp 171-188.

Bascom, W. N. 1951. "The Relationship Between Sand Size and Beach-Face Slope," Transactions American Geophysical Union, Vol 32, No. 6, pp 866-874.

Beach, R. A., and Sternberg, R. W. 1987. "The Influence of Infragravity Motions on Suspended Sediment Transport in the Inner Surf Zone," Proceedings of Coastal Sediments '87, American Society of Civil Engineers, pp 913-928.

Birkemeier, W. A., Savage, R. J., and Leffler, M. W. 1988. "A Collection of Storm Erosion Field Data," Miscellaneous Paper CERC-88-9, US Army Engineer Waterways Experiment Station, Coastal Engineering Research Center, Vicksburg, MS.

Bruun, P. 1988. "Profile Nourishment: Its Background and Economic Advantages," Journal of Coastal Research, Vol 4, pp 219-228.

Caldwell, J. M. 1959. "Shore Erosion by Storm Waves," Miscellaneous Paper No. 1-59, Beach Erosion Board, US Army Engineer Waterways Experiment Station, Coastal Engineering Research Center, Vicksburg, MS.

Corson, W. D., and Tracy, B. A. 1985. "Atlantic Coast Hindcast, Phase II Wave Information: Additional Extremal Estimates," Wave Information Studies Report 15, US Army Engineer Waterways Experiment Station, Coastal Engineering Research Center, Vicksburg, MS.

Dally, W. R., and Dean, R. W. 1984. "Suspended Sediment Transport and Beach Profile Evolution," Journal of Waterways, Ports, Coastal, and Ocean Engineering, Vol 110, No. 1, pp 15-33.

Dally, W. R., Dean, R. G., and Dalrymple, R. A. 1984. "A Model for Breaker Decay on Beaches," Proceedings of the 19th Coastal Engineering Conference, American Society of Civil Engineers, pp 82-98.

_____. 1985. "Wave Height Variation Across Beaches of Arbitrary Profile," Journal of Geophysical Research, Vol 90, No. 6, pp 11917-11927.

Dean, R. G. 1973. "Heuristic Models of Sand Transport in the Surf Zone," Proceedings of the Conference on Engineering Dynamics in the Surf Zone, Sydney, Australia, pp 208-214.

_____. 1977. "Equilibrium Beach Profiles: U.S. Atlantic and Gulf Coasts," Department of Civil Engineering, Ocean Engineering Report No. 12, University of Delaware, Newark, DE.

_____. 1987. "Coastal Sediment Processes: Toward Engineering Solutions," Proceedings of Coastal Sediments '87, American Society of Civil Engineers, pp 1-24.

_____. 1990. "Equilibrium Beach Profiles: Characteristics and Applications," Coastal and Oceanographic Engineering Department, Report No. UFL/COEL-90/001, University of Florida, Gainsville, FL.

Dette, H. H., and Uliczka, K. 1987. "Prototype Investigation on Time-Dependent Dune Recession and Beach Erosion," Proceedings of Coastal Sediments '87, American Society of Civil Engineers, pp 1430-1444.

Downing, J. P. 1984. "Suspended Sediment Transport on a Dissipative Beach," Proceedings of 19th Coastal Engineering Conference, American Society of Civil Engineers, pp 1765-1781.

Ebersole, B. A. 1987. "Measurements and Prediction of Wave Height Decay in the Surf Zone," Proceedings of Coastal Hydrodynamics, American Society of Civil Engineers, pp 1-16.

Gable, C. G., Ed. 1979. "Report on Data from the Nearshore Sediment Transport Study Experiment at Torrey Pines Beach, California, November-December 1978," IMR Ref. No. 79-8, Institute of Marine Resources, University of California, San Diego, CA.

Galvin, C. J. 1969. "Breaker Travel and Choice of Design Wave Height," Journal of Waterways and Harbors Division, American Society of Civil Engineers, Vol 95, No. 2, pp 175-200.

Gebert, J. A., Watson, K. D., and Hemsley, J. M. "Monitoring Completed Coastal Projects, Manasquan Inlet, New Jersey," Technical Report in preparation, US Army Engineer Waterways Experiment Station, Coastal Engineering Research Center, Vicksburg, MS.

Gorman, L. T., Stauble, D. K., and Reed, D. W. "Geomorphic Processes at Asbury Park to Manasquan River Inlet, New Jersey," Final Report in preparation, US Army Engineer District, New York, New York.

Greenwood, B., and Sherman, D. J. 1984. "Waves, Currents, Sediment Flux and Morphological Response in a Barred Nearshore System," Marine Geology, Vol 60, pp 31-61.

Guza, R. T., and Thornton, E. B. 1982. "Swash Oscillations on a Natural Beach," Journal of Geophysical Research, Vol 87, No. C1, pp 483-491.

Hallermeier, R. J. 1987. "Applying Large Replicas of Shore Erosion by Storms," Proceedings of Coastal Sediments '87, American Society of Civil Engineers, pp 1415-1429.

Hansen, M. "Preliminary Data Report on the Hurricane Protection Project: Ocean City, Maryland," Miscellaneous Paper in preparation, US Army Engineer Waterways Experiment Station, Coastal Engineering Research Center, Vicksburg, MS.

Hanson, H. 1989. "Genesis - a Generalized Shoreline Change Numerical Model," Journal of Coastal Research, Vol 5, No. 1, pp 1-27.

Hattori, M., and Kawamata, R. 1980. "Onshore-Offshore Transport and Beach Profile Change," Proceedings of the 17th Coastal Engineering Conference, American Society of Civil Engineers, pp 1175-1193.

Horikawa, K., and Kuo, C. 1966. "A Study on Wave Transformation Inside the Surf Zone," Proceedings of the 10th Coastal Engineering Conference, American Society of Civil Engineers, pp 217-233.

Howd, P. A., and Birkemeier, W. A. 1987. "Beach and Nearshore Survey Data: 1981-1984 CERC Field Research Facility," Technical Report CERC-87-9, US Army Engineer Waterways Experiment Station, Coastal Engineering Research Center, Vicksburg, MS.

Hughes, M. G., and Cowell, P. J. 1987. "Adjustment of Reflective Beaches to Waves," Journal of Coastal Research, Vol 3, No. 2, pp 153-167.

Hunt, I. A. 1959. "Design of Seawalls and Breakwaters," Journal of Waterways and Harbors Division, Vol 85, pp 123-152.

Hunt, J. N. 1979. "Direct Solution of Wave Dispersion Equation," Journal of Waterway, Ports, Coastal and Ocean Engineering, Vol 105, No. WW4, pp 457-459.

Iwagaki, Y., and Noda, H. 1962. "Laboratory Studies of Scale Effects in Two-Dimensional Beach Processes," Proceedings of the 8th Coastal Engineering Conference, American Society of Civil Engineers, pp 194-210.

Jansen, P. C. M. 1986. "Laboratory Observations of the Kinematics in the Aerated Region of Breaking Waves," Coastal Engineering, Vol 9, pp 453-477.

Jarrett, J. T., and Hemsley, J. M. 1988. "Beach Fill and Sediment Trap at Carolina Beach, North Carolina," Technical Report CERC-88-7, US Army Engineer Waterways Experiment Station, Coastal Engineering Research Center, Vicksburg, MS.

Jensen, R.E. 1983. "Atlantic Coast Hindcast, Shallow-Water Significant Wave Information," Wave Information Studies Report 9, US Army Engineer Waterways Experiment Station, Coastal Engineering Research Center, Vicksburg, MS.

Kadib, A., Fine, S., and Ryan, J. 1989. "Coast of California Storm and Tidal Wave Study, An Overview," Proceedings of Coastal Zone '89, American Society of Civil Engineers, pp 836-848.

Kajima, R., Shimizu, T., Maruyama, K., and Saito, S. 1982. "Experiments of Beach Profile Change with a Large Wave Flume," Proceedings of the 18th Coastal Engineering Conference, American Society of Civil Engineers, pp 1385-1404.

Kajima, R., Saito, S., Shimizu, T., Maruyama, K., Hasegawa, H., and Sakakiyama, T. 1983. "Sand Transport Experiments Performed by Using a Large Water Wave Tank," Data Report No. 4-1, Central Research Institute for Electric Power Industry, Civil Engineering Division, Abiko, Japan (in Japanese).

Keulegan, G. H. 1948. "An Experimental Study of Submarine Sand Bars," Technical Report No. 3, Beach Erosion Board, US Army Engineer Waterways Experiment Station, Coastal Engineering Research Center, Vicksburg, MS.

Kraus, N. C. 1983. "Applications of a Shoreline Prediction Model," Proceedings of Coastal Structures '83, American Society of Civil Engineers, pp 632-645.

_____. 1988. "The Effects of Seawalls on the Beach: An Extended Literature Review," In: N. C. Kraus and O. H. Pilkey, Eds., The Effects of Seawalls on the Beach, Journal of Coastal Research, Special Issue, Vol 4, No. 4, pp 1-28.

_____. 1989. "Beach Change Modeling and the Coastal Planning Process," Proceedings of Coastal Zone '89, American Society of Civil Engineers, pp 553-567.

Kraus, N. C., Hanson, H., and Harikai, S. 1984. "Shoreline Change at Oarai Beach, Japan: Past, Present and Future," Proceedings of the 19th Coastal Engineering Conference, American Society of Civil Engineers, pp 2107-2123.

Kraus, N. C., and Horikawa, K. 1990. "Nearshore Sediment Transport," In: B. Lé Mehauté and D. Hanes, Eds., The Sea, Vol 9, John Wiley and Sons, New York.

Kraus, N. C., and Larson, M. 1988. "Beach Profile Change Measured in the Tank for Large Waves, 1956-1957 and 1962," Technical Report CERC-88-6, US Army Engineer Waterways Experiment Station, Coastal Engineering Research Center, Vicksburg, MS.

_____. 1989. "Prediction of Initial Profile Adjustment of Nourished Beaches to Wave Action," Proceedings of Beach Technology '88, Florida Shore and Beach Preservation Association, pp 125-137.

_____. "NMLONG: Numerical Model of the Longshore Current," Technical Report in preparation, US Army Engineer Waterways Experiment Station, Coastal Engineering Research Center, Vicksburg, MS.

Kriebel, D. L. 1982. "Beach and Dune Response to Hurricanes," M.S. Thesis, University of Delaware, Newark, DE.

_____. 1986. "Verification Study of a Dune Erosion Model," Shore and Beach, Vol 54, No. 3, pp 13-21.

Kriebel, D. L., and Dean, R. G. 1985. "Numerical Simulation of Time-Dependent Beach and Dune Erosion," Coastal Engineering, Vol 9, pp 221-245.

Larson, M. 1988. "Quantification of Beach Profile Change," Report No. 1008, Department of Water Resources Engineering, University of Lund, Lund, Sweden.

Larson, M., and Kraus, N. C. 1989a. "SBEACH: Numerical Model for Simulating Storm-Induced Beach Change, Report 1: Theory and Model Foundation," Technical Report CERC-89-9, US Army Engineer Waterways Experiment Station, Coastal Engineering Research Center, Vicksburg, MS.

_____. 1989b. "Prediction of Beach Fill Response to Varying Waves and Water Level," Proceedings of Coastal Zone '89, American Society of Civil Engineers, pp 607-621.

_____. in press. "Numerical Modeling of the Short-Term Fate of Beach Nourishment," Coastal Engineering, Special Issue on Beach Nourishment.

Larson, M., Kraus, N. C., and Sunamura, T. 1988. "Beach Profile Change: Morphology, Transport Rate, and Numerical Simulation," Proceedings of the 21st Coastal Engineering Conference, American Society of Civil Engineers, pp 1295-1309.

Longuet-Higgins, M. S., and Stewart, R. W. 1962. "Radiation Stress and Mass Transport in Gravity Waves with Application to 'Surf Beats'," Journal of Fluid Mechanics, Vol 13, pp 481-504.

_____. 1963. "A Note on Wave Set-up," Journal of Marine Research, Vol 21, pp 4-10.

Miller, R. L. 1976. "Role of Vortices in Surf Zone Prediction: Sedimentation and Wave Forces," In: R. A. Davis and R. I. Ethington, Eds., Beach and Nearshore Sedimentation, Society of Economic Paleontologists and Mineralogists, Special Publication No. 24, pp 92-114.

Mimura, N., Otsuka, Y., and Watanabe, A. 1986. "Laboratory Study on Two-Dimensional Beach Transformation Due to Irregular Waves," Proceedings of the 20th Coastal Engineering Conference, American Society of Civil Engineers, pp 1393-1406.

Moore, B. D. 1982. "Beach Profile Evolution in Response to Changes in Water Level and Wave Height," M.S. Thesis, Department of Civil Engineering, University of Delaware, Newark, DE.

Nayak, I. V. 1970. "Equilibrium Profiles of Model Beaches," Technical Report HEL-2-25, Hydraulic Engineering Laboratory, University of California, Berkeley, CA.

Peregrine, D. H., and Svendsen, I. A. 1978. "Spilling Breakers, Bores, and Hydraulic Jumps," Proceedings of the 16th Coastal Engineering Conference, American Society of Civil Engineers, pp 540-550.

Raynor, A. C., and Simmons, G. W. 1964. "Summary of Capabilities," Miscellaneous Paper No. 3-64, US Army Engineer Waterways Experiment Station, Coastal Engineering Research Center, Vicksburg, MS.

Rector, R. L. 1954. "Laboratory Study of Equilibrium Profiles of Beaches," Technical Memorandum No. 41, Beach Erosion Board, US Army Engineer Waterways Experiment Station, Coastal Engineering Research Center, Vicksburg, MS.

Roelvink, J. A., and Stive, M. J. F. 1989. "Bar-Generating Cross-Shore Flow Mechanisms on a Beach," Journal of Geophysical Research, Vol 94, No. C4, pp 4785-4800.

Sallenger, A. S., Holman, R. A., and Birkemeier, W. A. 1985. "Storm-Induced Response of a Nearshore-Bar System," Marine Geology, Vol 64, pp 237-257.

Savage, R. J., and Birkemeier, W. A. 1987. "Storm Erosion Data from the United States Atlantic Coast," Proceedings of Coastal Sediments '87, American Society of Civil Engineers, pp 1445-1459.

Saville, T. 1957. "Scale Effects in Two Dimensional Beach Studies," Transactions from the 7th General Meeting of the International Association of Hydraulic Research, Vol 1, pp A3-1-A3-10.

Scheffner, N. W. 1988. "The Generation of Dune Erosion-Frequency of Occurrence Relationships," Proceedings of Symposium on Coastal Water Resources, Technical Publication Series TPS-88-1, American Water Resources Association, pp 33-47.

_____, 1989. "Dune Erosion-Frequency of Storm Occurrence Relationships," Proceedings of Coastal Zone '89, American Society of Civil Engineers, pp 595-606.

Seymour, R. J. 1986. "Results of Cross-Shore Transport Experiments," Journal of the Waterway, Port, Coastal, and Ocean Engineering, Vol 112, No. 1, pp 168-172.

_____. 1987. "An Assessment of NSTS," Proceedings of Coastal Sediments '87, American Society of Civil Engineers, pp 642-651.

Shepard, F. P. 1950. "Longshore-Bars and Longshore-Troughs," Technical Memorandum No. 15, Beach Erosion Board, US Army Engineer Waterways Experiment Station, Coastal Engineering Research Center, Vicksburg, MS.

Shimizu, T., Saito, S., Maruyama, K., Hasegawa, H., and Kajima, R. 1985. "Modeling of Onshore-Offshore Sand Transport Rate Distribution Based on the Large Wave Flume Experiments," Civil Engineering Laboratory Report No. 384028, Abiko City, Japan (in Japanese).

Singamsetti, S. R., and Wind, H. G. 1980. "Breaking Waves Characteristics of Shoaling and Breaking Periodic Waves Normally Incident to Plane Beaches of Constant Slope," Report M 1371, Delft Hydraulics Laboratory, Delft, The Netherlands.

Skjelbreia, J. E. 1987. "Observations of Breaking Waves on Sloping Bottoms by Use of Laser Doppler Velocimetry," Report No. KH-R-48, Division of Engineering and Applied Science, California Institute of Technology, Pasadena, CA.

Smith, E. R., and Kraus, N. C. "Laboratory Study of the Macrofeatures of Wave Breaking Over Bars and Reefs," Technical Report in preparation, US Army Engineer Waterways Experiment Station, Coastal Engineering Research Center, Vicksburg, MS.

Sternberg, R. W., Shi, N. C., and Downing, J. P. 1984. "Field Investigation of Suspended Sediment Transport in the Nearshore Zone," Proceedings of the 19th Coastal Engineering Conference, American Society of Civil Engineers, pp 1782-1798.

Sunamura, T. 1980a. "Parameters for Delimiting Erosion and Accretion of Natural Beaches," Annual Report of the Institute of Geoscience, the University of Tsukuba, Tsukuba, Japan, No. 6, pp 51-54.

_____. 1980b. "A Laboratory Study of Offshore Transport of Sediment and a Model for Eroding Beaches," Proceedings of the 17th Coastal Engineering Conference, American Society of Civil Engineers, pp 1051-1070.

Sunamura, T., and Horikawa, K. 1974. "Two-Dimensional Beach Transformation Due to Waves," Proceedings of the 14th Coastal Engineering Conference, American Society of Civil Engineers, pp 920-938.

Svendsen, I. A. 1987. "Analysis of Surf Zone Turbulence," Journal of Geophysical Research, Vol 92, No. C5, pp 5115-5124.

Svendsen, I. A., Madsen, P. A., and Buhr Hansen, J. 1978. "Wave Characteristics in the Surf Zone," Proceedings of the 14th Coastal Engineering Conference, American Society of Civil Engineers, pp 520-539.

Takeda, I., and Sunamura, T. 1983. "A Wave-Flume Experiment of Beach Steps," Annual Report No. 9, Institute of Geoscience, University of Tsukuba, Tsukuba, Japan, pp 45-48.

Thomas, K. V., and Baba, M. 1986. "Berm Development on a Monsoon-Influenced Microtidal Beach," Sedimentology, Vol 33, pp 537-546.

US Army Engineer District, New York. 1954. "Atlantic Coast of New Jersey, Sandy Hook to Barnegat Inlet," Beach Erosion Control Report on Cooperative Study (Survey), Serial No. 38, New York, NY.

_____, Los Angeles. 1984. "Sediment Sampling, Dana Point to the Mexican Border, Nov 83-Jan 84," CCSTWS 84-5, Los Angeles, CA.

van de Graaff, J. 1983. "Probabilistic Design of Dunes," Proceedings of Coastal Structures '83, American Society of Civil Engineers, pp 820-831.

van Hijum, E. 1974. "Equilibrium Profiles of Coarse Material Under Wave Attack," Proceedings of the 14th Coastal Engineering Conference, American Society of Civil Engineers, pp 939-957.

_____. 1976. "Equilibrium Profiles and Longshore Transport of Coarse Material Under Oblique Wave Attack," Proceedings of the 15th Coastal Engineering Conference, American Society of Civil Engineers, pp 1258-1276.

Vellinga, P. 1982. "Beach and Dune Erosion During Storm Surges," Publication No. 276, Delft Hydraulics Laboratory, Delft, The Netherlands.

Visser, P. J. 1982. "The Proper Longshore Current in a Wave Basin," Report No. 82-1, Department of Civil Engineering, Delft University of Technology, Delft, The Netherlands.

Watanabe, A. 1982. "Numerical Models of Nearshore Currents and Beach Deformation," Coastal Engineering in Japan, Vol 25, pp 147-161.

Waters, C. H. 1939. "Equilibrium Slopes of Sea Beaches," M.S. Thesis, Department of Civil Engineering, University of California, Berkeley, CA.

Wiegel, R. L. 1964. Oceanographical Engineering, Prentice-Hall, Englewood Cliffs, NJ.

Wright, L. D., and Short, A. D. 1984. "Morphodynamic Variability of Surf Zones and Beaches: A Synthesis," Marine Geology, Vol 56, pp 93-118.

Wu, C. S., Thornton, E. B., and Guza, R. T. 1985. "Waves and Longshore Currents: Comparison of a Numerical Model with Field Data," Journal of Geophysical Research, Vol 90, No. C3, pp 4951-4958.

APPENDIX A: NOTATION

A	Shape parameter for equilibrium beach profile, $m^{1/3}$
C	Wave phase speed, m/sec
C_g	Wave group speed, m/sec
C_o	Wave group speed in deep water, m/sec
d	Total water depth, m
D_{50}	Median grain diameter, mm
D	Wave energy dissipation per unit water volume, N-m/m^3-sec
D_{eq}	Equilibrium wave energy dissipation per unit water volume, N-m/m^3-sec
E	Wave energy density, N-m/m^2
E_s	Stable wave energy density, N-m/m^2
F	Wave energy flux, N-m/m-sec
F_s	Stable wave energy flux, N-m/m-sec
g	Acceleration due to gravity, m/sec^2
h	Still-water depth, m
H	Wave height, m
H_b	Breaking wave height, m
H_{mo}	Energy-based significant wave height, m
H_o	Deepwater wave height, m
H_{rms}	Root-mean-square wave height, m
H_{so}	Deepwater significant wave height, m
$\overline{H}$	Mean wave height, m
$\overline{H}_o$	Mean deepwater wave height, m
K	Sand transport rate coefficient, m^4/N
L	Wavelength, m
L_o	Deepwater wavelength, m
M	Dimensionless empirical coefficient
n	Ratio of wave group speed and wave phase speed
q	Net cross-shore sand transport rate, m^3/m-sec
S_{xx}	Radiation stress component directed onshore, N/m
t	Time, sec
T	Wave period, sec
w	Sand fall speed, m/sec
x	Cross-shore coordinate, m

y	Longshore coordinate, m
Z_R	Height of active subaerial profile, m
β	Local beach slope seaward of break point
γ	Ratio between wave height and water depth at breaking
Γ	Empirical stable wave height coefficient
Δ	Change in quantity
ε	Slope-related sand transport rate coefficient, m^2/sec
η	Mean water surface elevation (wave setup or setdown), m
κ	Wave decay coefficient
λ	Spatial decay coefficient, m^{-1}
θ	Wave angle with respect to bottom contours
ρ	Density of water, kg/m^3
ψ	Local profile slope
ψ_{iy}	Angle of initial yield
ψ_{ra}	Residual angle after shearing
ξ	Surf similarity parameter

Subscripts and Superscripts:

b	Breaking condition
eq	Equilibrium condition
o	Deepwater condition
i	Variable at grid point or cell i
k	Variable at time step k
N	Number of cells where avalanching occurs
p	Plunge point
r	Runup limit
s	Stable condition for depth-limited wave
z	End of surf zone
1	Specific value of variable in zone I
2	Specific value of variable in zone II
'	Denotes the smoothed transport rate